Institut für Theoretische Physik

Fakultät Mathematik und Naturwissenschaften

Technische Universität Dresden

On Quantum Simulators and Adiabatic Quantum Algorithms

Dissertation

zur Erlangung des akademischen Grades

Doctor rerum naturalium

vorgelegt von

Sarah Mostame

geboren am 27. July 1978 in Tabriz, Iran

Dresden 2008

Eingereicht am 02.10.2008

1. Gutachter: Prof. Dr Rüdiger Schmidt

2. Gutachter: Prof. Dr. Ralf Schützhold

3. Gutachter: Prof. Dr. Walter Strunz

Verteidigt am 28.11.2008

Abstract

This Thesis focuses on different aspects of quantum computation theory: adiabatic quantum algorithms, decoherence during the adiabatic evolution and quantum simulators. After an overview on the area of quantum computation and setting up the formal ground for the rest of the Thesis we derive a general error estimate for adiabatic quantum computing. We demonstrate that the first-order correction, which has frequently been used as a condition for adiabatic quantum computation, does not yield a good estimate for the computational error. Therefore, a more general criterion is proposed, which includes higher-order corrections and shows that the computational error can be made exponentially small – which facilitates significantly shorter evolution times than the first-order estimate in certain situations. Based on this criterion and rather general arguments and assumptions, it can be demonstrated that a run-time of order of the inverse minimum energy gap is sufficient and necessary. Furthermore, exploiting the similarity between adiabatic quantum algorithms and quantum phase transitions, we study the impact of decoherence on the sweep through a second-order quantum phase transition for the prototypical example of the Ising chain in a transverse field and compare it to the adiabatic version of Grover's search algorithm. It turns out that (in contrast to first-order transitions) the impact of decoherence caused by a weak coupling to a rather general environment increases with system size (i.e., number of spins/qubits), which might limit the scalability of the system. Finally, we propose the use of electron systems to construct laboratory systems based on present-day technology which reproduce and thereby simulate the quantum dynamics of the Ising model and the $O(3)$ nonlinear sigma model.

Contents

1 Introduction

In many areas of physics, progress has been thwarted by our lack of understanding strongly interacting quantum systems with *many degrees of freedom* such as quantum field theories. Beyond perturbation theory with respect to some parameter or semiclassical models/methods, there are not many analytical tools available for the treatment of these systems. Numerical methods are hampered by the exponentially increasing amount of resources required for the simulation of quantum systems with many degrees of freedom in general. This difficulty of simulating the dynamics of quantum systems by classical means was recognized by Feynman [1] more than two decades ago and bred widespread interest in quantum computation. Feynman himself expressed:

> *The full description of quantum mechanics for a large system with R particles is given by a function $\Psi(x_1, x_2, \cdots, x_R, t)$ which we call the amplitude to find the particles $x_1, x_2, \cdots, x_R$, and therefore, because it has too many variables it cannot be simulated with a normal computer with a number of elements proportional to R.*

He thought up the idea of a quantum computer which uses the effects of quantum theory instead of classical physics and will be able to simulate other quantum systems with polynomial effort. The computational power of quantum computers has been investigated extensively since Feynman's observation in 1982. Deutsch [3] was the first to establish a solid ground for the theory of quantum computation by introducing a fully quantum model for computation and giving the description of a *universal quantum computer* in 1985. But certainly, the strongest evidence for the power of quantum computers comes from Shor's discovery of a polynomial-time quantum algorithm [4] for finding the prime factors of composite numbers and computing the discrete logarithm. Although there is no proof, it is believed that no polynomial-time classical algorithm exists for these two problems. More recent results on quantum algorithms include Grover's quantum algorithm [5] for unstructured search problems which offers quadratic speedups over

classical search algorithms and Hallgren's quantum algorithm [6] for Pell's equation[1] which is exponentially faster than any known classical algorithm.

Quantum mechanics, in so far as it is a complete natural theory, describes every physical computing device and, so, even classical computers. Therefore, describing quantum computers as computing devices that operate according to the laws of quantum mechanics is not very informative. However, quantum computers can be distinguished from classical ones by their operation based on the two distinctively quantum-mechanical effects of interference and entanglement that do not appear in classical physics. Therefore, a quantum computer is an interference device of many entangled computation paths. Just as an interference pattern can appear by preparing a particle in a superposition of different geometric paths which are then combined to interfere, the output of a quantum computer is also obtained by preparing the quantum bits in a superposition of different classical computation states which are combined to interfere producing the final computation answer. This immediately leads to the problem of dealing with noise in quantum computation. We know that the interference pattern in a double-slit experiment disappears if it is in principle possible to know from which slit the particle has passed. So, if we think of a quantum computer as executing a computation which resembles a very complex interference experiment, it is natural to worry that the complexity of the computation will make it impossible in practice to maintain the complex superpositions of states and observe an interference effect at the end of the computation. In principle, the problem that non-controllable errors occur (decoherence problem) is an essential issue of studying in order to completely exploit the new possibilities opened by quantum mechanics. Any real-life device unavoidably interacts with its environment, which typically contains a huge amount of uncontrollable degrees of freedom. This interaction causes a corruption of the information stored in the system as well as errors in computation steps that eventually lead to wrong outputs. One of the possible approaches for overcoming this difficulty is an adiabatic quantum computation which has been proposed by Farhi et al. [7] and attracted considerable attention since it exhibits promising algorithmic capabilities as well as a good robustness against decoherence and control errors [8, 9, 10]. One of the main topics of this Thesis is on adiabatic quantum algorithms.

[1] Pell's equation is one of the oldest studied problems in number theory. Given a positive non-square integer d, Pell's equation is $x^2 - dy^2 = 1$ and the goal is to find its integer solutions. The original algorithm for solving this problem is the second oldest number theory algorithm after Euclid's algorithm. The algorithm is due to Indian mathematicians around 1000. In 1768 Lagrange showed that there are an infinite number of solutions of the equation, and we have the following theorem. If x_1, y_1 is the least positive solution of $x^2 - dy^2 = 1$, where d is a positive non-square integer, then all positive solutions are given by x_n, y_n for $n = 1, 2, 3, \cdots$, where $x_n + y_n\sqrt{d} = \left(x_1 + y_1\sqrt{d}\right)^n$.

1.1 Introduction to Quantum Information

In analogy with classical computation where the basic carriers of information are bits, in quantum computation the carriers of information are quantum bits or *qubits* for short. A qubit is a two-level quantum system[2] such as, e.g., spin 1/2 particles. The Hilbert space, $\mathcal{H}$, of a qubit, namely, a single-qubit space, is complex and two-dimensional with basis vectors

$$|0\rangle = \begin{pmatrix} 1 \\ 0 \end{pmatrix} \quad , \quad |1\rangle = \begin{pmatrix} 0 \\ 1 \end{pmatrix}, \tag{1.1}$$

a so-called computational basis. A basis for operators in a two-dimensional Hilbert space can be formed by the three Pauli matrices which are unitary and Hermitian

$$\sigma^x = \begin{pmatrix} 0 & 1 \\ 1 & 0 \end{pmatrix} \quad , \quad \sigma^y = \begin{pmatrix} 0 & -i \\ i & 0 \end{pmatrix} \quad , \quad \sigma^z = \begin{pmatrix} 1 & 0 \\ 0 & -1 \end{pmatrix}, \tag{1.2}$$

and the identity operator $\mathcal{I} = \mathrm{diag}(1, 1)$. Unlike the state of a bit which is either 0 or 1, the state of a qubit is a unit vector in a two-dimensional Hilbert space, $\mathcal{H} = \mathbb{C}^2$. Then, an arbitrary state of a single qubit is a vector

$$|\phi\rangle = c_0 \, |0\rangle + c_1 \, |1\rangle \ , \tag{1.3}$$

having unit length, i.e., $|c_0|^2 + |c_1|^2 = 1$. Qubits generalize classical bits since not only can they be in the two orthogonal states $|0\rangle$ and $|1\rangle$, but they can also be in superpositions of these two states. A signal or message in a quantum information processing system is the state of a set of (say n) qubits. The Hilbert space for such an n-digit quantum message is the n-tuple tensor product

$$\mathcal{H}_n := \mathcal{H}^{\otimes n} = \underbrace{\mathcal{H} \otimes \cdots \otimes \mathcal{H}}_{(n \text{ times})}, \tag{1.4}$$

which is a 2^n-dimensional complex space. A natural basis in $\mathcal{H}_n$ is provided by the vectors $|X\rangle$ where $X = (x_1, \cdots, x_n) \in \{0, 1\}^n$ is a binary string of length n. There are 2^n of these vectors which can be written in the tensor-product notation as

$$|X\rangle = |x_1\rangle \otimes \cdots \otimes |x_n\rangle \equiv |x_1 \, x_2 \, \cdots \, x_n\rangle \ . \tag{1.5}$$

The orthonormality of these basis vectors is expressed as $\langle X|X'\rangle = \delta_{XX'}$.

[2] Any two-level system can be used as a qubit. Multilevel systems can be used as well, if they possess two states that can be effectively decoupled from the rest (e.g., ground state and first excited state of a nonlinear oscillator). There are various proposals. Several physical implementations which approximate two-level systems to various degrees were successfully realized. Similarly to a classical bit where the state of a transistor in a processor, the magnetization of a surface in a hard disk and the presence of current in a cable can all be used to represent bits in the same computer, an eventual quantum computer is likely to use various combinations of qubits in its design.

Any vector (quantum register) $|\Psi\rangle \in \mathcal{H}_n$ is a (complex) linear combination of 2^n basis states and can be in a highly entangled state[3]

$$|\Psi\rangle = \sum_{X \in \{0,1\}^n} c_X \, |X\rangle \ , \tag{1.6}$$

with $c_X \in \mathbb{C}$. If

$$|\Psi'\rangle = \sum_{X' \in \{0,1\}^n} c'_{X'} \, |X'\rangle \ , \tag{1.7}$$

then the scalar product $\langle \Psi' | \Psi \rangle$ is given by

$$\langle \Psi' | \Psi \rangle = \sum_{X \in \{0,1\}^n} c'^*_X c_X \, . \tag{1.8}$$

The qubits can be transformed using the quantum logic gates, which are performed with the help of unitary transformations $\mathcal{U} : \mathcal{H} \to \mathcal{H}$, and transform initial state $|\Psi_0\rangle$ into final state $|\Psi_\mathrm{f}\rangle$ according to

$$|\Psi_\mathrm{f}\rangle = \mathcal{U} \, |\Psi_0\rangle \ . \tag{1.9}$$

In other words, a single-qubit quantum gate defines a linear operation

$$|0\rangle \to a \, |0\rangle + b \, |1\rangle \qquad , \qquad |1\rangle \to c \, |0\rangle + d \, |1\rangle \ , \tag{1.10}$$

such that the matrix

$$\begin{pmatrix} a & b \\ c & d \end{pmatrix} \tag{1.11}$$

is unitary.

1.2 Quantum Algorithms

A quantum algorithm consists of a sequence of unitary transformations (gates) applied on several distinguishable two-level quantum systems (qubits). To realize every possible quantum algorithm, one must be able to realize one qubit rotations and at least one two-qubit gate, i.e.

[3] This means that it cannot be written as a product of the states of n individual qubits

$$|\Psi\rangle \neq |\phi_1\rangle \otimes \cdots \otimes |\phi_n\rangle \ ,$$

where $|\phi_j\rangle \in \mathcal{H}$ for $1 \leq j \leq n$.

an interaction between two different qubits. A simple example for a one-qubit gate is a rotation by π

$$a\,|0\rangle + b\,|1\rangle \xrightarrow{\pi} b\,|0\rangle + a\,|1\rangle \ . \tag{1.12}$$

The *Hadamard gate* and the *controlled not gate* (CNOT or XOR) are frequently used gates. In the latter one, denoted by C_{12}, the first qubit is the control-qubit and the second one the target qubit. The target bit is flipped depending on whether the control bit is zero or one. Applied to the basis states of a combined two-qubit system, the CNOT has the following effect

$$\begin{aligned} |00\rangle &\xrightarrow{C_{12}} |00\rangle \qquad , \qquad |01\rangle \xrightarrow{C_{12}} |01\rangle \ , \\ |10\rangle &\xrightarrow{C_{12}} |11\rangle \qquad , \qquad |11\rangle \xrightarrow{C_{12}} |10\rangle \ . \end{aligned} \tag{1.13}$$

A Hadamard gate $H^{(2)}$ is a unitary and Hermitian one-qubit operation. It produces an equally weighted superposition of the two basis states according to the rule

$$|0\rangle \rightarrow \frac{1}{\sqrt{2}}\left(|0\rangle + |1\rangle\right) \qquad , \qquad |1\rangle \rightarrow \frac{1}{\sqrt{2}}\left(|0\rangle - |1\rangle\right) \ . \tag{1.14}$$

A n-qubit Hadamard gate $H^{(2^n)}$ is defined by the n-fold tensor product, i.e.

$$H^{(2^n)} = \underbrace{H^{(2)} \otimes \cdots \otimes H^{(2)}}_{n \text{ times}} \ . \tag{1.15}$$

1.3 Grover's Quantum Search Algorithm

Let us first of all consider a classical version of Grover's search algorithm. Consider an unsorted database with N items and a certain item w one is searching for. As a particular example one can imagine a telephone directory with N entries and a particular telephone number w she is looking for. Furthermore, assume that she is only given a black box for performing this data search. This black box, i.e. a so called *oracle*, can decide whether an item is w or not. Thus, in mathematical terms she is given a Boolean function

$$f(x) = \delta_{xw} = \begin{cases} 1 & x = w \\ 0 & x \neq w \end{cases} \tag{1.16}$$

The classical oracle allows her to evaluate this Boolean function for any element x of the database. Assuming that each application of this oracle requires one elementary step a classical random search process will require $N-1$ steps in the worst case and one step in the best possible case. Thus, for large values of N, on the average a classical algorithm will need $N/2$ steps to find the item w.

It has been shown by Grover [5] that with the help of his quantum search algorithm this task can be performed in $\sqrt{N}$ steps with a probability arbitrarily close to unity. Thereby, one exploits

the phenomenon of quantum interference. The basic idea of this quantum algorithm is to rotate an initial reference state of the qubit system representing the database in the direction of the searched state $|w\rangle$ with the help of a unitary quantum version of the oracle.
In Grover's quantum search algorithm the $N = 2^n$ elements of the database are represented by orthogonal states of a distinguishable n-qubit system. These orthogonal states constitute the computational basis of a quantum computer. The state $|0\cdots0110\cdots0\rangle$ of this computational basis, for example, corresponds to the element $0\cdots0110\cdots0$ of the database in binary notation. The quantum oracle $\mathcal{U}_f$ is determined completely by the Boolean function of Eq. (1.16) and is represented by a quantum gate, i.e. by the unitary and hermitian transformation

$$\mathcal{U}_f : |x, a\rangle \rightarrow |x, f(x) \oplus a\rangle \ . \tag{1.17}$$

Thereby $|x\rangle$ is an arbitrary element of the computational basis and $|a\rangle$ is the state of an additional ancilla qubit which is discarded later. The symbol $\oplus$ denotes addition modulo 2. It is important to note that the elementary rotations in the direction of the searched quantum state $|w\rangle$ which are the key ingredient in Grover's algorithm can be performed with the help of this unitary oracle. Thus such a rotation can be performed without explicit knowledge of the state $|w\rangle$. Its implicit knowledge through the values of the Boolean function $f(x)$ is already sufficient. For large values of N it turns out that the number of elementary rotations needed to prepare state $|w\rangle$ is $\mathcal{O}(\sqrt{N})$. To implement such an elementary rotation from the initial reference state $|s\rangle = |0\cdots0\rangle$, for example, towards the final state $|w\rangle$ two different types of quantum gates are needed, namely *Hadamard gates* and *controlled phase inversions*.
A controlled phase inversion with respect to a state $|w\rangle$ changes the phase of this particular state by an amount of π and leaves all other states unchanged. Thus the phase inversion I_s with respect to the initial state $|s\rangle$ is defined by

$$I_s\,|s\rangle = -\,|s\rangle \qquad , \qquad I_s\,|x\rangle = |x\rangle \quad (x \neq s)\,. \tag{1.18}$$

The controlled phase inversion I_w with respect to the searched state $|w\rangle$ is defined in an analogous way. As state $|w\rangle$ is not known explicitly but only implicitly through the property $f(w) = 1$, this transformation has to be performed with the help of the quantum oracle. This task can be achieved by preparing the ancilla of the oracle of Eq. (1.17) in state

$$|a_0\rangle = \frac{1}{\sqrt{2}}\,(|0\rangle - |1\rangle) \ . \tag{1.19}$$

As a consequence one obtains the following required properties for the phase inversion I_w

$$\begin{aligned} |x, f(x) \oplus a_0\rangle \equiv |x, 0 \oplus a_0\rangle &= \frac{1}{\sqrt{2}}\,(|x, 0\rangle - |x, 1\rangle) = |x, a_0\rangle \quad \text{for} \quad x \neq w\,, \\ |x, f(x) \oplus a_0\rangle \equiv |x, 1 \oplus a_0\rangle &= \frac{1}{\sqrt{2}}\,(|x, 1\rangle - |x, 0\rangle) = -\,|x, a_0\rangle \quad \text{for} \quad x = w\,. \end{aligned} \tag{1.20}$$

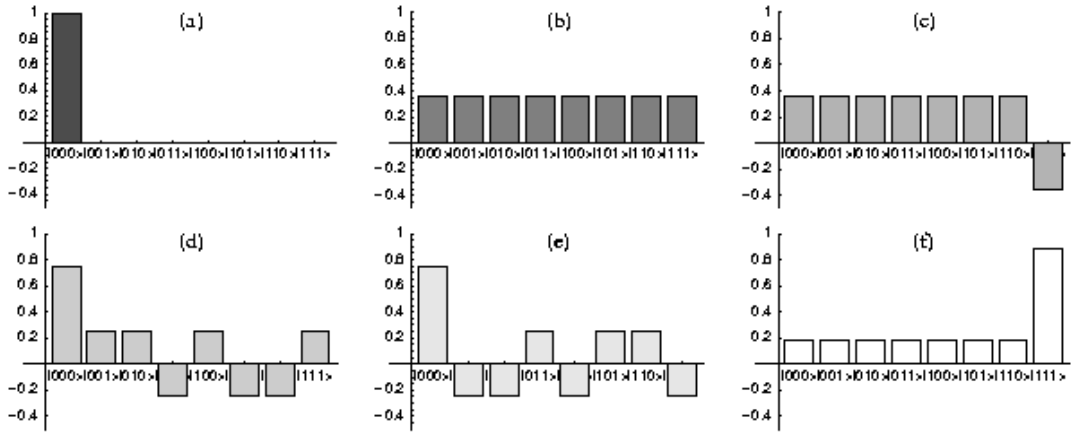

Figure 1.1: Amplitude distributions resulting from the various quantum gates involved in Grover's quantum search algorithm for the case of three qubits. The quantum states which are prepared by these gates are (a) $|s\rangle = |000\rangle$, (b) $H^{(2^n)}\,|s\rangle$, (c) $I_w\,H^{(2^n)}\,|s\rangle$, (d) $H^{(2^n)}\,I_w\,H^{(2^n)}\,|s\rangle$, (e) $-I_s\,H^{(2^n)}\,I_w\,H^{(2^n)}\,|s\rangle$, (f) $-H^{(2^n)}\,I_s\,H^{(2^n)}\,I_w\,H^{(2^n)}\,|s\rangle$. The searched state $|w\rangle$ is assumed to be state $|111\rangle$. The figure has been taken from [11].

This controlled phase inversion can be performed with the help of the quantum oracle without explicit knowledge of state $|w\rangle$.

Grover's algorithm starts by preparing all n qubits of the quantum computer in the reference state $|0\cdots0\rangle$. An elementary rotation in the direction of the searched state $|w\rangle$ with the property $f(w) = 1$ is achieved by the gate sequence

$$\mathcal{Q} = -I_s\,H^{(2^n)}\,I_w\,H^{(2^n)}\,|s\rangle\ , \tag{1.21}$$

where $H^{(2^n)}$ denotes the n-qubit Hadamard gate. In order to rotate the initial state $|s\rangle$ into state $|w\rangle$, one has to perform a sequence of τ such rotations and a final Hadamard transformation at the end

$$|f\rangle = H^{(2^n)}\mathcal{Q}^\tau\,|s\rangle\ . \tag{1.22}$$

The effect of one elementary rotation $\mathcal{Q}$ is demonstrated [11] in Fig. (1.1) for the case of three qubits ($n = 3$). The first Hadamard transformation $H^{(2^3)}$ prepares an equally weighted state,

$$H^{(2^3)}\,|000\rangle = \frac{1}{2^{3/2}}\left(|000\rangle + |001\rangle + |010\rangle + |011\rangle + |100\rangle + |101\rangle + |110\rangle + |111\rangle\right)\ .$$

The subsequent quantum gate I_w inverts the amplitude of the searched state $|w\rangle = |111\rangle$,

$$I_w H^{(2^3)}\,|000\rangle = \frac{1}{2^{3/2}}\left(|000\rangle + |001\rangle + |010\rangle + |011\rangle + |100\rangle + |101\rangle + |110\rangle - |111\rangle\right)\ .$$

Together with the subsequent Hadamard transformation and the phase inversion I_s this gate sequence $\mathcal{Q}$ amplifies the probability amplitude of the searched state $|111\rangle$. In this particular case an additional Hadamard transformation finally prepares the quantum computer in the searched state $|111\rangle$ with a probability of 0.88

$$\begin{aligned} H^{(2^3)}\mathcal{Q}\,|000\rangle &= -H^{(2^3)} I_s\, H^{(2^3)}\, I_w\, H^{(2^3)}\,|000\rangle \\ &= \frac{1}{2^{5/2}}\left(|000\rangle + |001\rangle + |010\rangle + |011\rangle + |100\rangle + |101\rangle + |110\rangle + 5\,|111\rangle\right) . \end{aligned} \tag{1.23}$$

In order to determine the dependence of the ideal number of repetitions τ on the number of qubits n it is convenient to analyze the repeated application of the gate sequence $\mathcal{Q}$. According to Eq. (1.22) in terms of the two states $|s\rangle$ and $|v\rangle = H^{(2^n)}\,|w\rangle$ the overlap is given by $u = \langle s|v\rangle = \langle s|\, H^{(2^n)}\,|w\rangle = 2^{-n/2}$ for n qubits. It is straightforward to show that the unitary gate sequence $\mathcal{Q}$ preserves the subspace spanned by these two states [5]

$$\mathcal{Q}\begin{pmatrix}|s\rangle\\|v\rangle\end{pmatrix} = \begin{pmatrix} 1-4u^2 & 2u \\ -2u & 1 \end{pmatrix}\begin{pmatrix}|s\rangle\\|v\rangle\end{pmatrix} . \tag{1.24}$$

Thus the gate sequence $\mathcal{Q}$ acts like a rotation in the plane spanned by states $|s\rangle$ and $|v\rangle$. The angle of rotation is given by $\theta = \arcsin(2u\sqrt{1-u^2})$. The initial state $|s\rangle$ can be decomposed in the following way

$$|s\rangle = \sin\beta\,|w\rangle + \cos\beta\,\left|w^{\perp}\right\rangle , \tag{1.25}$$

where $\left\langle w|w^{\perp}\right\rangle = 0$ and $\langle w|s\rangle = \sin\beta \approx u$ (for $2^n \gg 1$). After j iterations

$$\mathcal{Q}^j\,|s\rangle = \sin[(2j+1)\beta]\,|w\rangle + \cos[(2j+1)\beta]\,\left|w^{\perp}\right\rangle , \tag{1.26}$$

the amplitude of state $|v\rangle$ is given by $\sin[(2j+1)\beta]$. Therefore, the optimal number τ of repetitions of the gate sequence $\mathcal{Q}$ is approximately given by $\sin[(2\tau+1)\beta] \to 1$

$$\Rightarrow \quad \tau \approx \frac{\pi}{4\arcsin u} - \frac{1}{2} = \frac{\pi}{4\arcsin(2^{-n/2})} - \frac{1}{2} \approx \frac{\pi}{4}\sqrt{2^n} = \mathcal{O}(\sqrt{N}) , \tag{1.27}$$

for $N = 2^n \gg 1$.

1.4 NP-Complete Problems

Quantum computers could solve problems believed to be intractable on classical (i.e., nonquantum) computers. An intractable problem is one that takes too long to solve when the input gets too big. More precisely, a classically intractable problem is one that cannot be solved using any

classical algorithm whose running time grows only polynomially as a function of the length of the input. For example, all known classical factoring algorithms require a time that grows faster than any polynomial as a function of the number of digits in the integer to be factored. Shor's quantum algorithm [4] for the factoring problem can factor an integer in a time that grows polynomially with the number of digits. This raises the question of whether quantum computers could solve other classically difficult problems faster than classical computers. According to computational complexity, problems can be divided into two large groups. Those for which the time to find a solution grows polynomially with the size of the problem belong to the so-called **P** class (polynomial) and those that require polynomial time to verify the solution belong to **NP** (nondeterministic polynomial). An especially important subset of **NP** problems is called **NPC** (**NP**-complete), see, e.g., [12]. They have the property that any **NP** problem can be transformed to a **NPC** problem in a polynomial time. Hundreds of problems are known to be **NPC** (e.g., the Traveling Salesman problem) and they are all related in the following sense:

> *If someone finds a polynomial-time algorithm for one* **NPC** *problem, then this algorithm could be used as a subroutine in programs that would then solve all other* **NPC** *problems in polynomial time.*

That no one has succeeded in finding a classical polynomial-time algorithm for any of these problems is strong evidence for the intractability of all of them. On the other hand, no one has been able to prove that a polynomial-time algorithm cannot be constructed for any **NPC** problem. Settling the question of whether a polynomial-time algorithm does or does not exist for an **NPC** problem is one of the outstanding problems of classical computer science. It is also an open question whether an **NPC** problem could be solved in polynomial time on a quantum computer.

Saying that an algorithm solves a problem in polynomial time means that the algorithm succeeds in polynomial time on every possible input. On the other hand, an algorithm may succeed in polynomial time on a large set of inputs but not on all. This has led to efforts to identify sets of instances that are hard for particular classical algorithms. Recently, the quantum adiabatic algorithm[4] has been applied to a specific **NPC** problems, 3-bit Exact Cover [13] and 3-SAT (Three-Satisfiability) [14] and for the randomly generated instances of Exact Cover, it was found that the quantum algorithm succeeds in a time that seems to grow only quadratically in the length of the input.

[4]We will discuss extensively later on quantum adiabatic algorithm

1.5 The Physical Realization of Quantum Computers

In the last years we observed a rapid progress in the theory of quantum computing. Moreover, various physical realizations of quantum computations are intensively studied. According to the DiVincenzo criteria [15] a physical system suitable for quantum computing should satisfy the followings:

- First of all, a *scalable* physical system containing a collection of *well characterized qubits* is needed. A well characterized qubit means that its physical parameters should be accurately known, including the internal Hamiltonian, the presence of and coupling to other states of the qubit, the interactions with other qubits, and the couplings to external fields that might be used to manipulate the state of the qubit. If the qubit has higher levels (third, fourth, etc.), the computer's control apparatus should be designed so that the probability of the system ever going into these states is small.

- The second requirement is the *possibility to initialize the state of the qubit*. This arises from the elementary computing requirement that registers should be initialized to a known value before the start of computation. There are two main approaches to setting qubits to a standard state: the system can either be naturally cooled when the ground state of its Hamiltonian is the state of interest, or the standard state can be achieved by a measurement which projects the system either directly into the state desired or another state which can be rotated into it. These approaches are not fundamentally different from one another, since the projection procedure is a form of cooling, for instance, the laser cooling techniques used routinely now for the cooling ion state to near their ground state in a trap [16] are closely connected to the fluorescence techniques used to measure the state of these ions.

- The Physical system needs to have *long decoherence time compared with the gate operation time*. Decoherence is a subtler effect, in which the energy may be conserved but the relative phase of the different basis states of the qubit is changed. As a result of decoherence the qubit changes as follows

$$|\phi\rangle \rightarrow c_0 |0\rangle + e^{i\theta} c_1 |1\rangle \ , \tag{1.28}$$

  where the real number θ denotes the relative phase. The appearance of the non-zero relative phase results from the coupling of the quantum system with the environment and can lead to essential changes in the measurement statistics. For example, the quantum-mechanical expectation value of the measured quantity is changed. The decoherence time $T_{\rm de}$ is usually much shorter than the decay time, therefore, the decoherence can be treated

as the most detrimental effect for the quantum computations. The ratio of the decoherence time $T_{\rm de}$ to the gate operation time $T_{\rm op}$, i.e.,

$$R = \frac{T_{\rm de}}{T_{\rm op}}\,, \tag{1.29}$$

is an approximate measure of the number of computation steps performed before the coupling with the environment destroys the qubit.[5]

- It must provide a *universal set of gates*.[6] This requirement is of course at the heart of quantum computing. A quantum algorithm is typically specified as a sequence of unitary transformations $\mathcal{U}_1, \mathcal{U}_2, \mathcal{U}_3, \cdots$, each operating on a small number of qubits. The most common quantum gates operate on spaces of one or two qubits. The transcription of this into physical specification can be identified by Hamiltonians which generate these unitary transformations

$$\mathcal{U}_1 = e^{iH_1 t/\hbar}\,, \quad \mathcal{U}_2 = e^{iH_2 t/\hbar}\,, \quad \mathcal{U}_3 = e^{iH_3 t/\hbar}, \cdots\,. \tag{1.30}$$

  Then the physical apparatus should be designed so that H_1 can be turned on from time 0 to time t_1, then turned off and H_2 turned on from time t_1 to time t_2, etc.

- It should have *read-out* or *qubit measurement capability*. Finally, the result of a computation must be read out, and this requires the ability to measure specific qubits.

Besides theses rules there are two other necessary requirements for quantum teleportation[7] as well:

- *The ability to convert stationary and flying qubits*.[8] In a quantum computer, no qubit is an island. Memory qubits must converse with one another and with logic, control, input and output units. One possible way to achieve this goal is based on converting a *material qubit* to a *flying qubit* or photon.

[5] For example, assume that a gate operation takes some time, lets say 10 ns. If the decoherence time is, e.g., 1 μs, this means that in theory 100 gate operations can be performed before the system collapses.

[6] A set of universal quantum gates is any set of gates to which any operation possible on a quantum computer can be reduced. One simple set of two-qubit universal quantum gates is the Hadamard gate, a phase rotation gate, and the CNOT gate.

[7] In quantum teleportation, an unknown quantum state is faithfully transferred from a sender (Alice) to a receiver (Bob). To perform the teleportation, Alice and Bob must have a *classical communication channel* and must also share *quantum entanglement*. Alice makes an appropriate projective measurement of the unknown state together with her component of the shared entangled state. The result of this measurement is a random piece of classical information which Alice sends to Bob over their classical communication channel. Bob uses this information to choose a unitary transformation which he performs on his component of the shared entangled state, thus transforming it into an output state identical to the original (unknown) input [17].

[8] Flying qubits are typically photons that can transmit quantum information from one location to another, as opposed to stationary qubits – typically made of matter – that hold quantum memory.

- *The ability to faithfully transmit flying qubits* between specified locations.

These seven rules form the necessary and sufficient conditions for a physical realization of quantum information processing.

1.6 Quantum Simulators

As a matter of fact, Feynman's initial motivation for constructing a quantum computer was the efficient simulation of quantum dynamics. As an example, Feynman proposed a *universal quantum simulator* consisting of a lattice of spins with nearest neighbor interactions that are freely specifiable and can efficiently reproduce the dynamics of *any* other many-particle quantum system with a finite-dimensional state space [1, 2]. Thus, a universal quantum simulator is a controlled device that, operating itself at the quantum level, efficiently reproduces the dynamics of any other many-particle quantum system that evolves according to short range interactions, see also [18]. Here, the assumption of some degree of locality in the interactions, implying that the multi-particle Hamiltonian $H_N = \sum_j H_j$ is a sum of terms H_j each one involving only a few neighboring systems, is important to achieve an efficient simulation. In most cases of interest this requirement happens to be fulfilled. Consequently, a universal quantum simulator could be used to efficiently simulate the dynamics of a generic many-body quantum system and in this way function as a fundamental tool for research in quantum physics.
On the other hand, one of the main present motivation for building a quantum computer comes from the expected exponential gain in efficiency of certain quantum algorithms with respect to their classical counterparts. Shor's efficient factorization of large numbers is so far the most celebrated milestone of quantum computation [4]. However, for quantum computers to overcome classical ones in tasks such as factorization, they would have to coherently operate tens of thousands of two-level systems or qubits. This extraordinary enterprise requires technology that may only be at reach in several decades from now.
Because such universal quantum computers of sufficient size are not available yet, it appears as a more feasible task to design a special quantum system in the laboratory which simulates the quantum dynamics of a particular model of interest. Such a designed quantum system can be thought of as a special type of quantum computer optimized to investigate specific, complex physical problems that classical computation methods do not efficiently solve, thus developing a quantum simulator would be a major step towards a practical quantum computer.

1.7 Adiabatic Quantum Computing

Unfortunately, the actual realization of usual sequential quantum algorithms (where a sequence of quantum gates is applied to some initial quantum state, see, e.g., [19]) goes along with the

problem that errors accumulate over many operations and the resulting decoherence tends to destroy the fragile quantum features needed for the computation. Therefore, adiabatic quantum algorithms have been suggested [7], where the solution to a problem is encoded in the (unknown) ground state of a (known) Hamiltonian. Since there is evidence that, in adiabatic quantum computing the ground state is more robust against decoherence[9] [8, 9, 10], this scheme offers fundamental advantages compared to sequential quantum algorithms.
Suppose we have to solve a problem that may be reformulated as preparing a quantum system in the ground state of a Hamiltonian H_{f} . The adiabatic theorem [20] then provides a straightforward method to solve this problem:

- Prepare the quantum system in the (known and easy-to-prepare) ground state of another Hamiltonian H_0.

- Apply H_0 on the system and slowly modify it to H_{f}.

The adiabatic theorem ensures that if this has been done slowly enough, the system will end up in a state close to the ground state of H_{f}. Therefore, a measurement of the final state will yield a solution of the problem with high probability.
Furthermore, adiabatic quantum algorithms display a remarkable similarity with sweeps through quantum phase transitions [21, 22]. During the adiabatic interpolation, the ground state changes from the simple initial ground state of H_0 to the unknown solution of some problem encoded in H_{f}. Typically, on the way from H_0 to H_{f}, one encounters a critical point where the fundamental gap (which is sufficiently large initially and finally) becomes very small. Near the position of this minimum gap, the ground state will change more drastically than in other time intervals of the interpolation and therefore bears strong similarities to a quantum phase transition.

1.8 Overview of This Thesis

This Thesis is organized as follows: The first sections of the second chapter are devoted to a brief introduction into the adiabatic theorem together with a discussion of adiabatic quantum computation. Most investigations dedicated to the conditions for adiabatic quantum computing are based on the first-order correction. However, it is demonstrated that this first-order correction does not yield a good estimate for the computational error. After having established the basic principles of adiabatic quantum algorithms, we derive a more general criterion which includes higher-order corrections as well and shows that the computational error can be made exponentially small. Based on the similarity between adiabatic quantum algorithms and quantum phase transitions, it seems that adiabatic quantum algorithms corresponding to second-order

[9] The ground state cannot decay and phase errors do not play any role, i.e., errors can only result from excitations – a sufficiently cold reservoir provided.

quantum phase transitions should be advantageous compared to isolated avoided level crossings – which are analogous to first-order transitions. The impact of decoherence on the sweep through a second-order quantum phase transition for the prototypical example of the Ising chain in a transverse field is studied in the third chapter after a brief introduction into quantum phase transition. We discuss quantum simulators in the forth chapter of this Thesis. Quantum simulators for the examples of the $O(3)$ nonlinear sigma model and quantum Ising model with electron systems are proposed. We demonstrate that these quantum simulators can be constructed using present-day technology.

2 Adiabatic Quantum Computation

2.1 The Adiabatic Theorem

The adiabatic approximation is a standard method of Quantum Mechanics used to derive approximate solutions of the Schrödinger equation in the case of a slowly varying Hamiltonian. Its basic principle is quite simple:

> *If a quantum system is prepared in its ground state and its Hamiltonian varies slowly enough, it will stay in a state close to the instantaneous ground state of this Hamiltonian as time goes on.*[1]

The Hamiltonian of a physical system gives a complete specification of the time evolution of this system. At a given time t, let $|\Psi(t)\rangle$ denote the state of the system under the influence of the Hamiltonian $H(t)$. The differential equation that describes the time evolution is the well-known Schrödinger equation

$$i\frac{d}{dt}|\Psi(t)\rangle = H(t)\,|\Psi(t)\rangle \tag{2.1}$$

with the initial condition that $|\Psi(0)\rangle$ is the ground state of $H(0)$. First of all, we need to define the instantaneous eigenstates $|n(t)\rangle$ of the Hamiltonian $H(t)$

$$H(t)\,|n(t)\rangle = E_n(t)\,|n(t)\rangle\ , \tag{2.2}$$

where $E_n(t)$ are the corresponding eigenenergies and the set of eigenvectors $|n(t)\rangle$ chosen to be orthonormal. To solve the Schrödinger equation, we expand its solution $|\Psi(t)\rangle$ in the basis formed by the eigenstates $|n(t)\rangle$

$$|\Psi(t)\rangle = \sum_n a_n(t)\exp\left\{-i\int_0^t E_n(t')dt'\right\}|n(t)\rangle\ . \tag{2.3}$$

[1] A rigorous proof of the adiabatic theorem can be found in [20]

Inserting this expansion into the Schrödinger equation (2.38) and projecting onto $\langle m(t)|$, we get the following evolution equations for the coefficients

$$\dot{a}_m = -\sum_n a_n \, \langle m|\dot{n}\rangle \exp\left\{-i\int_0^t \Delta E_{nm}(t')dt'\right\} \tag{2.4}$$

with the energy gap $\Delta E_{nm}(t) = E_n(t) - E_m(t)$. A useful expression to evaluate the matrix elements $\langle m|\dot{n}\rangle$, for $m \neq n$, can be found by taking a time derivative of (2.2) and multiplying the resulting expression by $\langle m(t)|$, which reads

$$\langle m|\dot{n}\rangle = \frac{\langle m|\,\dot{H}\,|n\rangle}{\Delta E_{nm}(t)} \qquad \forall\, m \neq n \tag{2.5}$$

and therefore (2.4) can be written as

$$\dot{a}_m = -a_m \langle m|\dot{m}\rangle - \sum_{n\neq m} a_n \frac{\langle m|\,\dot{H}\,|n\rangle}{\Delta E_{nm}(t)} \exp\left\{-i\int_0^t \Delta E_{nm}(t')dt'\right\}\,, \tag{2.6}$$

With some algebra, this equation can be rewritten as follows

$$\frac{\partial}{\partial t}\left(a_m e^{-i\vartheta_m}\right) = -\sum_{n\neq m} a_n \, \frac{\langle m|\,\dot{H}\,|n\rangle}{\Delta E_{nm}} \, e^{-i\vartheta_m} \exp\left\{-i\int_0^t \Delta E_{nm}(t')dt'\right\} \tag{2.7}$$

with the Berry phase [23]

$$\vartheta_n(t) = i\int_0^t dt' \, \langle n(t')|\dot{n}(t')\rangle\,. \tag{2.8}$$

The integration of Eq. (2.7) yields

$$a_m(s)e^{-i\vartheta_m}(s) = a_m(0) - \sum_{n\neq m}\int_0^s ds'\Delta E_{nm}(s')A_{mn}(s')\exp\left\{-iT\int_0^{s'}\Delta E_{nm}(s'')ds''\right\}\,, \tag{2.9}$$

where T is the total evolution time and $s = t/T$ with $s \in [0,1]$. The elements A_{mn} are defined as

$$A_{mn}(s) = \, a_n(s)\frac{\langle m(s)|\,\dot{H}\,|n(s)\rangle}{\Delta E_{nm}^2(s)}\, e^{-i\vartheta_m(s)}\,. \tag{2.10}$$

The integral on the right-hand side of Eq. (2.9) can be evaluated by subsequently using

$$\exp\left\{-iT\int_0^s \Delta E_{nm}(s')ds'\right\} = \frac{i}{T\,\Delta E_{nm}}\frac{d}{ds}\exp\left\{-iT\int_0^s \Delta E_{nm}(s')ds'\right\} \tag{2.11}$$

and performing an integration by parts results in

$$a_m(s)e^{-i\vartheta_m}(s) = a_m(0) + \frac{i}{T}\sum_{n\neq m} A_{mn}(0) - \frac{i}{T}\sum_{n\neq m} A_{mn}(s)\exp\left\{-iT\int_0^s \Delta E_{nm}(s')ds'\right\} + \frac{i}{T}\sum_{n\neq m}\int_0^s ds'\left[\frac{d}{ds'}A_{mn}(s')\right]\exp\left\{-iT\int_0^{s'}\Delta E_{nm}(s'')ds''\right\} . \quad (2.12)$$

A condition for the adiabatic regime can be obtained from Eq. (2.12) if the last integral vanishes for large evolution time T. Let us assume that, as $T\to\infty$, the energy difference ΔE_{nm} remains nonvanishing. We further assume that $dA_{mn}(s')/ds'$ is integrable on the interval $[0,1]$. Then it follows from the Riemann-Lebesgue lemma [24] that the last integral in Eq. (2.12) vanishes in the limit $T\to\infty$ (due to the fast oscillation of the integrand). Thus, a general estimate of the time rate at which the adiabatic regime is approached can be expressed by

$$T \gg \frac{\mathcal{E}}{(\Delta E)^2}\,, \quad (2.13)$$

with

$$\mathcal{E} = \max_{s\in[0,1]}\left|\langle m(s)|\,\frac{dH(s)}{ds}\,|n(s)\rangle\right| , \quad (2.14)$$

and

$$\Delta E = \min_{s\in[0,1]}\Delta E_{nm}(s) = \min_{s\in[0,1]}\left[E_n(s) - E_m(s)\right] . \quad (2.15)$$

2.2 Adiabatic Quantum Algorithm

The adiabatic quantum algorithm works by applying a time-dependent Hamiltonian that interpolates smoothly from an initial Hamiltonian H_0 to a final Hamiltonian $H_{\rm f}$. As an example, one can consider the linear interpolation path between these two Hamiltonians

$$H(s) = [1-s(t)]H_0 + s(t)H_{\rm f}\,, \quad (2.16)$$

with $s(0)=0$ and $s(T)=1$, where T is the total evolution time or the *run-time* of the algorithm. Thus, this Hamiltonian interpolates between H_0 and $H_{\rm f}$ as s varies from 0 to 1. We prepare the ground state of H_0 at time $t=0$, and then the state evolves from $t=0$ to T according to the Schrödinger equation. At time T, we measure the state. According to the adiabatic theorem, if there is a nonzero gap between the ground state and the first excited state of $H(s)$ for all $s\in[0,1]$ then the success probability[2] of the algorithm approaches 1 in the limit $T\to\infty$. How

[2] If $|\Phi\rangle$ denotes the ground state of $H_{\rm f}$ for a given instance of the problem, then the success probability of the algorithm for this instance is given by $|\langle\Phi|\Psi(T)\rangle|^2$.

large a T is large enough is given by the condition expressed in Eq. (2.13)

$$T \gg \frac{\mathcal{E}}{(\Delta E)^2}\,, \tag{2.17}$$

with

$$\mathcal{E} = \max_{s\in[0,1]} \left| \langle 1, s| \frac{dH(s)}{ds} |0, s\rangle \right| , \tag{2.18}$$

and

$$\Delta E = \min_{s\in[0,1]} \left[E_1(s) - E_0(s)\right] , \tag{2.19}$$

where $E_0(s)$ is the lowest eigenvalue of $H(s)$, $E_1(s)$ is the second-lowest eigenvalue, and $|0, s\rangle$ and $|1, s\rangle$ are the corresponding eigenstates, respectively. Hence, the required run time T will be bounded by a polynomial in the number of qubits so long as Δ and $\mathcal{E}$ are polynomially bounded.

2.3 Examples

2.3.1 Adiabatic Quantum Search Algorithm

One can apply this adiabatic-evolution method to the problem of finding an item in an unsorted database, discussed in Sec. (1.3) of this Thesis. Consider a set of N items among which one is marked, the goal being to find it in minimum time. We use n qubits to label the items, so that the Hilbert space is of dimension $N = 2^n$. In this space, the basis states are written as $|x\rangle$, with $x = 0, \cdots, N-1$, while the marked state is denoted by $|w\rangle$. At time $t = 0$, the quantum mechanical system is described by the Hamiltonian

$$H_0 = \mathbf{1} - |\mathrm{in}\rangle \langle \mathrm{in}| \,, \tag{2.20}$$

whose ground state is an equal superposition of all basis states

$$|\mathrm{in}\rangle = \frac{1}{\sqrt{N}} \sum_{x=0}^{N-1} |x\rangle \tag{2.21}$$

with energy zero. Next, this system is slowly transformed to its final Hamiltonian

$$H_\mathrm{f} = \mathbf{1} - |w\rangle \langle w| \,, \tag{2.22}$$

whose ground state is the marked state $|w\rangle$ (unknown). The fact that H_f can be applied without explicitly knowing w is equivalent to the assumption, in the standard description of Grover's

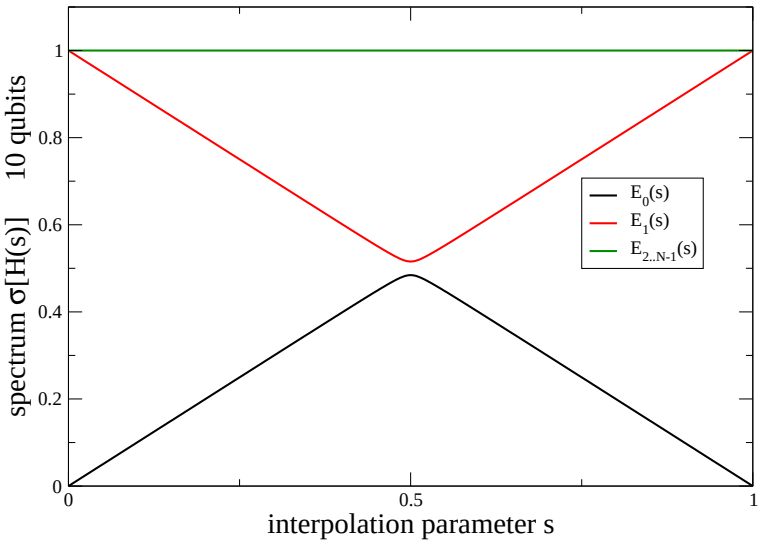

Figure 2.1: Energy spectrum of the time-dependent Hamiltonian $\widetilde{H}(s)$ given in Eq. (2.23) as a function of interpolation parameter $s = t/T$.

algorithm (see, Sec. (1.3) of this Thesis), that a quantum oracle is available. One can write the time-dependent Hamiltonian as a linear interpolation between these two Hamiltonians

$$H(t) = (1 - t/T)H_0 + t/T H_{\rm f}\,. \tag{2.23}$$

The algorithm consists in preparing the system in the state $|{\rm in}\rangle$ and then applying the Hamiltonian $H(t)$ during a time T. Now the Hamiltonian $H(t)$ is well defined and the eigenproblem $H(t)\,|n(t)\rangle = E_n(t)\,|n(t)\rangle$ in Eq. (2.2) can be solved to find the eigenvalues and eigenstates, and then to evaluate the matrix element in Eq. (2.18) and the gap in Eq. (2.19). It is easy to see that the two lowest eigenvalues E_0 and E_1 are separated by a time-dependent gap [25]

$$\Delta E_{10} = \sqrt{1 - 4\left(1 - \frac{1}{N}\right) s(1-s)} \tag{2.24}$$

with $s = t/T$. Then, the minimum gap in Eq. (2.19) $\Delta E = 1/\sqrt{N}$ is attained for $s = 1/2$. The matrix element in Eq. (2.18) can be rewritten by using the variable transformation $t = sT$

$$\langle 1, s|\,\frac{dH(t)}{dt}\,|0, s\rangle = \frac{ds}{dt}\,\langle 1, s|\,\frac{d\widetilde{H}(s)}{ds}\,|0, s\rangle = \frac{1}{T}\,\langle 1, s|\,\frac{d\widetilde{H}(s)}{ds}\,|0, s\rangle \tag{2.25}$$

with $\widetilde{H}(s) = (1-s)H_0 + sH_{\rm f}$ and $d\widetilde{H}(s)/ds = H_{\rm f} - H_0$. The eigenvalues of $\widetilde{H}(s)$ are plotted as a function of s in Fig. (2.1). Therefore, knowing that

$$\left|\langle 1, s|\,\frac{d\widetilde{H}(s)}{ds}\,|0, s\rangle\right| \leq 1\,, \tag{2.26}$$

provides the adiabatic condition in Eq. (2.17) for the problem

$$T \geq \frac{N}{\epsilon}\,, \tag{2.27}$$

where $\epsilon \ll 1$. Therefore, the computation time is of order N, and there is no advantage of this method compared to a classical search.

Applying Eq. (2.17) globally, i.e., to the entire time interval T, imposes a limit on the evolution rate during the whole computation while this limit is only severe around $s = 1/2$, where the gap ΔE_{10} is minimum. Thus, by dividing T into infinitesimal time intervals dt and applying the adiabaticity condition locally to each of these intervals, one can vary the evolution rate continuously in time, thereby speeding up the computation. In other words, instead of using the linear evolution function $s(t) = t/T$, one can adapt the evolution rate ds/dt to the local adiabaticity condition. The new condition is obtained by applying Eq. (2.17) to each infinitesimal time interval [25]

$$\epsilon\,\Delta E_{10}^2 \geq \left|\frac{ds}{dt}\right| \left|\langle 1,s|\,\frac{d\widetilde{H}(s)}{ds}\,|0,s\rangle\right|\,, \tag{2.28}$$

for all times t. Insertion of Eqs. (2.24), (2.26) into the Eq. (2.28) yields

$$\frac{ds}{dt} = \epsilon\,\Delta E_{10}^2 = \epsilon\left[1 - 4\left(1 - \frac{1}{N}\right)s(1-s)\right]\,. \tag{2.29}$$

After integration, we have

$$t = \frac{N}{2\epsilon(N-1)^{1/2}}\left\{\arctan\left[\sqrt{N-1}(2s-1)\right] + \arctan\sqrt{N-1}\right\}\,. \tag{2.30}$$

We may now evaluate the computation time of the new algorithm by taking $s = 1$, which gives

$$T = \frac{N}{\epsilon(N-1)^{1/2}}\arctan\sqrt{N-1}\,. \tag{2.31}$$

For large N, we get

$$T \approx \frac{\pi}{2\epsilon}\sqrt{N} \qquad (N \gg 1)\,. \tag{2.32}$$

Thus, one obtains a quadratic speed-up with respect to a classical search, so that this algorithm can be viewed as the adiabatic-evolution version of Grover's algorithm.[3]

[3] See also section (1.3) of this Thesis.

2.3.2 The Exact Cover Problem

The second example for the application of adiabatic quantum algorithms is the NP-complete problem *three-bit Exact Cover* [13]. Consider n bits $v_1, v_2, \cdots, v_n$ each of which can take the value 0 or 1. An n-bit instance of Exact Cover is a list of triples (v_i, v_j, v_k) indicating which groups of three bits are involved in clauses. The constraint is that one of the three bits must have the value 1 and the other two must have the value 0. The problem is to determine whether there is some assignment of the n-bit values that satisfies all of the clauses. Given an assignment of values for $v_1, v_2, \cdots, v_n$, we can easily check whether the assignment satisfies all of the clauses. But determining whether at least one of the 2^n assignments of $v_1, v_2, \cdots, v_n$ satisfies all the clauses is in fact an NP-complete problem.
Let $f(v)$ be a function of n bits $(v_1, v_2, \cdots, v_n)$, and consider the computational problem of finding a value of v that minimizes $f(v)$ and we will typically be interested in the case where this value of v is unique. Defining this function as a sum of three-bit clauses

$$f(v) = \sum_C f_C(v_{i_C}, v_{j_C}, v_{k_C}) \tag{2.33}$$

with

$$f_C(v_{i_C}, v_{j_C}, v_{k_C}) = \begin{cases} 0, & (v_{i_C}, v_{j_C}, v_{k_C}) \quad \text{satisfies clause } C\,, \\ 1, & (v_{i_C}, v_{j_C}, v_{k_C}) \quad \text{violates clause } C\,, \end{cases} \tag{2.34}$$

the final Hamiltonian of the adiabatic quantum algorithm may be written as follows

$$H_{\mathrm{f}} = \sum_{\boldsymbol{v}\in\{0,1\}^n} f(v)\,|\boldsymbol{v}\rangle\,\langle\boldsymbol{v}| \tag{2.35}$$

with $\boldsymbol{v} = (v_n, \cdots, v_1) \in \{0,1\}^n$. The computational basis state $|\boldsymbol{v}\rangle$ is an eigenstate of H_{f} with eigenvalue $f(v)$. Then the problem is to determine which state $|\boldsymbol{v}\rangle$ is the ground state (eigenstate with lowest eigenvalue) of H_{f}. To solve the Exact Cover problem by the adiabatic algorithm, one choice [8] for the initial Hamiltonian is

$$H_0 = \frac{1}{2}\sum_C \left\{ \left(1 - \sigma_x^{(i_C)}\right) + \left(1 - \sigma_x^{(j_C)}\right) + \left(1 - \sigma_x^{(k_C)}\right) \right\}\,, \tag{2.36}$$

where σ_x is the Pauli operator. The ground state of the i-th qubit corresponding to spin aligned in the x-direction is $|{\rightarrow}\rangle_i = \left(\,|0\rangle_i + |1\rangle_i\,\right)/\sqrt{2}$. The ground state of H_0 for the n-qubit quantum system is therefore

$$|\Psi(0)\rangle = \frac{1}{2^{n/2}} \sum_{\boldsymbol{v}\in\{0,1\}^n} |\boldsymbol{v}\rangle\ . \tag{2.37}$$

The resulting $H(t) = [1-s(t)]H_0 + s(t)H_{\mathrm{f}}$ is local in the sense that it is a sum of terms, each of which acts on only a few qubits. A stronger kind of locality may be imposed by restricting the

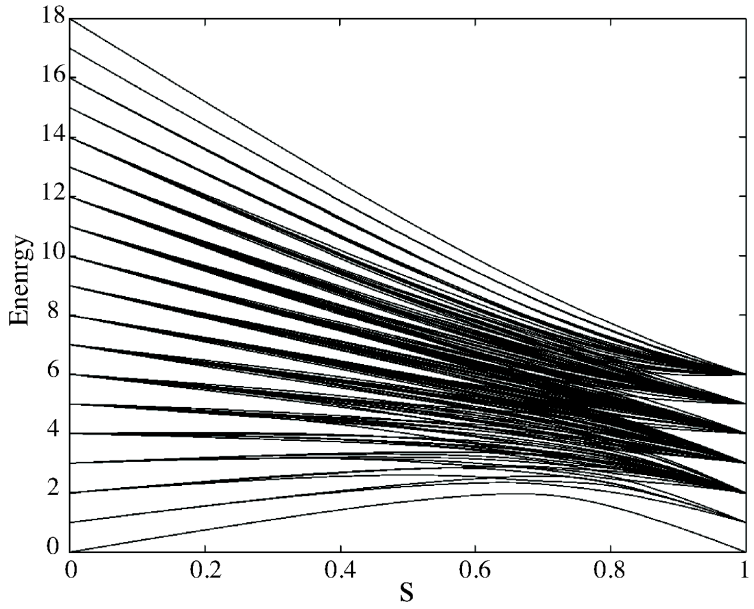

Figure 2.2: Spectrum of a randomly generated $n = 7$ bit instance of three-bit Exact Cover with a unique satisfying assignment. The energy gap between the ground state and the first excited state is significantly larger than all other gaps. This figure has been taken from [8].

instances so that each bit is involved in at most a fixed number of clauses. The computational complexity of the problem is unchanged by this restriction. Numerical studies of the adiabatic algorithm applied to this problem were reported in [13, 26]. Instances of Exact Cover with n bits were generated by adding random clauses until there was a unique satisfying assignment, giving a distribution of instances that one might expect to be computationally difficult to solve. The results for a small number of bits ($n \leq 20$) were consistent with the possibility that the *adiabatic algorithm* requires a time that grows only as a *polynomial* in n for typical instances drawn from this distribution. For example, Fig. (2.2) shows the spectrum of a randomly generated seven-bit instance of three-bit Exact Cover. Although the typical spacing between levels must be exponentially small, since there are an exponential number of levels in a polynomial range of energies, it is possible that the gap at the bottom is larger, see, e.g., [8].

2.4 General Error Estimate for Adiabatic Quantum Computing

Determining the achievable speed-up of adiabatic quantum algorithms (compared to classical methods) for many problems is still a matter of investigation and debate, see, e.g., [25, 26],

[27]-[31]. For example, it has been argued in [29] that all conventional (sequential) quantum algorithms can be realized as adiabatic quantum computation schemes with polynomial overhead via the history interpolation (polynomial equivalence). The rest of the second chapter of this Thesis based on publication[4] [32] and we derive a general error estimate as a function of the run-time T (the main measure for the computational complexity of adiabatic quantum algorithms) for very general gap structures $\Delta E(s)$ and interpolation velocities $s(t)$.

2.4.1 Analytic Continuation of the Adiabatic Expansion

The evolution of a system state $|\Psi(t)\rangle$ subject to a time-dependent Hamiltonian $H(t)$ is described by the Schrödinger equation

$$i\left|\dot{\Psi}(t)\right\rangle = H(t)\,|\Psi(t)\rangle\ . \tag{2.38}$$

Using the instantaneous energy eigenbasis defined by $H(t)\,|n(t)\rangle = E_n(t)\,|n(t)\rangle$, the system state $|\Psi(t)\rangle$ can be expanded to yield

$$|\Psi(t)\rangle = \sum_n a_n(t)\exp\left\{-i\int_0^t E_n(t')dt'\right\}|n(t)\rangle\ . \tag{2.39}$$

Insertion into the Schrödinger equation yields – after some algebra (see, the first parts of this chapter) – the evolution equations for the coefficients

$$\frac{\partial}{\partial t}\left(a_m e^{-i\vartheta_m}\right) = -\sum_{n\neq m} a_n\,\frac{\langle m|\,\dot{H}\,|n\rangle}{\Delta E_{nm}(t)}\,e^{-i\vartheta_m}\exp\left\{-i\int_0^t \Delta E_{nm}(t')dt'\right\}\ , \tag{2.40}$$

where $\Delta E_{nm}(t) = E_n(t) - E_m(t)$ and ϑ_m is the Berry phase given in Eq. (2.8). If the external time-dependence $\dot{H}$ is slow (adiabatic evolution), the right-hand side of Eq. (2.40) is small and the solution can be obtained perturbatively. After an integration by parts, the first-order contribution yields

$$a_m(t) \;\approx\; a_m^0 e^{i\vartheta_m(t)} - i\left[\sum_{n\neq m} a_n^0\,\frac{\langle m|\,\dot{H}\,|n\rangle}{\Delta E_{nm}^2}\,e^{i\varphi_{nm}}\right]_0^t\ , \tag{2.41}$$

where $\varphi_{nm}\in\mathbb{R}$ denotes a pure phase. Consequently, if the local adiabatic condition

$$\frac{\langle m|\,\dot{H}\,|n\rangle}{\Delta E_{nm}^2} = \epsilon \ll 1\,, \tag{2.42}$$

[4] G. Schaller, S. Mostame, and R. Schützhold, *General error estimate for adiabatic quantum computing*, Phys. Rev. A **73**, 062307 (2006).

is fulfilled for all times, the system approximately stays in its instantaneous eigen (e.g., ground) state throughout the (adiabatic) evolution. This above constraint has frequently been used as a condition for adiabatic quantum computation [7, 26]. However, since the solution to a problem is encoded in the ground state of the final Hamiltonian in adiabatic quantum computation schemes, it is not really necessary to be in the instantaneous ground state *during* the dynamics – the essential point is to obtain the desired ground state *after* the evolution. Since the external time-dependence $\dot{H}$ could realistically be extremely small (or even practically vanish) at the end of the computation $t = T$, the first-order result Eq. (2.41) does not always provide a good error estimate. Similar to the theory of quantum fields in curved space-times [33], the difference between the adiabatic and the instantaneous vacuum should not be confused with real excitations (particle creation). Therefore, it is necessary to go beyond the first-order result above and to estimate the higher-order contributions.

Evidently, the Schrödinger equation is covariant under simultaneous transformations of time and energy, such that the runtime of an adiabatic algorithm can be reduced to constant if the energy of the system is modified accordingly [31]. Here, we want to exclude a mixing of these effects and will therefore assume

$$\mathrm{tr}\{H[s(t)]\} = \mathrm{const.} \qquad \forall\, s \in [0,1]\,, \tag{2.43}$$

where $0 \leq s(t) \leq 1$ is an interpolation function which will be specified below. In practice, the above condition can even be relaxed to the demand that the trace should not vary by orders of magnitude (during $0 \leq s \leq 1$). With suitable initial and final Hamiltonians H_0 and H_f, the above condition can be satisfied for all s by using the linear interpolation scheme

$$H(t) = [1 - s(t)]\, H_0 + s(t) H_\mathrm{f}\,. \tag{2.44}$$

For simplicity, we restrict our considerations in this section to an instantaneous non-degenerate ground state $n = 0$ and one single first exited state $m = 1$ with $\Delta E = \Delta E_{10}$. Similarly, all energies will be normalized in units of a typical energy scale corresponding to the initial/final gap, i.e., $\Delta E(s = 0) = \mathcal{O}(1)$ and $\Delta E(s = 1) = \mathcal{O}(1)$. We classify the dynamics of $s(t)$ via a function $h(s) \geq 0$

$$\frac{ds}{dt} = \Delta E(s) h(s)\,, \tag{2.45}$$

where the function $h(s) \geq 0$ is constrained by the conditions $s(0) = 0$ and $s(T) = 1$. Insertion of this ansatz into Eq. (2.40) yields the exact formal expression for the non-adiabatic corrections to a system starting in the ground state, i. e., with $a_1(0) = 0$ one obtains after time T

$$a_1(1) e^{-i\vartheta_1(1)} = -\int_0^1 ds\; a_0(s) e^{-i\vartheta_1(s)}\, \frac{F_{01}(s)}{\Delta E(s)} \exp\left\{ -i \int_0^s \frac{ds'}{h(s')} \right\} \tag{2.46}$$

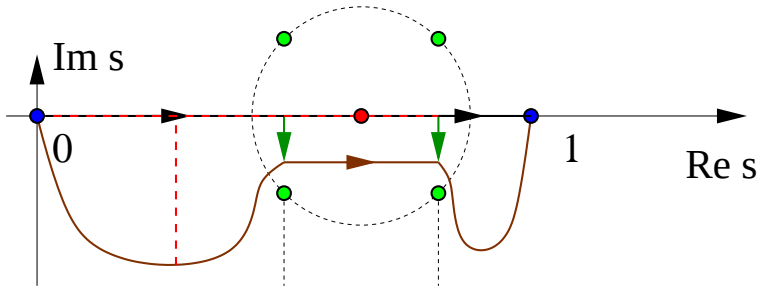

Figure 2.3: The original integration contour (black line along real axis) of Eq. (2.46) is shifted to the complex plane (curved line). The gap structure $\Delta E(s)$ leads to singularities near the real axis – green hollow circles, here displayed for $2a = 4$ in Eq. (2.55) – which limit the deformation of the integration contour. The integral in the exponent (dashed line) in Eq. (2.46) ranges from 0 to s', which gives rise to a real contribution to the exponent off the real axis only.

with the matrix elements $F_{nm}(s) = \langle m(s)| H'(s) |n(s)\rangle$ which simplify in the case (2.44) of linear interpolation to $F_{nm}(s) = \langle m(s)| H_\mathrm{f} - H_0 |n(s)\rangle$. The advantage of the form in Eqs. (2.45) and (2.46) lies in the fact that different time-dependences $s(t)$ and hence different choices for $h(s)$ solely modify the exponent.

We assume that all involved functions can be analytically continued into the complex s-plane and are well-behaved near the real s-axis. Given this assumption, we may estimate the integral in Eq. (2.46) via deforming[5] the integration contour into the lower complex half-plane (to obtain a negative exponent – which is the usual procedure in such estimates) until we hit a saddle point, a singularity, or a branch cut, see Fig. (2.3). Since the gap $\Delta E(s)$ usually has a pronounced minimum at $s_\mathrm{min} \in (0, 1)$, the first obstacle we encounter[6] will be a singularity at $\tilde{s}$ close to the real axis, i.e.,

$$|\Im(\tilde{s})| \ll 1 \quad \text{and} \quad \Re(\tilde{s}) \approx s_\mathrm{min}\,, \tag{2.47}$$

where $\Delta E(\tilde{s}) = 0$. Let us first consider a constant function $h(s) = h$: Assuming $h \ll 1$ (i.e., slow evolution), the exponent in Eq. (2.46) acquires a large negative real part for $\Im(s) < 0$ and thus, the absolute value of the integrand decays rapidly if we depart from the real s-axis in the lower complex half-plane. Imposing the even stronger constraint $h \ll |\Im(\tilde{s})| \ll 1$, the decay

[5] Deforming the integration contour into the upper complex half-plane would of course not change the result, but there the integrand is exponentially large and strongly oscillating such that the integral is hard to estimate.

[6] Since the functions $\vartheta_1(s)$, $F_{01}(s)$, and $\Delta E(s)$ are supposed to be well-behaved near the real s-axis, there are no small (or large) numbers in the problem apart from those generated by the minimum of the gap $\Delta E(s)$. Thus the significant changes of the eigenvectors are also localized around this minimum. In the complex plane, this minimum along the real axis becomes a saddle point. For analytic functions, the characteristic length scale of variation must be the same along the real axis and into the complex plane (of order $|\Im(\tilde{s})| \ll 1$) and is determined by the lowest non-trivial Taylor coefficient at that point.

of the exponent dominates all the other s-dependences [$\vartheta_1(s)$, $F_{01}(s)$, and $\Delta E(s)$] since their typical scale of variation is $|\Im(\tilde{s})| \ll 1$. In view of the complex continuation of Eq. (2.40), the same applies to the amplitude $a_0(s)$. As a result, the above integral (2.46) will be exponentially suppressed

$$\sim \exp\left\{-\mathcal{O}\left(\frac{|\Im(\tilde{s})|}{h}\right)\right\}, \tag{2.48}$$

if $h \ll |\Im(\tilde{s})| \ll 1$ holds, which (as one would expect) implies a large evolution time T via the side condition $s(T) = 1$.

The general situation with varying $h(s)$ can be treated in complete analogy – the integral in Eq. (2.46) is suppressed provided that the condition

$$1 \ll \Re\left(i \int_0^{\Re(\tilde{s})+i\Im(\tilde{s})/2} \frac{ds}{h(s)}\right) \quad \wedge \quad h(0) + h(1) \ll 1\,, \tag{2.49}$$

holds for all singularities $\tilde{s}$ (and saddle points etc.) in the lower complex half-plane (which limit the deformation of the integration contour). Together with

$$T = \int_0^1 \frac{ds}{\Delta E(s) h(s)}\,, \tag{2.50}$$

this determines an upper bound for the necessary runtime T of the quantum adiabatic algorithm. Note that the constraint $\dot{s} \ll |\Im(\tilde{s})|\,\Delta E$ derived from $h \ll |\Im(\tilde{s})|$, is not necessarily equivalent to $\dot{s} \ll \Delta E^2$, which one would naively deduce from Eq. (2.42).

2.4.2 Evolution Time

The general criterion in Eq. (2.49) can now be used to estimate the necessary run-time via Eq. (2.50). Typically, the inverse energy gap $1/\Delta E(s)$ is strongly peaked (along the real axis) around $\Re(\tilde{s})$ with a width of order $|\Im(\tilde{s})|$. Therefore, assuming $h(s)$ to be roughly constant across the peak and respecting $h\,|_{\rm peak} \ll |\Im(\tilde{s})|$, yields the following estimate of the integral in Eq. (2.50)

$$T = \mathcal{O}\left(\Delta E_{\rm min}^{-1}\right)\,, \tag{2.51}$$

where $\Delta E_{\rm min}$ denotes the minimum energy gap. Note that this estimate is only valid for one (or a few) relevant excited state(s).

Intuitively, the same order of magnitude estimate for the evolution time can also be derived from the local adiabatic condition (2.42): Inverting this condition, we find the relationship

$$T = \frac{1}{\epsilon} \int_0^1 ds\, \frac{F_{01}(s)}{\Delta E^2(s)}\,. \tag{2.52}$$

Assuming that $F_{01}(s)$ does not oscillate strongly, e.g., that the ground state of $H(s)$ travels on a reasonably direct path from the initial to the final state, we can make the following estimate

$$T = \frac{\mathcal{O}(\Delta E_{\min}^{-1})}{\epsilon} \int_0^1 ds \, \frac{F_{01}(s)}{\Delta E(s)} \, . \tag{2.53}$$

Now we may exploit the advantage of the representation in Eq. (2.46), which is valid for general dynamics $s(t)$ corresponding to different functions $h(s)$ and hence for arbitrary evolution times T. In the limit of very fast evolution $T \to 0$ (which implies $h \to \infty$), we have large excitations $a_1(T) = \mathcal{O}(1)$ and thus the remaining integral in the above equation can be estimated via inserting this limit into Eq. (2.46)

$$\int_0^1 ds \, \frac{F_{01}(s)}{\Delta E(s)} = \mathcal{O}(1) \, . \tag{2.54}$$

By comparing Eqs. (2.54) and (2.52), we again obtain the estimate (2.51). Note that the quantities $F_{01}(s)$ and $\Delta E(s)$ appearing in the integrals in Eqs. (2.52-2.54) do not depend on the dynamics $s(t)$ which allows us to perform the integration independently of $s(t)$.

2.4.3 Gap Structure

Let us illustrate the above considerations by means of the rather general ansatz for the behavior of the gap

$$\Delta E(s) = \left[(s - s_{\min})^{2a} + \Delta E_{\min}^{b} \right]^{1/b} \tag{2.55}$$

with the minimal gap $0 < \Delta E_{\min} \ll 1$ at $s_{\min} \in (0, 1)$, $b > 0$, and $a \in \mathbb{N}$. An avoided level crossing in an effectively two-dimensional subspace corresponds to $2a = b = 2$, see Eq. (2.24). This is the typical situation if the commutator of the initial and the final Hamiltonian $[H_{\rm i}, H_{\rm f}]$ is small, since, in this case, the two operators can almost be diagonalized independently and thus the energy levels are nearly straight lines except at the avoided level crossing(s), where $[H_{\rm i}, H_{\rm f}]$ becomes important. In the continuum limit, such an (Landau-Zener type[7]) avoided level crossing corresponds to a first-order quantum phase transition. The finite-size analogue of a second-order phase transition corresponds to $a = b$ (and accordingly for even higher orders), which may occur if $[H_{\rm i}, H_{\rm f}]$ is not small or if the interpolation is not linear, i.e.,

$$H(s) \neq [1 - s] H_{\rm i} + s H_{\rm f} \, . \tag{2.56}$$

[7]The Landau-Zener formula is an analytic solution to the equations of motion governing the transition dynamics of a 2-level quantum mechanical system, with a time-dependent Hamiltonian varying such that the energy separation of the two states is a linear function of time. The formula, giving the probability of a nonadiabatic transition between the two energy state, was published separately by Lev Landau [34] and Clarence Zener [35] in 1932, (for more details see the appendix of this Thesis).

$\Delta E(s) =$	$\sqrt{(s-1/2)^2+\Delta E_{\min}^2}$	$\sqrt{(s-1/2)^4+\Delta E_{\min}^2}$
$d=-1$	$\Delta E_{\min}^{-2}$	$\Delta E_{\min}^{-3/2}$
$d=0$	$\Delta E_{\min}^{-1}\ln\Delta E_{\min}^{-2}$	$\Delta E_{\min}^{-1}$
$d\geq 1$	$\Delta E_{\min}^{-1}$	$\Delta E_{\min}^{-1}$

Table 2.1: Scaling of the runtime T necessary to obtain a fixed fidelity for different gap structures (top row) and varying interpolation velocities (first column). The best improvement possible scales as the inverse of the minimum gap $\Delta E_{\min}^{-1}$.

The inverse gap $1/\Delta E(s)$ has singularities, compare Fig. (2.3), around $s_{\min}$ at

$$\Im(\tilde{s}) = \mathcal{O}(\Delta E_{\min}^{b/2a})\,. \tag{2.57}$$

The total running time T for different choices of $h(s)=\alpha_d\Delta E^d(s)$ satisfying the criterion (2.49) can be obtained from Eq. (2.50). Here, the exponent d determines the scaling of the interpolation dynamics, whereas the coefficient α_d is adapted such that $s(T)=1$, cf. Eqs. (2.45) and (2.50). For

$$\frac{2a}{b}(d+1)>1\,, \tag{2.58}$$

one easily shows that

$$\frac{1}{\alpha_d} = \mathcal{O}\left(T\Delta E_{\min}^{d+1-b/2a}\right) \tag{2.59}$$

satisfies the criterion (2.49) with the evolution time obeying $T=\mathcal{O}(\Delta E_{\min}^{-1})$. If d is smaller, the necessary evolution time will be larger. In Table (2.1), the scaling of the run-time (for two examples of the gap structure) is derived for three cases:

(a) Constant velocity $\dot{s}=\alpha_{-1}$, i.e., $d=-1$.

(b) Constant function $h(s)=\alpha_0$, i.e., $d=0$.

(c) The local adiabatic evolution with $h(s)=\alpha_1\Delta E(s)$, i.e., $d=+1$, investigated in [25].

2.4.4 Grover's Algorithm

In the frequently studied adiabatic realization of Grover's algorithm[8] the initial Hamiltonian reads $H_0=\mathbf{1}-|\mathrm{in}\rangle\langle\mathrm{in}|$ with the initial superposition state $|\mathrm{in}\rangle=\sum_{x=0}^{N-1}|x\rangle/\sqrt{N}$, and the final Hamiltonian is given by $H_\mathrm{f}=\mathbf{1}-|w\rangle\langle w|$, where $|w\rangle$ denotes the marked state. In this case,

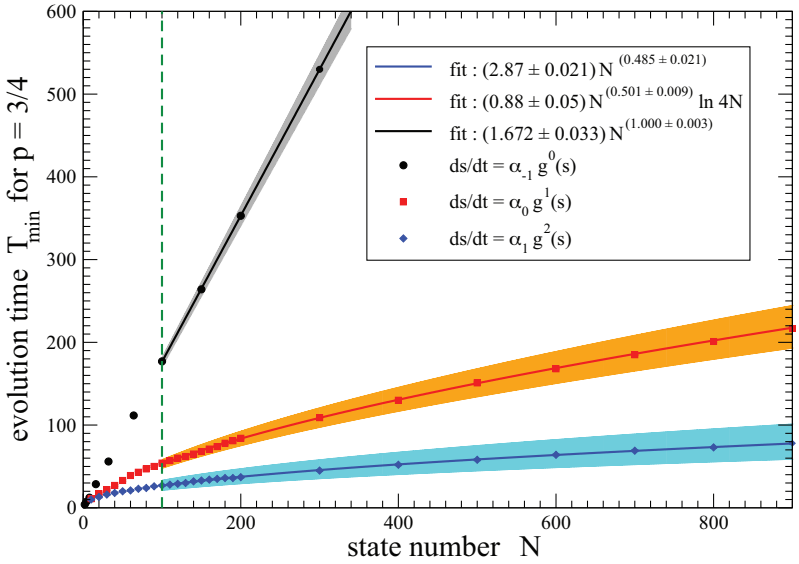

Figure 2.4: Runtime scaling of the adiabatic Grover search for different interpolation functions $s(t)$ and a target fidelity of $3/4$. Solid lines represent fits to full symbol data for $N \geq 100$ and shaded regions correspond to fit uncertainties (99% confidence level). These uncertainties arise from the finite resolution when determining the necessary runtime.

the commutator is very small $[H_0, H_\mathrm{f}] = (|\mathrm{in}\rangle\langle w| - |w\rangle\langle \mathrm{in}|)/\sqrt{N}$ and one obtains for the time-dependent gap

$$\Delta E(s) = \sqrt{1 - 4\left(1 - \frac{1}{N}\right) s(1-s)} \approx \sqrt{4\left(s - \frac{1}{2}\right)^2 + \frac{1}{N}}\,. \tag{2.60}$$

Comparing with Eq. (2.55), we identify $\Delta E_\mathrm{min} \approx 1/\sqrt{N}$ and $2a = b = 2$ (the pre-factor does not affect the scaling behavior). Consequently, our analytical estimate implies

$$\begin{cases} T = \mathcal{O}(N) & \text{for} \quad d = -1\,, \\ T = \mathcal{O}(\sqrt{N}\ln 4N) & \text{for} \quad d = 0\,, \\ T = \mathcal{O}(\sqrt{N}) & \text{for} \quad d > 0\,. \end{cases} \tag{2.61}$$

We have solved the Schrödinger equation numerically by using a fourth order Runge-Kutta integration scheme with an adaptive step-size [36]. By restarting the code with different T until agreement with desired fidelity was sufficient, we could confirm these runtime scaling predictions numerically, see Fig. (2.4). The dependence of the final error on the run-time T for fixed $N = 100$ and constant h is depicted in Fig. (2.5), where the exponential decay becomes evident.

[8] See Sec. (2.2) of this Thesis.

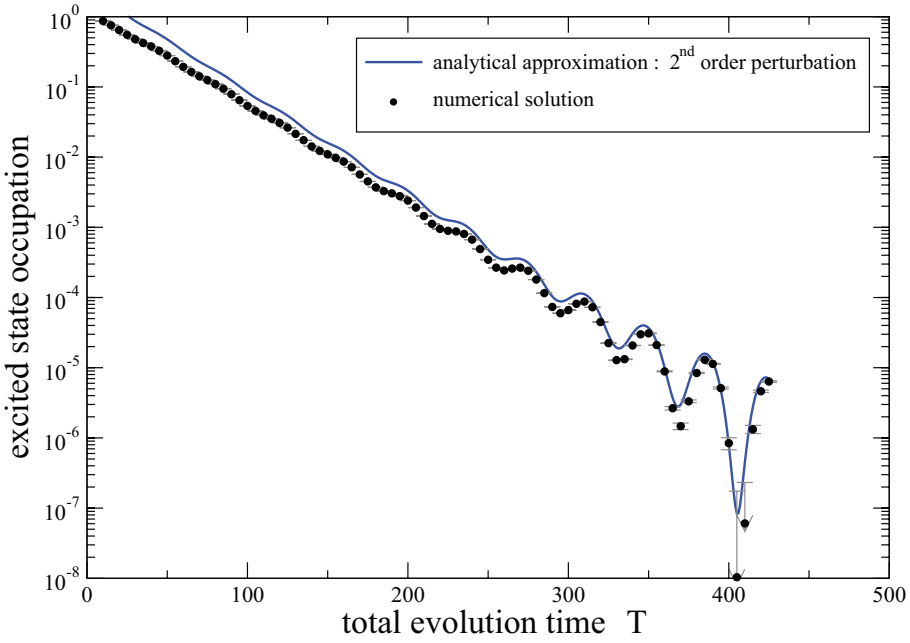

Figure 2.5: Final error probability $|a_1(T)^2|$ as a function of run-time T for Grover's algorithm with $N = 100$ and $h = \text{const}$. The oscillations stem from the time-dependence of a_0 in Eq. (2.46). The solid (blue) line represents the second-order perturbative solution of Eq. (2.46).

2.4.5 Summary

The advantage of adiabatic quantum computation scheme, which is believed to be polynomially equivalent to sequential quantum computation [29], lies in the inherent robustness of the ground state against the influences of decoherence - a sufficiently cold reservoir provided. The ground state cannot decay and phase errors do not play any role, i.e., errors can only result from excitations. However, the instantaneous occupation of the first excited state during the adiabatic evolution in Eq. (2.41) and Eq. (2.42) does not provide a good error estimate. Instead, a better estimate is given by the remaining real excitations *after* the dynamics.
Moreover, the final error can be made extremely (in fact, with $h(0)+h(1) \lll 1$, exponentially) small

$$a_1(T) = \mathcal{O}\left(h(0) + h(1) + \exp\left\{-\frac{|\Im(\tilde{s})|}{h(s_{\min})}\right\}\right) , \tag{2.62}$$

cf. Fig. (2.5). For the Grover example, the last term was dominant.
Based on general arguments, the optimal run-time scales as $T = \mathcal{O}(\Delta E_{\min}^{-1})$ contrary to what one might expect from the Landau-Zener [34, 35] formula (with $T \propto \Delta E_{\min}^{-2}$). In view of the fact that the minimum energy gap $\Delta E_{\min}$ is a measure of the coupling between the known initial state and the unknown final state, this result is very natural. For the Grover algorithm,

it is known that the $\sqrt{N}$-scaling is optimal [25]. This optimal scaling $T = \mathcal{O}(\Delta E_{\min}^{-1})$ can already be achieved with interpolation functions $s(t)$ which vary less strongly (e.g., $d = 0$) than demanded by locally [25] adiabatic evolution ($d = 1$) – and hence should be easier to realize experimentally.

Unfortunately, a constant velocity with $d = -1$ does not produce the optimal result in general. The Grover example has the advantage that the spectrum can be determined analytically, which is for example not the case for the more involved satisfiability problems [7]. Therefore, some knowledge of the spectral properties $\Delta E(s)$ is necessary for achieving the optimal result $T = \mathcal{O}(\Delta E_{\min}^{-1})$ also in the general case of adiabatic quantum computing. For systems with an analytically unknown gap structure, some knowledge about the spectrum can be obtained by extrapolating the scaling behavior of small systems. A related interesting point is the impact of the gap structure (corresponding to the first or second order transition etc.) in Eq. (2.55). The derived constraint for the velocity at the transition $\dot{s} \ll |\Im(\tilde{s})|\, \Delta E$ is only for first-order transitions equivalent to $\dot{s} \ll \Delta E^2$, which one would naively deduce from Eq. (2.42).

Note that the improvement $T = \mathcal{O}(\Delta E_{\min}^{-1})$ compared with the conventional runtime estimate $T = \mathcal{O}(\Delta E_{\min}^{-2})$ is merely polynomial (same complexity class). Though this is not as impressive as an exponential speedup, in practice a polynomial improvement may be useful. For time-dependent Hamiltonians where the inverse of the minimum gap scales exponentially with the size of the problem, we would still expect an exponential scaling of the optimal runtime T. On the other hand, the exponential suppression of the final error in Eq. (2.62) may become important in certain cases such as in the presence of degeneracy and may yield an exponential speedup in comparison with the conventional estimate.

3 Decoherence in a Dynamical Quantum Phase Transition

3.1 Introduction

In contrast to thermal phase transitions occurring when the strength of the thermal fluctuations equals a certain threshold, during recent years, a different class of phase transitions has attracted the attention of physicists, namely transitions taking place at zero temperature. A non-thermal control parameter such as pressure, magnetic field, or chemical composition is varied to access the transition point. There, order is changed solely by quantum fluctuations. Let us consider a quantum system (at zero temperature) described by the Hamiltonian H depending on some external parameter g. At a certain critical value of this parameter g_c, the system is supposed to undergo a phase transition, i.e., the ground state $|\Psi_<(g)\rangle$ of $H(g)$ for $g < g_c$ is different from the ground state $|\Psi_>(g)\rangle$ of $H(g)$ for $g > g_c$. For example, $|\Psi_<(g)\rangle$ and $|\Psi_>(g)\rangle$ could have different global/topological properties (such as magnetization) in the thermodynamic limit.
A quantum phase transition is a non-analyticity of the ground state properties of the system as a function of the control parameter. If this singularity arises from a simple level crossing in the ground state, see Fig. (3.1)-(a), then we have a first-order quantum phase transition. The situation is different for continuous transitions, where a higher-order discontinuity in the ground state energy occurs. Typically, for any finite-size system a continuous transition will be rounded into a crossover, this is nothing but an avoided level-crossing in the ground state, see Fig. (3.1)-(b). Continuous transitions can usually be characterized by an order parameter[1] which is a quantity that is zero in one phase (the disordered) and non-zero and possibly non-unique in the other (the ordered) phase. If the critical point is approached, the spatial correlations of the order parameter fluctuations become long-ranged. Close to the critical point the correlation

[1]The choice of an order parameter for a particular transition is often obvious – e.g., for the ferromagnetic transition where the total magnetization is an order parameter. However, in some cases finding an appropriate order parameter is complicated – e.g., for the interaction-driven metal-insulator transition in electronic systems (the Mott transition).

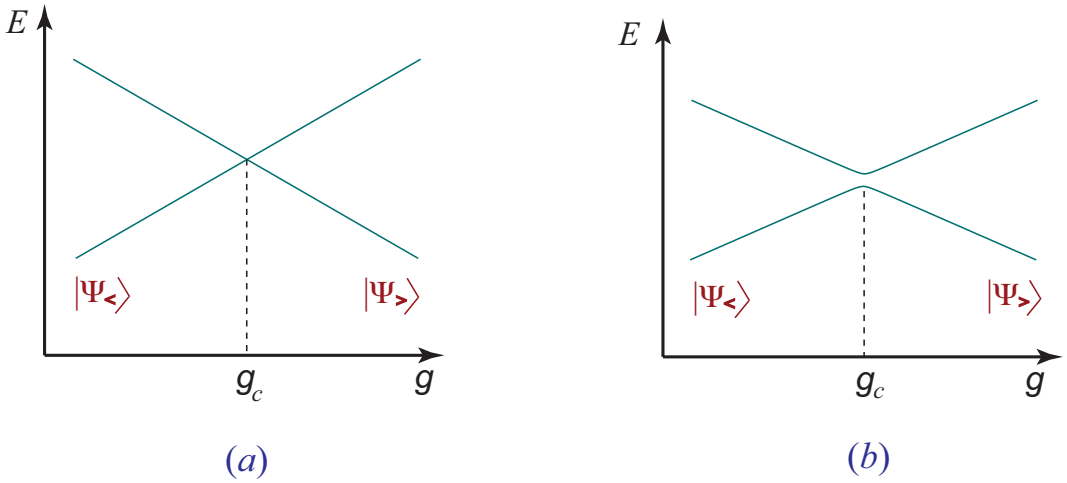

Figure 3.1: Sketch of the lowest eigenvalues of a Hamiltonian $H(g)$ as a function of some external parameter g. At the critical point $g = g_c$, the ground state changes from $|\Psi_<(g)\rangle$ to $|\Psi_>(g)\rangle$. (a) A level-crossing. (b) An avoided level-crossing.

length Υ diverges as

$$\Upsilon^{-1} \propto \Lambda |g - g_c|^{\mathfrak{d}} , \tag{3.1}$$

where $\mathfrak{d}$ is a critical exponent and Λ is an inverse length scale of order the inverse lattice spacing. Let Δ denotes the energy excitation gap above the ground state. In most cases, it has been found [37] that as g approaches g_c, Δ vanishes as

$$\Delta \propto \Upsilon^{-z} , \tag{3.2}$$

where z is the dynamic critical exponent.

For all interesting systems are discussed later, adiabatic quantum computation inherently brings the quantum system near to a point where is similar to the critical point in a quantum phase transition. Somewhere on the way from the simple initial configuration H_0 to the unknown solution of some problem encoded in $H_{\rm f}$, there is typically a critical point which bears strong similarities to a quantum phase transition [21, 22]. During the adiabatic interpolation, one encounters a critical point where the fundamental gap (which is sufficiently large initially and finally) becomes very small, see, e.g., Fig. (2.1). Near the position of the minimum gap, the ground state will change more drastically than in other time intervals of the interpolation. This can be seen from the time-derivative of the eigenvalue equation $H(t)\,|\psi_n(t)\rangle = E_n(t)\,|\psi_n(t)\rangle$

$$||\dot{\psi}_0(t)||^2 = \left\langle \dot{\psi}_0(t) | \dot{\psi}_0(t) \right\rangle \geq \sum_{n>0} \left| \frac{\langle \psi_0(t)|\, \dot{H}(t)\, |\psi_n(t)\rangle}{E_n(t) - E_0(t)} \right|^2 . \tag{3.3}$$

In the continuum limit, one would expect that the minimum value of the fundamental gap in adiabatic computation will vanish identically and that the ground state will change non-analytically

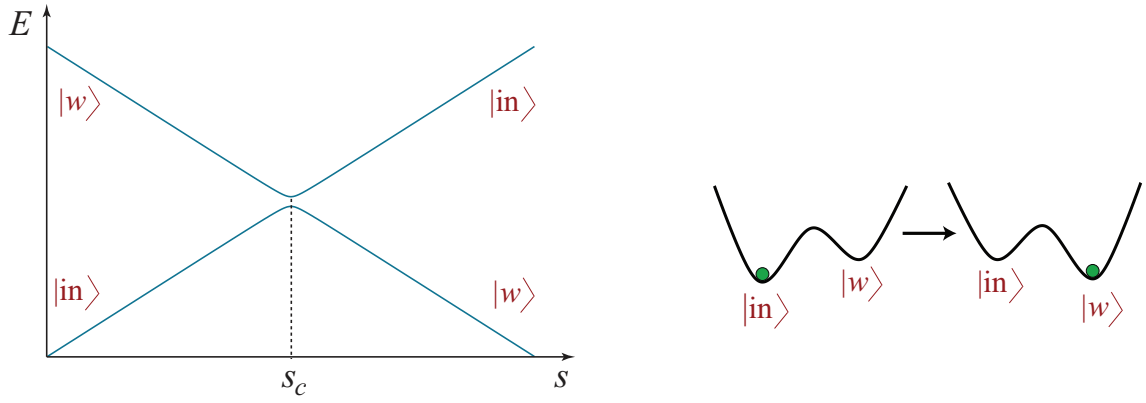

Figure 3.2: Sketch of the two lowest energy eigenvalues of the Grover Hamiltonian (left). In the continuum limit, this corresponds to the time evolution of the energy landscape for a first-order transition (right). The green dot in the energy landscape denotes the ground state.

at the critical point. This is similar to what happens in quantum phase transition when g approaches g_c, see Eq. (3.2). Based on this similarity, it seems [22] that adiabatic quantum algorithms corresponding to second-order quantum phase transitions should be advantageous compared to isolated avoided level crossings (which are analogous to first-order transitions). A brief review of this idea comes in the following section.

3.2 Examples

3.2.1 First-Order Transition – Grover's Algorithm

An adiabatic version of Grover's algorithm is defined by the Hamiltonian

$$H(s) = (1-s)H_0 + sH_{\mathrm{f}}\,, \tag{3.4}$$

where the initial Hamiltonian is given by $H_0 = \mathbf{1} - |\mathrm{in}\rangle\langle\mathrm{in}|$ with the initial superposition state $|\mathrm{in}\rangle = \sum_{x=0}^{N-1}|x\rangle/\sqrt{N}$, and the final Hamiltonian reads $H_{\mathrm{f}} = \mathbf{1} - |w\rangle\langle w|$, where $|w\rangle$ denotes the marked state.[2] In this case, the commutator is very small $[H_0, H_{\mathrm{f}}] = (|\mathrm{in}\rangle\langle w| - |w\rangle\langle\mathrm{in}|)/\sqrt{N}$ and one can nearly diagonalize them simultaneously and the s-dependent spectrum will consist of nearly straight lines – except near $s_c = 1/2$, where we have an avoided level-crossing, see Fig. (3.2). In the continuum limit of $n \to \infty$, this corresponds to a first-order quantum phase transition from $|\mathrm{in}\rangle = |{\to}\cdots{\to}\rangle$ to $|w\rangle = |{\uparrow\downarrow}\cdots{\uparrow\downarrow\downarrow}\rangle$, for example, at the critical point $s_c = 1/2$. Such a first-order transition is characterized by an abrupt change of the ground

[2] For more details about Grover's adiabatic algorithm see Sec. (2.2) of this Thesis.

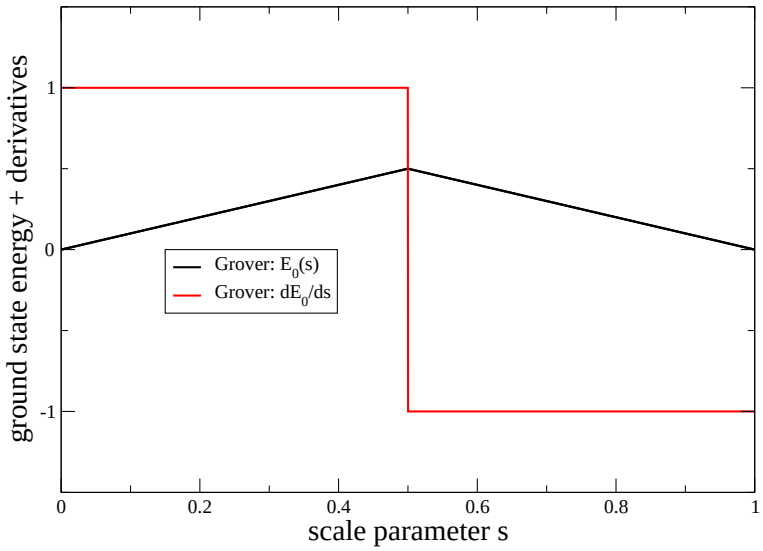

Figure 3.3: The ground-state energy of the Grover Hamiltonian and its first-order derivative. The discontinuity in the first-order derivative of the ground state suggests the first-order quantum phase transition in adiabatic quantum search algorithm.

state – $|\mathrm{in}\rangle$ for $s < s_c$ and $|w\rangle$ for $s > s_c$ – resulting in a discontinuity of a corresponding order parameter, see Fig. (3.3),

$$\langle\psi_0(s)|\,\frac{dH}{ds}\,|\psi_0(s)\rangle = \frac{dE_0}{ds}\,. \tag{3.5}$$

First-order quantum phase transitions are typically associated with an energy landscape pictured in Fig. (3.2), where the two competing ground states are separated by an energy barrier. In order to stay in the ground state, the system has to tunnel through the barrier between the initial ground state $|\mathrm{in}\rangle$ and the final ground state $|w\rangle$ during the quantum phase transition. The natural increase of the strength of the barrier with the system size n yields to the tunneling time which scales exponentially with the system size – as we have seen in the second chapter of this Thesis, the optimal run-time for the adiabatic search algorithm behaves as $T = \mathcal{O}(\sqrt{N}) = \mathcal{O}\left(2^{n/2}\right)$. Therefore, the abrupt change of the ground state and the energy barrier between the initial and final ground states suggest that the first-order transitions are not the best choice for the realization of adiabatic quantum algorithms. Thus, it would be relevant to study higher-order quantum phase transitions for this purpose.

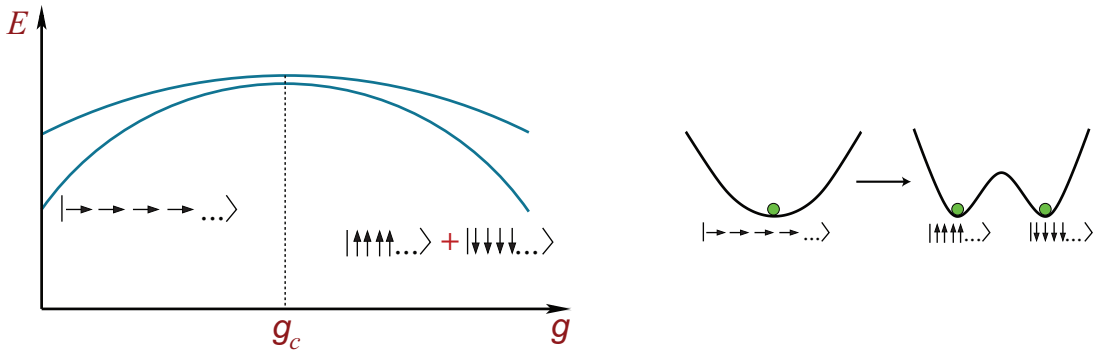

Figure 3.4: Sketch of the two lowest energy levels of the Ising Hamiltonian (left) given in Eq. (3.6) and the time evolution of the energy landscape for a second-order transition (right). A symmetry-breaking transition corresponds to the deformation of the energy landscape. The green dot in the energy landscape denotes the ground state.

3.2.2 Second-Order Transition – Ising Model

The one-dimensional quantum Ising model is one of the two paradigmatic examples [37] for second-order quantum phase transition (the other is Bose-Hubbard model). Of this two, only the former model is exactly solvable [38].[3] Quantum Ising model has been employed in the study of quantum phase transitions and percolation theory [37], spin glasses [37, 39], as well as quantum annealing [40, 41, 42] etc. Although its Hamiltonian is quite simple and can be diagonalized analytically, the Ising model is rich enough to display most of the basic phenomena near quantum critical points. Furthermore, the transverse Ising model can also be used to study the order-disorder transitions at zero temperature driven by quantum fluctuations [37, 40]. Finally, two-dimensional generalizations of the Ising model can be mapped onto certain adiabatic quantum algorithms (see, e.g., [43]). However, due to the evanescent excitation energies, such a phase transition is rather vulnerable to decoherence, which must be taken into account [44].
The one-dimensional transverse Ising chain of n spins exhibits a time-dependent nearest-neighbor interaction $g(t)$ plus transverse field $B(t) = 1 - g(t)$

$$H_{\mathrm{sys}}(t) = -\sum_{j=1}^{n} \left\{ [1 - g(t)]\, \sigma_j^x + g(t)\, \sigma_j^z \sigma_{j+1}^z \right\} , \tag{3.6}$$

where $\boldsymbol{\sigma}_j = (\sigma_j^x, \sigma_j^y, \sigma_j^z)$ are the spin-1/2 Pauli matrices acting on the jth qubit and periodic boundary conditions $\boldsymbol{\sigma}_{n+1} = \boldsymbol{\sigma}_1$ are imposed. This Hamiltonian is invariant under a global 180-

[3] The Ising model in a transverse field is a special case of the XY model (which can also be diagonalized completely).

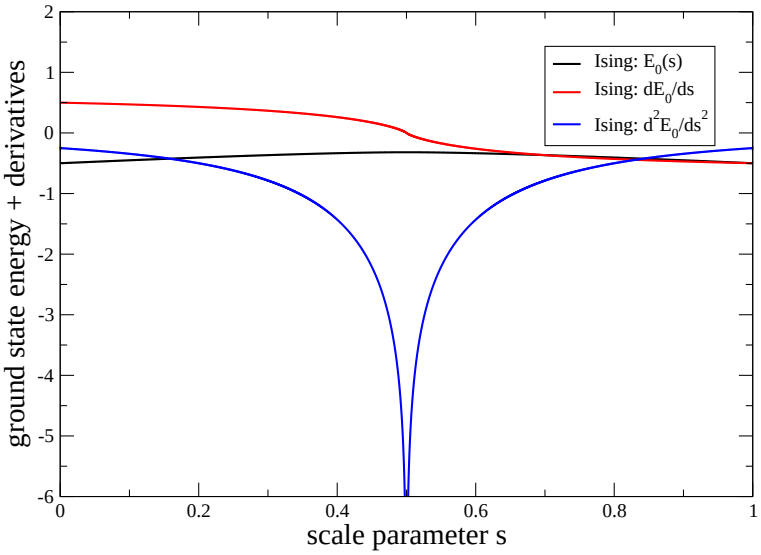

Figure 3.5: The ground-state energy for the Ising model and its first and second derivatives. The discontinuity in the second-order derivative of the ground state suggests a second-order quantum phase transition.

degree rotation around the σ_j^x-axes (bit flip) which transforms all qubits according to $\sigma_j^z \rightarrow -\sigma_j^z$

$$\left[H_0, \prod_{j=1}^{n} \sigma_j^x\right] = \left[H_{\rm f}, \prod_{j=1}^{n} \sigma_j^x\right] = 0\,, \tag{3.7}$$

where

$$H_0 = -\sum_{j=1}^{n} \sigma_j^x \qquad , \qquad H_{\rm f} = -\sum_{j=1}^{n} \sigma_j^z \sigma_{j+1}^z\,. \tag{3.8}$$

Choosing $g(0) = 0$ and $g(T) = 1$ where T is the evolution time, the quantum system evolves from the unique paramagnetic state $|{\rm in}\rangle = |{\rightarrow}{\rightarrow}{\rightarrow}\ldots\rangle$ through a second-order quantum phase transition at $g_{\rm cr} = 1/2$ to the two-fold degenerate ferromagnetic state, see Fig. (3.4)

$$|w\rangle = \frac{|{\uparrow}{\uparrow}{\uparrow}\ldots\rangle + |{\downarrow}{\downarrow}{\downarrow}\ldots\rangle}{\sqrt{2}}\,. \tag{3.9}$$

At the critical point $g_{\rm cr}$ the excitation gap vanishes (in the thermodynamic limit $n \uparrow \infty$) and the response time diverges. As a result, driving the system through its quantum critical point at a finite sweep rate entails interesting non-equilibrium phenomena such as the creation of topological defects, i.e., kinks [45].

Since the initial ground state $|{\rm in}\rangle$ reflects the bit-flip invariance (3.7) of the Hamiltonian (3.6) whereas the final ground states break this symmetry, we have a symmetry-breaking quantum

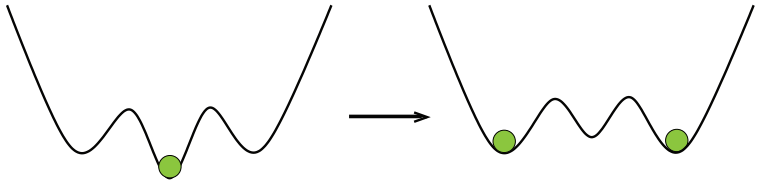

Figure 3.6: Sketch of the time evolution of the energy landscape for a symmetry-breaking quantum phase transition – which is, however, not of second but of first order. The green dot denotes the ground state. This figure has been taken from [46].

phase transition. Typically, such a symmetry-breaking change of the ground state corresponds to a second-order phase transition [22]. For such a transition, the ground state changes continuously[4] and the energy barrier observed in first-order transitions is absent:

> *Initially, there is a unique ground state but at the critical point, this ground state splits up into two degenerate ground states which are the mirror image of each other. Therefore, the ground state does not change abruptly in this situation and the system does not need to tunnel through a barrier in order to stay in the ground state, see Figs. (3.4) and (3.5).*

Consequently, we expect that in this case, the quantum system should find its way from the initial to the final ground state easier. This expectation is confirmed in the following sections of this chapter: Since the minimum gap behaves as $\mathcal{O}(1/n)$, the optimal run-time in order to stay in the ground state scales polynomially for the Ising model.

3.2.3 Mixed Case

Looking at Fig. (3.4), it seems that a symmetry-breaking quantum phase transition typically corresponds to a second-order phase transition, but there are counter-examples. Let us consider the energy landscape in Fig. (3.6) which is more complicated but nevertheless possible. In spite of the symmetry-breaking, there is a tunneling barrier throughout the interpolation and a jump between the initial and the final ground state(s).
An analytic example for a symmetry-breaking first-order transition [46] is given by a combination of the initial Hamiltonian from the Grover problem with the final Hamiltonian of the Ising model

$$H_0 = \mathbf{1} - |\mathrm{in}\rangle\langle\mathrm{in}| \qquad , \qquad H_\mathrm{f} = \frac{1}{2}\sum_{j=1}^{n}\left(\mathbf{1} - \sigma_j^z\sigma_{j+1}^z\right) , \tag{3.10}$$

[4] There is no jump in an order parameter.

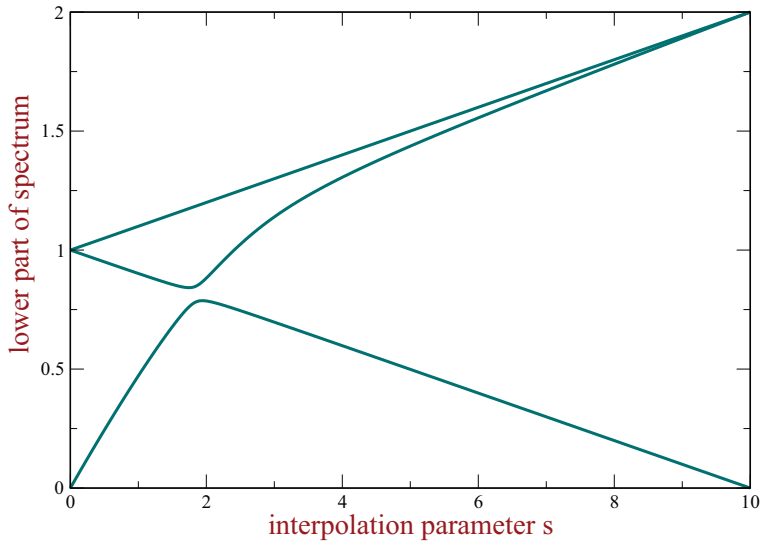

Figure 3.7: Sketch of the lowest eigenvalues of the Hamiltonian (3.10). One can clearly see that the spectrum displays an avoided-level crossing at the critical point – thus corresponding to a first-order transition [46].

where $H_{\rm f}$ has been shifted and scaled in order to preserve the positive definiteness and the fundamental energy gap of H_0. Even though this Hamiltonian possesses the same bit-flip symmetry in Eq. (3.7) as the Ising model, its level structure displays an avoided-level crossing at the critical point, i.e., it corresponds to a first-order phase transition, see Fig. (3.7). It can also be shown analytically that the fundamental gap of the combined Hamiltonian $H(s) = (1-s)H_0 + sH_{\rm f}$ scales exponentially with the system size, i.e. number of qubits, see, e.g., [28, 47].

3.3 Decoherence

In all of the above examples, we have already seen that at the critical point, the energy levels become arbitrarily close and thus, the response times diverge (in the continuum limit). Consequently, during the sweep through such a phase transition by means of a time-dependent external parameter, small external perturbations or internal fluctuations become strongly amplified – leading to many interesting effects, see, e.g., [48]-[53]. One of them is the anomalously high susceptibility to decoherence (see also [54]):

Due to the convergence of the energy levels at the critical point, even low-energy modes of the environment may cause excitations and thus perturb the system.

Based on the similarity between the quantum adiabatic algorithms and critical phenomena, we have argued that adiabatic quantum algorithms corresponding to the higher-order quantum phase transitions should be advantageous in comparison to those of first order. However, in the above arguments, the impact of decoherence has not been considered.
In order to study the impact of decoherence, we consider an open system described by the total Hamiltonian $H(t)$ which can be split up into that of the closed system $H_{\rm sys}$ and the bath $H_{\rm bath}$ acting on independent Hilbert spaces $\mathcal{H}_{\rm sys} \otimes \mathcal{H}_{\rm bath} = \mathcal{H}$

$$H(t) \;=\; H_{\rm sys}(t) + H_{\rm bath}(t) + \lambda\, H_{\rm int}(t)\,, \tag{3.11}$$

plus an interaction $\lambda\, H_{\rm int}$ between the two, which is supposed to be weak $\lambda \ll 1$ in the sense that it does not perturb the state of the system drastically. Note that the change of the bath caused by the interaction need not be small. To describe the evolution of the combined quantum state $|\Phi(t)\rangle \in \mathcal{H}$, we expand it into the instantaneous system energy eigenbasis

$$H_{\rm sys}(t)\,|\psi_s(t)\rangle = E_s(t)\,|\psi_s(t)\rangle\ , \tag{3.12}$$

in $\mathcal{H}_{\rm sys}$ via

$$|\Phi(t)\rangle = \sum_s a_s(t)\,|\psi_s(t)\rangle \otimes |\alpha_s(t)\rangle\ , \tag{3.13}$$

where a_s are the corresponding amplitudes and $|\alpha_s\rangle \in \mathcal{H}_{\rm bath}$ denote the associated (normalized but not necessary orthogonal) states of the reservoir. Insertion of this expansion into the Schrödinger equation $i\left|\dot\Phi(t)\right\rangle = H(t)\,|\Phi(t)\rangle$ yields

$$\frac{\partial}{\partial t}\left(a_s e^{-i\varphi_s}\right) = e^{-i\varphi_s}\sum_{r\neq s} a_r\left(\frac{\langle\psi_s|\,\dot H_{\rm sys}\,|\psi_r\rangle}{\Delta E_{sr}}\,\langle\alpha_s|\alpha_r\rangle - i\,\langle\alpha_s|\,\langle\psi_s|\,\lambda H_{\rm int}\,|\psi_r\rangle\,|\alpha_r\rangle\right)\ , \tag{3.14}$$

with the energy gaps $\Delta E_{sr}(t) = E_s(t) - E_r(t)$ of the system and the total phase (including the Berry phase)

$$\varphi_s(t) = -\int_0^t dt'\Big\{E_s(t') + H^{ss}_{\rm bath}(t') + \lambda H^{ss}_{\rm int}(t') - i\langle\psi_s(t')|\dot\psi_s(t')\rangle - i\langle\alpha_s(t')|\dot\alpha_s(t')\rangle\Big\}\,, \tag{3.15}$$

whith the energy shift

$$H^{sr}_{\rm int} = \langle\alpha_s|\,\langle\psi_s|\,H_{\rm int}\,|\psi_r\rangle\,|\alpha_r\rangle \qquad , \qquad H^{sr}_{\rm bath} = \langle\alpha_s|\,H_{\rm bath}\,|\alpha_r\rangle\ . \tag{3.16}$$

Evidently, there are two contributions for transitions in the Hilbert space $\mathcal{H}_{\rm sys}$ of the system:

- The first term on the right-hand side of Eq. (3.14) describes the transitions caused by a non-adiabatic evolution.[5] Note, however, that the factor $\langle\alpha_s|\alpha_r\rangle$ and the additional phases in Eq. (3.15) give rise to extra terms in the adiabatic expansion.

- The last term in Eq. (3.14) directly corresponds to transitions caused by the interaction of the quantum system with its environment.

Since we are mainly interested in the impact of the coupling to the bath, we shall assume a perfectly adiabatic evolution[6] of the system itself

$$\langle\psi_s|\,\dot{H}_{\rm sys}\,|\psi_r\rangle \ll \Delta E_{sr}^2\,, \tag{3.17}$$

such that the first term in Eq. (3.14) is negligible and the second one dominates. Starting in the system's ground state $a_0(t=0)=1$, which is relevant for adiabatic quantum computation, the excitations $s>0$ caused by the weak interaction $\lambda H_{\rm int}$ with the bath

$$\mathfrak{A}_s = a_s(T)\exp\{-i\varphi_s(T)\} \tag{3.18}$$

can be calculated via response theory, i.e., the solution of Eq. (3.14) to first order in $\lambda \ll 1$

$$\mathfrak{A}_s \approx -i\sum_{r\neq s}\int_0^T dt\; e^{i\Delta\varphi_{rs}}\,\langle\alpha_s|\,\langle\psi_s|\,\lambda H_{\rm int}\,|\psi_r\rangle\,|\alpha_r\rangle\;, \tag{3.19}$$

where $\Delta\varphi_{rs}=\varphi_r(t)-\varphi_s(t)$. This is rather a general result. In the following, after a brief review of the impact of decoherence on the sweep through a first-order quantum phase transition [55], we study the decoherence caused by a small coupling to a general reservoir for the quantum Ising chain in a transverse field, which is considered a prototypical example for a second-order quantum phase transition.

3.4 Decoherence in the Adiabatic Search Algorithm

This section based on publication[7] [55], which we rederive in our framework to describe the impact of decoherence on Grover's quantum search algorithm based on a single isolated level crossing – which are analogous to first-order transitions – in order to compare with the Ising

[5] See the second chapter of this Thesis and also, e.g., [30].

[6] Without the coupling to the environment $\lambda = 0$, the system would stay in its ground state. Thus, the only decoherence channel available is heating (i.e., excitations), the phase damping and decay channels, for example, play no major role here.

[7] M. Tiersch and R. Schützhold, *Non-Markovian decoherence in the adiabatic quantum search algorithm*, Phys. Rev. A **75**, 062313 (2007).

model in the next section of this Thesis. For this purpose, it is natural to assume the following expansion of the interaction Hamiltonian

$$\lambda H_{\rm int} = \lambda \sum_{j=1}^{n} \boldsymbol{\sigma}_j \cdot \boldsymbol{A}_j + \lambda^2 \sum_{\ell,j=1}^{n} \boldsymbol{\sigma}_\ell \cdot \boldsymbol{B}_{\ell j} \cdot \boldsymbol{\sigma}_j + \mathcal{O}(\lambda^3) \tag{3.20}$$

with $\lambda \ll 1$. The n qubits are labeled by j and $\boldsymbol{\sigma}_j(t) = (\sigma_j^x, \sigma_j^y, \sigma_j^z)$ is the vector of their Pauli matrices in the interaction picture[8] with the corresponding bath operators $\boldsymbol{A}_j(t)$ and $\boldsymbol{B}_{\ell j}(t)$, etc. Recalling the adiabatic version of Grover's search algorithm in Eq. (3.4), at the beginning of the evolution the system of qubits has to be realized in – or close to – the ground state $|{\rm in}\rangle = \sum_{x=0}^{N-1} |x\rangle / \sqrt{N}$. Therefore, one can assume that the initial full density operator is a direct product

$$\varrho(0) = \varrho_{\rm sys}(0) \otimes \varrho_{\rm bath}(0)\,, \tag{3.21}$$

i.e., system and environment are not entangled at the beginning. In coupling an adiabatic quantum computer to an environment, an essential quantity is the probability of measuring the ground state at the end of the computation, at time T. Since, in the weak-coupling limit the adiabaticity condition for the open system dynamics is still in leading order the same as for the closed system, similar to former discussions, one can assume perfect adiabatic evolution of the unperturbed system and hence only consider perturbations due to the interaction with the environment.

The spectrum of the Grover's Hamiltonian (3.4) consists of the ground state $|\psi_0(s)\rangle$ and the first excited state $|\psi_1(s)\rangle$, which come very close $\left(\Delta E_{\rm min} = 1/\sqrt{N}\right)$ at $s = 1/2$, whereas all other states $|\psi_{k>1}(s)\rangle$ are degenerate – have the same constant energy – and well separated from the ground state by an energy gap of order one, see also Fig. (2.1). Since the temperature and hence the energies available in the environment are supposed to be much smaller than that gap of order one, transitions from the ground state to these states $|\psi_{k>1}(s)\rangle$ are exponentially suppressed. Thus, the final probability of the transitions to the first excited state

$$|\mathfrak{A}_s|^2 \approx \lambda^2 \sum_{\substack{\ell,j=1 \\ \mu,\nu=x,y,z}}^{n} \int_0^T dt_1 \int_0^T dt_2 \, \left\langle A_\ell^\mu(t_1) A_j^\nu(t_2) \right\rangle \left\langle w^\perp \right| \sigma_\ell^\mu(t_1) \left| w \right\rangle \left\langle w \right| \sigma_j^\nu(t_2) \left| w^\perp \right\rangle \,, \tag{3.22}$$

provides a good measure for the success probability[9] [55]. Since $N = 2^n \ggg 1$, the terms of order $1/\sqrt{N} \lll 1$ have been neglected and $|w\rangle$ denotes the marked state for Grover's problem,

[8] The Pauli operators can be transformed to the interaction picture by applying the unitary time evolution operator $\mathcal{U}_{\rm sys}$ which is implied by the system Hamiltonian $H_{\rm sys}$ and can be calculated with the adiabatic expansion for perfectly adiabatic evolution and in the large-N limit [55].

[9] The success of the Grover's algorithm corresponds to $|\mathfrak{A}_s|^2 \ll 1$.

see Eq. (3.4). The expression (3.22) is a combination of the system dynamics with the properties of reservoir. Of the system matrix elements $\langle w^\perp | \, \sigma_j^\mu(t) \, |w\rangle$ only those with $\mu = x, z$ contribute – the $\mu = y$ term is suppressed by a factor $1/\sqrt{N}$

$$\langle w^\perp | \, \sigma_j^x(t) \, |w\rangle \approx \frac{1-s(t)}{\sqrt{N}\Delta E(t)} \exp\left\{-i\int_0^t dt' \Delta E(t')\right\} , \tag{3.23}$$

for large N. It is the same for $\langle w^\perp | \, \sigma_j^z(t) \, |w\rangle$ apart from an additional sign $(-1)^{w_j+1}$, where w_j is the j-th bit of w, i.e., $|w\rangle$ is an eigenstate of the operators σ_j^z with eigenvalues $(-1)^{w_j}$. Assuming a stationary reservoir $[H_{\rm bath}, \varrho_{\rm bath}] = 0$ allows for a Fourier decomposition of the bath correlation function

$$\left\langle A_\ell^\mu(t_1) A_j^\nu(t_2)\right\rangle = \int d\omega \, e^{-i\omega(t_1-t_2)} f_{\ell j}^{\mu\nu}(\omega) \, , \tag{3.24}$$

where $f_{\ell j}^{\mu\nu}(\omega)$ depends on the spectral distribution of the bath modes and the temperature, etc. Insertion of (3.23) and (3.24) into Eq. (3.22) yields

$$|\mathfrak{A}_s|^2 \approx \lambda^2 \int d\omega \sum_{\ell,j=1}^n f_{\ell j}^{xx}(\omega) \left| \int_0^T dt \, \frac{1-s(t)}{\sqrt{N}\Delta E(t)} \exp\left\{ i\omega t + i\int_0^t dt' \Delta E(t')\right\}\right|^2 \tag{3.25}$$

plus similar terms including $f_{\ell j}^{xz}$, $f_{\ell j}^{zx}$ and $f_{\ell j}^{zz}$ with the associated signs (-1) and $(-1)^{w_j}$ for x and z, respectively [55]. In order to evaluate the time integrations, it is useful to distinguish different domains of ω:

- For large frequencies $|\omega| \gg \Delta E_{\rm min}$, the time integral can be calculated via the saddle-point approximation. The saddle points t_ω^* are given by a vanishing derivative of the exponent

$$\omega + \Delta E(t_\omega^*) = 0 \, , \tag{3.26}$$

  which corresponds to energy conservation. Hence large positive frequencies $\omega \gg \Delta E_{\rm min}$ do not contribute at all which is quite natural.[10]

- The saddle-point approximation cannot be applied for small frequencies $\omega = \mathcal{O}(\Delta E_{\rm min})$ and energy conservation is also not well-defined. In this case, one might estimate an upper bound for the time integral by omitting all phases.

[10] This corresponds to the transfer of a large energy from the system – which is in its ground state – to the reservoir. However, since the temperature of the bath is typically much larger than $\Delta E_{\rm min}$, the opposite process is possible in general.

These, altogether yield

$$|\mathfrak{A}_s|^2 \approx \lambda^2 N \int_{-\Delta E_{\min}}^{+\Delta E_{\min}} d\omega\, f(\omega) + \frac{\pi\lambda^2}{2N} \int_{\Delta E_{\min}}^{1} d\omega\, \frac{f(-\omega)}{\omega^2 \dot{s}(t^*_\omega)}\,, \tag{3.27}$$

where $f(\omega)$ is the appropriate sum of the $f^{xx}_{\ell j}$, $f^{xz}_{\ell j}$, $f^{zx}_{\ell j}$ and $f^{zz}_{\ell j}$ contributions. The second term of the above equation depends on the interpolation function $s(t)$. Considering three scenarios given in the former chapter (see Sec. (2.4) of this Thesis)

(a) $\ddot{s} = 0$

(b) $\dot{s} \propto \Delta E$

(c) $\dot{s} \propto \Delta E^2$

the second integrand scales as

(a) $N f(-\omega)/\omega^2$

(b) $\sqrt{N}\, f(-\omega)/\omega^3$

(c) $f(-\omega)/\omega^4$,

respectively. In all of these cases, the bath modes with large frequencies $|\omega| \gg \Delta E_{\min}$ do not cause problems in the large-N limit, since the spectral function $f(-\omega)$ is supposed to decrease for large $|\omega|$ as the bath does not contain excitations with large energies – the environment is cold enough. Therefore, the low-energy modes of the reservoir $\omega = \mathcal{O}(\Delta E_{\min})$ give the potentially dangerous contributions. Independent of the dynamics $s(t)$ both the first integral and the lower limit of the second integral yield the same order of magnitude [55]

$$|\mathfrak{A}_s|^2 \approx \lambda^2\, \frac{f\left[\mathcal{O}(\Delta E_{\min})\right]}{\Delta E_{\min}}\,. \tag{3.28}$$

Since $\Delta E_{\min}$ decreases as $1/\sqrt{N}$ in the large-N limit, the spectral function $f(\omega)$ must vanish in the infrared limit as ω or even faster in order to keep the error $|\mathfrak{A}_s|^2$ under control. Thus, one can conclude that:

> *The spectral function $f(\omega)$ of the bath provides a criterion to favor or disfavor certain physical implementations. If $f(\omega)$ vanishes in the infrared limit faster than ω, the computational error does not grow with increasing system size – the quantum computer is scalable.*

3.5 Decoherence in the Transverse Ising Chain

This section based on publication[11] [44], where we study the decoherence caused by a small coupling to a rather general reservoir for the quantum Ising chain in a transverse field. As we shall see below, the situation may be very different for second-order transitions compared to the first-order transitions. These investigations are particularly relevant in view of the announcement (see, e.g., [43]) regarding the construction of an adiabatic quantum computer with 16 qubits in the form of a two-dimensional Ising model.

A major advantage of the Ising Hamiltonian in Eq. (3.6) is that it can be diagonalized analytically [37]. First of all, we briefly review the main steps of the diagonalization of $H_{\rm sys}$, where we switch temporarily to the Heisenberg picture for convenience: The set of n qubits in Eq. (3.6) can be mapped to a system of n spinless fermions c_j via the *Jordan-Wigner* transformation [56] given by

$$\begin{aligned} \sigma_j^x(t) &= 1 - 2c_j^\dagger(t)\, c_j(t)\,, \\ \sigma_j^z(t) &= -\prod_{\ell<j} \Big[1 - 2c_\ell^\dagger(t)\, c_\ell(t)\Big] \Big[c_j(t) + c_j^\dagger(t)\Big] \end{aligned} \tag{3.29}$$

with $\sigma_j(t)$ indicating the Pauli operators in Heisenberg picture

$$\sigma_j(t) = \mathcal{U}_{\rm sys}^\dagger(t)\, \sigma_j\, \mathcal{U}_{\rm sys}(t)\,, \tag{3.30}$$

where $\mathcal{U}_{\rm sys}(t)$ is the unitary time evolution operator of the system. The fermionic operators c_j and $c_j^\dagger$ are related to $\sigma_j^+ = (\sigma_j^x + i\sigma_j^y)/2$ and $\sigma_j^- = (\sigma_j^x - i\sigma_j^y)/2$, respectively,

$$\sigma_j^+ = \prod_{\ell<j} \Big(1 - 2c_\ell^\dagger\, c_\ell\Big)\, c_j \quad , \quad \sigma_j^- = \prod_{\ell<j} \Big(1 - 2c_\ell^\dagger\, c_\ell\Big)\, c_j^\dagger\,. \tag{3.31}$$

These relations can also be rewritten in the inverse form

$$c_j = \prod_{\ell<j} \sigma_\ell^z\, \sigma_j^+ \quad , \quad c_j^\dagger = \prod_{\ell<j} \sigma_\ell^z\, \sigma_j^-\,. \tag{3.32}$$

Since the Pauli operators obey the following commutation relations

$$\big[\sigma_\ell^+, \sigma_j^-\big] = \delta_{\ell j}\, \sigma_j^z \qquad , \qquad \big[\sigma_\ell^z, \sigma_j^\pm\big] = \pm 2\delta_{\ell j}\, \sigma_j^\pm\,, \tag{3.33}$$

it is easy to verify that the fermionic operators anticommutation relations satisfy

$$\Big\{c_\ell, c_j^\dagger\Big\} = \delta_{\ell j} \qquad , \qquad \{c_\ell, c_j\} = \Big\{c_\ell^\dagger, c_j^\dagger\Big\} = 0\,. \tag{3.34}$$

[11] S. Mostame, G. Schaller, and R. Schützhold, *Decoherence in a dynamical quantum phase transition of the Ising chain*, Phys. Rev. A **76**, R030304 (2007).

Insertion of Eq. (3.29) into the system Hamiltonian in Eq. (3.6) yields

$$H_{\rm sys}(t) = \sum_{j=1}^{n} \Big\{ \left[1 - g(t)\right] \Big(1 - 2c_j^\dagger\, c_j\Big) + \; g(t) \Big(c_{j+1}\, c_j + c_{j+1}^\dagger\, c_j + c_j^\dagger\, c_{j+1} + c_j^\dagger\, c_{j+1}^\dagger\Big) \Big\}\,, \tag{3.35}$$

where the time-dependency of the c_j has been dropped for brevity. This fermionic Hamiltonian has terms that violate the fermion conservation number, $c_{j+1}\, c_j$ and $c_j^\dagger\, c_{j+1}^\dagger$. This bilinear form can now be diagonalized by a *Fourier* transformation

$$c_j(t) = \frac{1}{\sqrt{n}} \sum_k \tilde{c}_k(t)\, e^{-ik(ja)}\,, \tag{3.36}$$

followed by a *Bogoliubov* transformation [57]. Here a is lattice spacing. The Bogoliubov transformation

$$\tilde{c}_k(t) = u_k(t)\; \gamma_k + i v_k^*(t)\; \gamma_{-k}^\dagger \tag{3.37}$$

maps the Hamiltonian into a new set of fermionic operators γ_k whose number is conserved. The same anticommutation relations as in Eq. (3.34) are also satisfied by γ_k and $\gamma_k^\dagger$

$$\Big\{\gamma_k, \gamma_{k'}^\dagger\Big\} = \delta_{kk'} \qquad , \qquad \{\gamma_k, \gamma_{k'}\} = \Big\{\gamma_k^\dagger, \gamma_{k'}^\dagger\Big\} = 0\,. \tag{3.38}$$

Since these fermionic operators are supposed to be time-independent, the Bogoliubov coefficients u_k and v_k must satisfy [45] the equations of motion

$$\begin{aligned} i\frac{du_k}{dt} &= -\alpha_k(t) u_k(t) \; + \; \beta_k(t) v_k(t)\,, \\ i\frac{dv_k}{dt} &= \alpha_k(t) v_k(t) \; + \; \beta_k(t) u_k(t)\,, \end{aligned} \tag{3.39}$$

where

$$\alpha_k = 2 - 4g(t)\cos^2\left(\frac{ka}{2}\right) \qquad , \qquad \beta_k = 2g(t)\sin(ka)\,. \tag{3.40}$$

For an adiabatic evolution $\langle\psi_s|\, \dot{H}_{\rm sys}\, |\psi_r\rangle \ll \Delta E_{sr}^2$, these equations of motion can be solved approximately

$$\begin{aligned} u_k(t) &\approx \frac{\alpha_k(t) + \mathscr{E}_k(t)}{\mathcal{N}_k} \exp\Big\{-i \textstyle\int_0^t\, dt' \mathscr{E}_k(t')\Big\} \\ v_k(t) &\approx -\frac{\beta_k(t)}{\mathcal{N}_k}\; \exp\Big\{-i \textstyle\int_0^t\, dt' \mathscr{E}_k(t')\Big\} \end{aligned} \tag{3.41}$$

with the normalization $\mathcal{N}_k = \sqrt{2\mathscr{E}_k^2 + 2\alpha_k \mathscr{E}_k}$ ensuring $|u_k|^2 + |v_k|^2 = 1$ and the single-particle energies

$$\mathscr{E}_k(t) = 2\sqrt{1 - 4g(t)\left[1 - g(t)\right]\cos^2\left(ka/2\right)}\,. \tag{3.42}$$

All the excitation energies $\mathscr{E}_k$ take their minimum values

$$\mathscr{E}_k^{\min} = 2\left|\sin\left(\frac{ka}{2}\right)\right| , \tag{3.43}$$

at the critical point $g_{\rm cr} = 1/2$. The pseudo-momenta k take half-integer values

$$k \in \frac{(1+2\mathbb{Z})\pi}{na} \;:\; |ka| < \pi\,. \tag{3.44}$$

In view of the k-spectrum the minimal gap between the ground state and the first excited state scales as $\Delta E_{\min} = \mathcal{O}(1/n)$. Finally, the Hamiltonian (3.6) reads

$$H_{\rm sys}(t) = \sum_k \mathscr{E}_k(t)\left(\gamma_k^\dagger\gamma_k - \frac{1}{2}\right) \tag{3.45}$$

with fermionic creation and annihilation operators $\gamma_k^\dagger, \gamma_k$. Hence, its (instantaneous) ground state contains no fermionic quasi-particles $\forall_k \gamma_k\,|\psi_0(t)\rangle = 0$. Without the environment, the number of fermionic quasi-particles $\gamma_k^\dagger\gamma_k$ would be conserved and the system would stay in an eigenstate (e.g., ground state) for an adiabatic evolution. The coupling to the bath, however, may cause excitations and thus the creation of quasi-particles due to decoherence.

3.5.1 Decoherence Channel

Of course, the impact of decoherence depends on the properties of the bath and its interaction with the system (decoherence channels). In order to derive generally applicable results, we do not specify the bath $H_{\rm bath}$ in much detail and start with an interaction $\lambda\, H_{\rm int}$ which is always present: In the Hamiltonian $H_{\rm sys}$ in Eq. (3.6), the transverse field $B(t) = 1 - g(t)$ appears as a classical control parameter $B_{\rm cl}$. However, the external field $B \to B_{\rm cl} + \delta B$ does also possess (quantum) fluctuations δB, which couple to the system of Ising spins. Therefore, we start with the following interaction Hamiltonian

$$H_{\rm int} = \delta B \sum_j \sigma_x^j\,, \tag{3.46}$$

where δB denotes the bath operator. Incidentally, this interaction Hamiltonian yields the same matrix elements as the non-adiabatic corrections $\langle\psi_s|\,\dot{H}_{\rm sys}\,|\psi_r\rangle$ in Eq. (3.14), which can therefore be calculated analogously. Insertion of $\lambda H_{\rm int}$ into Eq. (3.19) yields

$$\mathfrak{A}_s \approx -i\lambda \int d\omega\, f_s(\omega) \int_0^T dt\; \langle\psi_s(t)|\sum_j \sigma_j^x\,|\psi_0(t)\rangle \exp\left\{i\left[-\omega t + \int_0^t dt'\,\Delta E_{s0}(t')\right]\right\}\,. \tag{3.47}$$

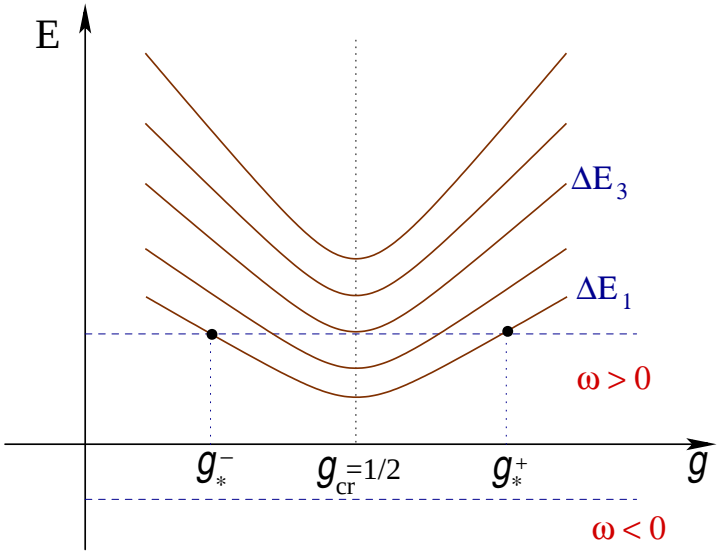

Figure 3.8: Sketch of the excitation spectrum of the Ising chain $H_{\rm sys}$ as a function of g. For a given frequency $\omega > 0$, real saddle points correspond to intersections of the (solid) energy level curves (e.g., ΔE_1) with the (dashed) vertical ω-line which occur shortly before (g_*^-) and after (g_*^+) the quantum phase transition at $g_{\rm cr} = 1/2$. The saddle-point approximation can only be applied if the intersection angle is large enough, i.e., for the drawn $\omega > 0$ line, it would work for ΔE_1, but not for ΔE_3 etc.

We have subsumed all relevant properties of the environment into the spectral function $f(\omega)$ of the bath

$$e^{-i\Delta\varphi_s'(t)} \langle\alpha_s(t)| \, \delta B(t) \, |\alpha_0(t)\rangle = \int_{-\infty}^{+\infty} d\omega \, e^{-i\omega t} f_s(\omega) \, , \tag{3.48}$$

where $\Delta\varphi_s'$ coincides with $\varphi_s - \varphi_0$ in Eq. (3.15) apart from the system's energy gap ΔE_{s0} and is typically dominated by the contribution from $H_{\rm bath}^{ss} - H_{\rm bath}^{00}$. As a first approximation, we assume that $f(\omega)$ does not change significantly if we increase the system size n (scaling limit). After inserting the Jordan-Wigner transformation [56], the matrix element in Eq. (3.47) reads

$$\sum_j \langle\psi_s| \, \sigma_x^j(t) \, |\psi_0\rangle \approx \frac{2ig(t)\sin(ka)}{\mathscr{E}_k(t)} \langle\psi_s| \, \gamma_k^\dagger \gamma_{-k}^\dagger \, |\psi_0\rangle \ , \tag{3.49}$$

where the $\approx$ sign refers to the adiabatic approximation. Thus, it is only non-vanishing for excited states $|\psi_s\rangle$ containing two quasi-particles $s = (k, -k)$ with opposite momenta and hence we get $\Delta E_{s0} = 2\mathscr{E}_k$.

3.5.2 Different Domains of ω

In order to solve the remaining time integrals in Eq. (3.47), it is useful to distinguish different ω-regimes:

– Cold Environment

First of all, in order to have a *quantum* phase transition (or a working adiabatic quantum computer), the environment should be cold enough to permit the preparation of the system in the initial ground state

$$\omega \ll 2 = \mathscr{E}_k(t=0)\,. \tag{3.50}$$

– Intermediate Positive Frequencies

We may solve the time integral via the saddle-point (or stationary phase) approximation for intermediate positive frequencies,

$$2 \gg \omega \gg \Delta E_{s0}^{\min} \approx 2|ka|\,. \tag{3.51}$$

For the exponent in Eq. (3.47) the saddle-point condition reads

$$\left[\frac{\partial h_k(t,\omega)}{\partial t}\right]_{t=t_*} = 0 \;\rightsquigarrow\; \omega = \Delta E_{s0}(t_*) = 2\mathscr{E}_k(t_*)\,, \tag{3.52}$$

where $h_k(t,\omega) = i\left[-\omega t + 2\int_0^t dt'\,\mathscr{E}_k(t')\right]$ and t_* denotes the saddle points. This condition yields two saddle points shortly before and after the transition, see also Fig. (3.8)

$$g(t_*^{\pm}) = \frac{1}{2} \pm \frac{\left[\omega^2 - 16\sin^2(ka/2)\right]^{1/2}}{8\cos(ka/2)}\,. \tag{3.53}$$

For the spectral excitation amplitude $\mathfrak{A}_s^{\omega}$ defined via

$$\mathfrak{A}_s = \int d\omega\, f_s(\omega)\,\mathfrak{A}_s^{\omega}\,, \tag{3.54}$$

the saddle-point approximation yields

$$\mathfrak{A}_s^{\omega\gg 2|ka|} \approx \left(\frac{\pm 32\pi i\lambda^2 \sin(ka)\sin(ka/2)\,\exp\left[2h_k(t_*,\omega)\right]}{\omega\dot{g}(t_*)g^{-2}(t_*)\sqrt{\omega^2 - 16\sin^2(ka/2)}}\right)^{1/2}, \tag{3.55}$$

which depends on the interpolation dynamics $g(t)$. The minimum gap can be obtained from Eq. (3.42) and does indeed scale polynomially $\Delta E_{\min} = \mathcal{O}(1/n)$ and, thus:

	$1 \gg \omega \gg 2ka$	$1 \gg \omega \approx 2ka$
$\ddot{g}(t) = 0$	$\mathcal{O}\left(\lambda ka\omega^{-1}n\right)$	$\mathcal{O}\left(\lambda n^2\omega\ln\omega\right)$
$\dot{g}(t) \propto \Delta E(t)$	$\mathcal{O}\left(\lambda ka\omega^{-3/2}\sqrt{n}\right)$	$\mathcal{O}\left(\lambda n\ln n\right)$
$\dot{g}(t) \propto \Delta E^2(t)$	$\mathcal{O}\left(\lambda ka\omega^{-2}\right)$	$\mathcal{O}\left(\lambda n\right)$

Table 3.1: Scaling of the spectral excitation amplitude $\mathfrak{A}_s^\omega$ in the saddle-point approximation ($\omega \gg 2ka$) and its upper bound ($\omega \approx 2ka$) for different interpolation dynamics $g(t)$, where $\Delta E(t) = 2\mathscr{E}_{k=\pi/(an)}(t)$ denotes the fundamental gap. In all cases, the total excitation probability (sum over all ω and k) increases with system size n.

- For a constant speed interpolation $g(t) = t/T$, the necessary run-time for an adiabatic evolution T scales polynomially $T = \mathcal{O}\left(\Delta E_{\min}^{-2}\right) = \mathcal{O}(n^2)$.
- For adapted interpolation dynamics $\dot{g}(t) \propto \Delta E(t)$ or $\dot{g}(t) \propto \Delta E^2(t)$, however, one may achieve shorter run-times of $T = \mathcal{O}(n\ln n)$ or $T = \mathcal{O}(n)$, respectively [32] and therefore better results for the spectral excitation amplitude, see Table 3.1.

– Near the Minimum Gap

Higher order terms of the saddle-point expansion scale with

$$\mathcal{O}\left(\frac{\lambda\dot{g}(t_*)}{\omega\sqrt{\omega^2 - 4k^2a^2}}\right), \tag{3.56}$$

and hence the saddle-point approximation breaks down if ω approaches the minimum gap $\Delta E_{s0}^{\min} \approx 2|ka|$, see Fig. (3.8). In this case, we may obtain an upper bound for the time integral in Eq. (3.47) via omitting all phases. For a constant speed interpolation $g(t) = t/T$

$$\mathfrak{A}_s^{\omega\approx 2|ka|} \approx \frac{2\lambda\sin(ka)}{T}\int_0^T dt\,\frac{t}{\mathscr{E}_k(t)} = \mathcal{O}\left(\lambda n^2\omega\ln\omega\right). \tag{3.57}$$

Similarly, one can get better results for adapted interpolation dynamics, see Table 3.1.

– Positive Frequencies Below the Minimum Gap

For positive frequencies which are far below $2|ka|$, the saddle points at

$$g(t_*^\pm) \approx \frac{1}{2} \pm \frac{1}{8}\sqrt{\omega^2 - 4k^2a^2}, \tag{3.58}$$

move away from the real axis and thus the exponent in Eq. (3.47) contains real terms. The constant speed interpolation leads to

$$i\left[-\omega t_* + 2\int_0^{t_*} dt\,\mathscr{E}_k(t)\right] \approx i\eta - \frac{1}{4}\Big[\omega|ka| + 2\,(ka)^2\Big]T, \tag{3.59}$$

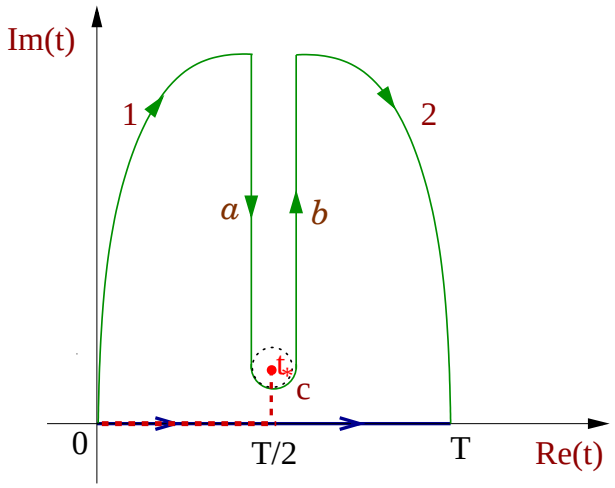

Figure 3.9: A sketch of the deformed integration contour. The original integration contour (blue line along the real axis) is shifted to the complex plane (curved line), where t_* indicates the singular point, $t_* = T/2 + iT/2 \tan(ka/2)$. Only paths a and b contribute significantly to the integral.

where η is a real value. Therefore, the spectral excitation amplitude is exponentially suppressed in the adiabatic limit

$$\mathfrak{A}_s^{\omega \ll 2|ka|} = \mathcal{O}\left(\exp\left\{-\frac{1}{2}\,T(ka)^2\right\}\right) . \tag{3.60}$$

– Negative Frequencies

Finally, for negative frequencies $\omega < 0$, the saddle points collide with the branch cut generated by the square-root in $\mathscr{E}_k$. In this case, we may also estimate the spectral excitation amplitude $\mathfrak{A}_s^\omega$ in Eq. (3.54) by deforming the time integration contour into the complex plane. We assume that all involved functions can be analytically continued into the complex plane and are well-behaved near the real axis. Given this assumption, we deform the integration contour into the upper complex half-plane to obtain a negative exponent which is the usual procedure in such estimates until reaching a saddle point, a singularity, or a brunch cut, see Fig. (3.9). Deforming the integration contour into the lower complex half-plane would of course not change the result, but there the integrand is exponentially large and strongly oscillating such that the integral is hard to estimate. Since the integral in the complex plane is zero around path c and the integrals on the paths 1 and 2 cancel each other, only paths a and b give the main contribution to the integral.

Let us first consider a constant interpolation function $g(t) = t/T$ which leads to singular points

$$t_* = \frac{T}{2} \pm i\frac{T}{2}\tan\left(\frac{ka}{2}\right), \tag{3.61}$$

in the complex plane. Performing the time integral in the exponent of Eq. (3.47) acquires a large negative real term in the exponent

$$\int_0^t dt'\,\Delta E_{s0}(t') = \left\{\int_0^{T/2} + \int_{T/2}^{t_*} + \int_{t_*}^{t}\right\} dt'\,\Delta E_{s0}(t') \approx \xi' \pm 2t^2 + \frac{i\pi T}{16}(ka)^2\,, \tag{3.62}$$

where ξ' is a constant and real value. Insertion of Eq. (3.62) into Eq. (3.47) and doing some algebra yields the exponential suppression for the amplitudes in the upper complex half-plane

$$\mathfrak{A}_s^{\omega<0} \approx \exp\left\{-\frac{\pi T}{16}(ka)^2\right\}\int_{a,b} dt\,F(t)\exp\left\{i\left(2t^2-\omega t+\tau\right)\right\} \tag{3.63}$$

with $F(t) = \langle\psi_s(t)|\sum_j \sigma_j^x\,|\psi_0(t)\rangle$ and τ is a real constant. Therefore, applying the inequality

$$|\mathfrak{H}| \le \int dy\,|\phi(y)| \quad \text{with} \quad \mathfrak{H} = \int dy\,\phi(y)\,, \tag{3.64}$$

the amplitudes for negative frequencies are also exponentially suppressed for $g(t) = t/T$ and similarly for the other interpolations. This result can be understood in the following way: For frequencies ω below the lowest excitation energies, the energy ω of the reservoir modes is not sufficient for exciting the system via energy-conserving transitions. Hence excitations can only occur via non-adiabatic processes for which energy-conservation becomes ill-defined, but these processes are suppressed if the evolution is slow enough.

3.5.3 Summary

In summary, we studied the quantum phase transition from paramagnetic to ferromagnetic phase in the quantum Ising chain in a transverse field via its analytical diagonalization and estimated the excitation probabilities caused by a weak coupling to a rather general environment (including possible non-perturbative behavior of the reservoir). Since the Ising model is considered [37] as a prototypical example for a second-order quantum phase transition, we expect our results to reflect general features of second-order transitions. For the decoherence channel (3.46) which is always present (though possibly not the dominant channel), we already found that the total excitation probability increases with system size n (continuum limit): Even though the probability for the *lowest* excitation $k = \pm\pi/(an)$ can be kept under control for a bath which is well-behaved in the infra-red limit – see also Sec. (3.4) – the existence of *many* excited states $k \in \pi(1+2\mathbb{Z})/(an) \;:\; |ka| < \pi$ converging near the critical point causes the growth of the error probability for large systems. This growth can be slowed down a bit via adapted interpolation schemes $g(t)$, but not stopped. Other decoherence channels will display the same general

behavior: E.g., for $\omega \gg |ka|$, the associated amplitudes scale as

$$\mathfrak{A}_s^{\omega} = \mathcal{O}\left(\frac{\lambda\phi_s(t_*)}{\sqrt{\dot{g}(t_*)}}\right) , \tag{3.65}$$

where ϕ_s denotes the matrix element in analogy to (3.49). Typically, for a homogeneous coupling to the bath, ϕ_s does not strongly depend on the system size n (for given ka and ω). Since $\dot{g}(t_*)$ decreases for $n \uparrow \infty$ or at least remains constant – for $\dot{g}(t) \propto \Delta E^2(t)$ – the total excitation probability again increases with system size n.[12]

According to the analogy between adiabatic quantum algorithms and quantum phase transitions [21, 22], this result suggests scalability problems of the corresponding adiabatic quantum algorithm – unless the temperature of the bath stays below the (n-dependent) minimum gap [8] or the coupling to the bath decreases with increasing n. These problems are caused by the accumulation of many levels at the critical point $g = 1/2$, which presents the main difference to isolated avoided level crossings (corresponding to first-order phase transitions) discussed earlier. It also causes some difficulties for the idea of thermally assisted quantum computation (see, e.g., [58]) since, in the presence of too many available levels, the probability of hitting the ground state becomes small.

Therefore, in order to construct a scalable adiabatic quantum algorithm in analogy to the Ising model, suitable error-correction methods will be required. As one possibility, one might exploit the quantum Zeno effect and suppress transitions in the system by constantly measuring the energy, see for example [59]. As another interesting idea, let us study a spatial sweep through the phase transition, i.e., we do not cross the critical point in a homogeneous way, but adopt the following step-wise interpolation [60]: Starting from the initial Hamiltonian

$$H_0 = -\sum_{j=1}^{n} \sigma_j^x = -\left\{\sigma_1^x + \sigma_2^x + \sigma_3^x + \sigma_4^x + \dots\right\} , \tag{3.66}$$

we change it slowly to H_1 and afterwards to H_2, $\cdots$

$$\begin{aligned}
H_1 &= -\sigma_1^z\sigma_2^z - \sum_{j=3}^{n} \sigma_j^x \, , \\
H_2 &= -\sigma_1^z\sigma_2^z - \sigma_2^z\sigma_3^z - \sum_{j=4}^{n} \sigma_j^x \, , \\
&\vdots \\
H_\ell &= -\sum_{j=1}^{\ell} \sigma_j^z\sigma_{j+1}^z - \sum_{j=\ell+2}^{n} \sigma_j^x \, ,
\end{aligned}$$

[12] If only a few spins are coupled to the environment, the matrix element ϕ_s (for given ka and ω) will generically decrease $\phi_s = \mathcal{O}(1/n)$ and then the error probability may be kept under control – for $\dot{g}(t) \propto \Delta E^2(t)$.

$$
\begin{aligned}
H_\ell &= -\sum_{j=1}^{\ell} \sigma_j^z \sigma_{j+1}^z - \sum_{j=\ell+2}^{n} \sigma_j^x \,, \\
&\vdots \\
H_{n-1} &= -\sum_{j=1}^{n-1} \sigma_j^z \sigma_{j+1}^z \,, \\
H_n &= -\sum_{j=1}^{n} \sigma_j^z \sigma_{j+1}^z = H_{\rm f} \,.
\end{aligned} \tag{3.67}
$$

This corresponds to a nonlinear interpolation path between the initial and final Hamiltonians in Eq. (3.6)

$$H(t) \neq [1-g(t)]H_0 + g(t)H_{\rm f} \,. \tag{3.68}$$

Physically, such a scheme could be approximated by a transverse magnetic field that within the distance between two spins rises linearly from zero to maximum and then travels at constant speed along the spin chain [60]. Note that this interpolation path does not destroy the bit-flip symmetry

$$\left[H_\ell, \prod_{j=1}^{n} \sigma_j^x \right] = 0 \,. \tag{3.69}$$

In this case, the minimum gap (in the relevant subspace that is even under bit flip) remains independent of the system size n and the run-time T scales linear in n (number of steps), see, e.g., [60]. Hence, decoherence could be strongly suppressed for a low-temperature bath. Of course, the generalization of all these concepts and results to more interesting cases such as the (NP-complete) two-dimensional Ising model is highly non-trivial and requires further investigations.

4 Quantum Simulators

4.1 Quantum Simulator with Electrons Floating on a Helium Film

As we discussed in the introduction, as long as universal quantum computers of sufficient size are not available, one has to search for alternatives. One possibility is to design a *quantum simulator* in the laboratory. Quantum simulator is an experimental study of an interesting quantum system by use of an alternative quantum system in which the same Hamiltonian is implemented. The first section of this chapter based on publication[1] [61] and we suggest using a set of electrons trapped at a thin superfluid Helium film interface for designing a quantum simulator for the Ising spin chain in a transverse field. A similar idea based on trapped ions has been pursued in [62]. Nevertheless, since different experimental realizations possess distinct advantages and drawbacks, it is still worthwhile to study an alternative set-up. For example, the number of coherently controlled ions in a trap is rather limited at present, whereas our proposal can be scaled up to a large number of electrons more easily – which is important for exploring the continuum limit and scaling properties etc.

4.1.1 Electrons above Helium Films

The system of electrons formed on a surface of superfluid helium has been the subject of a great number of experimental and theoretical studies. Because of very unique features of the system, these wide-ranging studies relate to a variety of topics of modern many-electron physics, see e.g. [63]. One of these unique properties is its nearly ideal two-dimensionality (2D) in a very clean surrounding with well-defined interactions, namely the Coulomb interactions, the electron-helium gas scattering at high temperature ($\mathcal{T} \geq 1$ K), see e.g. [64], and the interaction of electrons on the surface of liquid helium with the liquid surface waves (the electron-ripplon interaction), see e.g. [64, 65]. For $\mathcal{T} < 0.7$ K, the vapor pressure of helium atoms above the

[1] S. Mostame and R. Schützhold, *Quantum simulator for the Ising model with electrons floating on a helium film*, pre-print: `arXiv:0803.1093` (2008).

liquid is basically zero, so that the only significant electron coupling to the outside world is to thermally excited height variations of the helium surface. A brief review of the electronic surface state and the proper form of the electron-ripplon interaction is given below.

Let us assume that the helium film occupies the half space $z < 0$ and electrons are located outside the film. The binding potential, due to the interaction between the electron and the dielectric, is easily derived by putting an image charge in the dielectric. Asymptotically, the interaction takes the classical form

$$V_{\mathrm{B}} \approx -\frac{\varepsilon - \varepsilon_0}{4\varepsilon_0(\varepsilon + \varepsilon_0)} \frac{e^2}{z} \,. \tag{4.1}$$

Since the polarizability $\varepsilon \approx 1.06$ of the helium film is larger than the vacuum value $\varepsilon_0 = 1$, the classical image potential acting on an electron is attractive. The motion along the surface is free-electron like and the wavefunction in the z direction satisfies the Schrödinger equation

$$\frac{1}{2m_e}\left[-\frac{d^2}{dz^2} + 2m_e V(z)\right]\Phi(z) = E_z \Phi(z)\,, \tag{4.2}$$

with

$$V(z) = -\frac{1}{m_e a_0 z} + V_0(z) + eF_{\mathrm{H}} z\,, \tag{4.3}$$

where m_e is the electron mass, a_0 the effective Bohr radius defined by

$$a_0 = \frac{4\varepsilon_0(\varepsilon + \varepsilon_0)}{m_e e^2(\varepsilon - \varepsilon_0)}\,, \tag{4.4}$$

$V_0(z)$ the barrier potential of the film, and F_{H} the effective electric field which is the sum of the applied holding field F_z and the Hartree field due to other electrons. Total electron energy is the sum of the energy due to the perpendicular motion to the surface E_z, and of the energy due to the free motion parallel to the surface $\mathcal{E}_{k_e} = k_e^2/2m_e$, where $\boldsymbol{k}_e$ is the two-dimensional wavevector of an electron. Since the barrier height is of order of 1 eV (see e.g. [66]), and $a_0 = 76$ Å is much larger than the atomic distance of helium, we can practically approximate $V_0(z)$ by the infinite barrier

$$V_0(z) = \begin{cases} \infty & z < 0 \\ 0 & z > 0 \end{cases} \tag{4.5}$$

The wavefunction should be solved with the boundary condition $\Phi(0) = 0$. For the ground state we assume the trial form

$$\Phi_0(z) = 2\, b^{-3/2}\, z \exp\left(-z/b\right)\,, \tag{4.6}$$

for which a variational ansatz yields

$$b = \frac{4a_0}{3\eta} \sinh\left(\frac{1}{3}\sinh^{-1}\frac{9\eta}{4}\right)\,, \tag{4.7}$$

where $\eta = \sqrt{2m_e a_0^3 e F_{\rm H}}$. When $F_{\rm H} \to 0$, the trial form reduces to the exact solution of the Schrödinger equation and the ground state energy is $E_z^{(0)} = 1/2m_e a_0^2$ which is about 0.66 meV or 7.6 K. The smallness of $E_z^{(0)}$ justifies the use of the infinite barrier approximation.
One can also consider the effect of the surface roughness, i.e., the fact that the surface is deformed to $z = u(\boldsymbol{r})$ from $z = 0$ where $\boldsymbol{r}$ is the two dimensional position vector on the surface. This may be described by the ripplon normal coordinate $\mathfrak{Q}_{\boldsymbol{q}}$

$$u(\boldsymbol{r}) = \frac{1}{\sqrt{S}} \sum_{\boldsymbol{q}} \mathfrak{Q}_{\boldsymbol{q}} \ \exp(i\boldsymbol{q}\cdot\boldsymbol{r})\,, \tag{4.8}$$

where $\boldsymbol{q}$ is the two-dimensional momentum vector and S the surface area of the system. In the adiabatic approximation, the interaction potential U_{er} between electrons and ripplons is given by [67]

$$U_{er} = \frac{1}{\sqrt{S}} \sum_{\boldsymbol{q}} \mathfrak{Q}_{\boldsymbol{q}} \exp(i\boldsymbol{q}\cdot\boldsymbol{r}) \left[\zeta_q(z) + eF_z\right]\,, \tag{4.9}$$

with

$$\zeta_q(z) = -\frac{q^2}{m_e a_0} \left\{ \frac{K_1(qz)}{qz} - \frac{1}{(qz)^2} + \frac{\varepsilon - \varepsilon_0}{2(\varepsilon + \varepsilon_0)} K_0(qz) \right\}\,, \tag{4.10}$$

where K_1 and K_0 are modified Bessel functions of the second kind. When U_{er} is projected onto the electron ground state, $\zeta_q(z)$ has to be replaced by its expectation value at the ground state. In the infrared limit, we obtain

$$\zeta_q = \int_0^\infty dz\, \Phi_0^2(z)\, \zeta_q(z) \approx \frac{q^2}{2m_e a_0} \ln \frac{4}{ebq}\,, \tag{4.11}$$

where the small corrections due to the third term in Eq. (4.10) have been discarded. The ripplon normal coordinate $\mathfrak{Q}_{\boldsymbol{q}}$ is related to the creation and annihilation operators of a ripplon, $a_{\boldsymbol{q}}^\dagger$ and $a_{\boldsymbol{q}}$, which is given by [68]

$$\mathfrak{Q}_{\boldsymbol{q}} = \sqrt{\frac{q}{2\rho\,\omega_q}} \ \left(a_{\boldsymbol{q}} + a_{-\boldsymbol{q}}^\dagger\right)\,, \tag{4.12}$$

where ω_q denotes the ripplon angular frequency given by the hydrodynamic equation

$$\omega_q^2 = g_e q + q^3 \xi/\rho\,, \tag{4.13}$$

while $\rho = 0.145\ \mathrm{g/cm^3}$, $\xi = 0.37 \times 10^{-3}\ \mathrm{J/m^2}$ and g_e are the density of the liquid helium, the surface tension and the acceleration due to gravity plus *van der Waals* attraction, respectively. In practice, the first term in the right hand side of this equation is negligible and one can use

the simplified form $\omega_q = (\xi/\rho)^{1/2} q^{3/2}$. Finally, the average mean-square displacement of the surface determined by thermal fluctuations [69] is given by

$$\delta h = \sqrt{\frac{k_{\rm B}\mathcal{T}}{\xi}}\,. \tag{4.14}$$

Unlike in semiconductors, where two-dimensional electron systems have been studied extensively, the electron density above the helium film is significantly lower and can easily be varied over at least four orders of magnitude. By increasing the electron density one can study the phase transition from a classical dilute electron gas into the Wigner crystal.[2] The second phase transition occurs at even higher electron densities, when the Wigner crystal melts into a degenerated Fermi gas (i.e., quantum melting). However, the surface of charged bulk helium becomes unstable at densities greater than $2.4 \times 10^{13}\ \mathrm{m}^{-2}$. The instability grows when the electronic pressure exceeds the gravitational and surface tension restoring pressures. For the case of thin films, the gravitational pressure can be replaced by *van der Waals* attraction to the substrate. The van der Waals attraction greatly increases the stability of the charged film and higher electron densities $(2 \times 10^{16}\ \mathrm{m}^{-2})$ can be reached above thin helium films [71, 72].

4.1.2 The Model

We want to simulate the quantum dynamics of the one-dimensional Ising model which has been introduced in Sec. (3.2.2) of this Thesis. The model consists of n spins with nearest-neighbor interaction J plus a transverse field Γ along the x-direction – which has been introduced in Eq. (3.6)

$$H = -\sum_{j=1}^{n} \left\{ \Gamma\, \sigma_j^x + \, J\, \sigma_j^z \sigma_{j+1}^z \right\}\,, \tag{4.15}$$

where $\sigma_j = (\sigma_j^x, \sigma_j^y, \sigma_j^z)$ are the spin-1/2 Pauli matrices acting on the jth qubit. For $\Gamma \gg J$, the ground state is paramagnetic $|{\rightarrow}{\rightarrow}{\rightarrow}\ldots\rangle$ with all spins polarized along the x axis. In the opposite limit $\Gamma \ll J$, the nature of the ground state(s) changes qualitatively and there are two degenerate ferromagnetic phases with all spins pointing either up or down along the z axis $|{\uparrow}{\uparrow}{\uparrow}\ldots\rangle$ or $|{\downarrow}{\downarrow}{\downarrow}\ldots\rangle$. The two regimes are separated by a quantum phase transition at the critical point $\Gamma_{\rm cr} = J$, where the excitation gap vanishes (in the thermodynamic limit $n \uparrow \infty$) and the response time diverges.

[2] A Wigner crystal is the solid (crystalline) phase of electrons first predicted by Eugene Wigner [70] in 1934. A gas of electrons moving in 2D or 3D in a uniform, inert, neutralizing background will crystallize and form a lattice if the electron density is less than a critical value. This is because the potential energy dominates the kinetic energy at low densities, so the detailed spatial arrangement of the electrons becomes important. To minimize the potential energy, the electrons form a triangular lattice in 2D and a body-centered cubic lattice in 3D. A crystalline state of the 2D electron gas can also be realized by applying a sufficiently strong magnetic field. More generally, a Wigner crystal phase can also refer to a crystal phase occurring in non-electronic systems at low density.

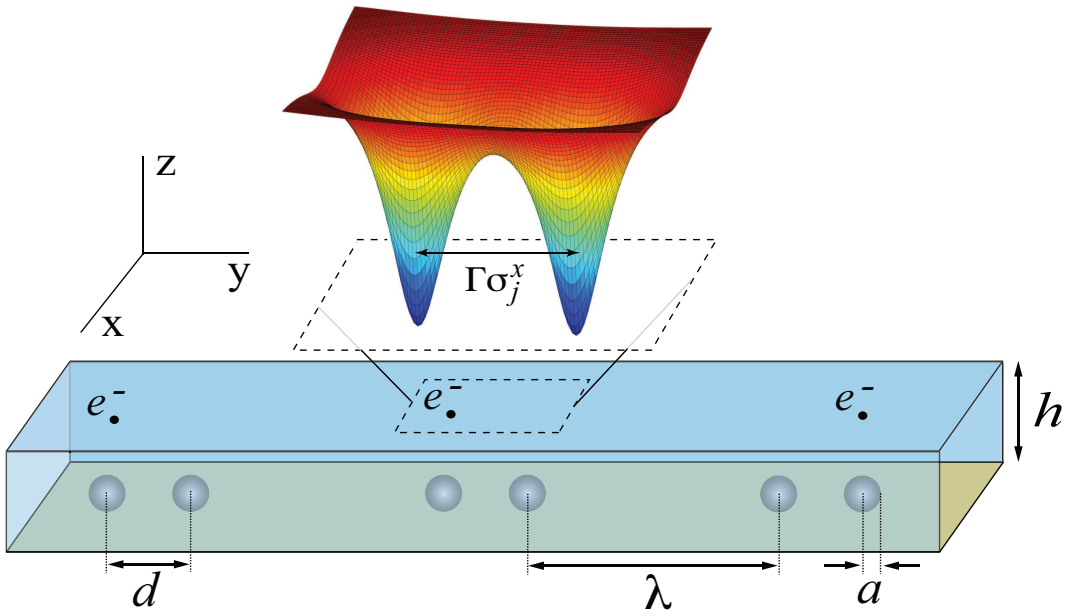

Figure 4.1: Sketch of the proposed analogue quantum simulator. Electrons (e^-) are floating on a low-temperature helium film of height h adsorbed on a silicon substrate. A double-well potential for each single electron is created by a pair of golden spheres of radius a and distance d on the bottom of the helium film. The double wells at each site provide two lowest states of the electron and model the spin states $|\uparrow\rangle$ and $|\downarrow\rangle$ at each site j. The tunneling rate between the two wells corresponds to the transverse field term $\Gamma\sigma_j^x$. The electrons are lined up at distances λ and interact via Coulomb forces, which creates the term $J\sigma_j^z\sigma_{j+1}^z$.

4.1.3 The Analogue

In order to reproduce the quantum dynamics of the 1+1 dimensional Ising model (4.15), we propose trapping a large number of electrons on a low-temperature helium film of thickness h (e.g., $h = 110$ nm) adsorbed on a silicon substrate. Due to the polarizability $\varepsilon \approx 1.06$ of the Helium film, the electrons are bound to its surface (i.e., in z-direction) via their image charges and the large potential barrier (around 1 eV) for penetration into the helium film. Since the binding energy of around 8 K is much larger than the temperature $\mathcal{T}$ (below 1 K) and the width of the electron wave packet in z-direction (of order 8 nm) is much smaller than all other relevant length scales, the electron motion is approximately two-dimensional (x, y-plane).

In our scheme, each single electron on top of the helium film is trapped by a pair of golden spheres of radius a (e.g., $a = 10$ nm) and distance d (e.g., $d = 60$ nm) attached to the silicon substrate, i.e., on the bottom of the helium film, cf. Fig. (4.1). Depending on its position x, y,

the electron will also induce image charges in the two golden spheres (which act as a pair of quantum dots) and hence experience a double-well potential

$$U_{\rm w}(x,y) = -\frac{ae^2}{4\pi\varepsilon}\frac{x^2+y^2+\alpha^2+\beta^2}{\left(x^2+y^2+\alpha^2+\beta^2\right)^2-4\alpha^2y^2}\,, \tag{4.16}$$

with $\alpha = d/2 + a$ and $\beta^2 = h^2 - a^2$. Since this potential is quite deep and symmetric $U_{\rm w}(x,y) = U_{\rm w}(x,-y)$, cf. Fig. (4.2), the ground state wave-function $\psi_{\rm S}(x,y)$ is given by the symmetric superposition of the two Wannier states $\psi_0(x,\pm y)$ while the first excited state $\psi_{\rm A}(x,y)$ is the anti-symmetric combination

$$\begin{aligned}\psi_{\rm S}(x,y) &= \frac{\psi_0(x,y)+\psi_0(x,-y)}{\sqrt{2}} \;\rightarrow\; \frac{|\uparrow\rangle+|\downarrow\rangle}{\sqrt{2}}\,,\\ \psi_{\rm A}(x,y) &= \frac{\psi_0(x,y)\;-\;\psi_0(x,-y)}{\sqrt{2}} \;\rightarrow\; \frac{|\uparrow\rangle-|\downarrow\rangle}{\sqrt{2}}\,.\end{aligned} \tag{4.17}$$

For a sufficiently high potential barrier between the two wells, the Wannier state $\psi_0(x,y)$ is strongly concentrated in the left well and models the spin state $|\uparrow\rangle$ and vice versa. The tunneling between the two states is then described by the Pauli operator σ^x with $\sigma^x|\uparrow\rangle = |\downarrow\rangle$ and $\sigma^x|\downarrow\rangle = |\uparrow\rangle$ such that the tunneling rate, given by the difference of the eigenenergies $E_A - E_S$ of $\psi_{\rm S}$ and $\psi_{\rm A}$, corresponds to the transverse field Γ in Eq. (4.15). In the limit of strong localization (i.e., weak tunneling), the energy splitting $E_A - E_S$ between the two levels can be estimated via the WKB approximation [74]

$$2\Gamma = E_{\rm A} - E_{\rm S} \approx \frac{\omega}{\pi}\exp\left[-\int_{-y_0}^{y_0} dy\;|p(y)|\right]\,. \tag{4.18}$$

Here $\pm y_0$ are the two inner (classical) turning points, cf. Fig. (4.2), and $\omega = 2\pi/T_0$ is the oscillation frequency (within one well) where

$$T_0 = 2m_e\int_{-y_1}^{-y_0}\frac{dy}{p(y)}\,, \tag{4.19}$$

is the period. The integrand is given by $p(x,y) = \sqrt{2m_e\left[E_0 - U_{\rm w}(x,y)\right]}$, where we can set $x = 0$ since the tunneling probability away from the $x = 0$-axis is strongly suppressed. Finally, the energy E_0 determines the turning points and m_e is the electron mass. For the parameters above, each valley can well be approximated by a harmonic oscillator

$$U_{\rm w}(x, y \approx \pm y_{\rm min}) \approx \frac{ae^2}{4\pi\varepsilon\beta^4}(x^2 + [y \mp y_{\rm min}]^2)\,, \tag{4.20}$$

and thus we obtain

$$E_0 \approx \sqrt{\frac{ae^2}{2\pi\varepsilon m_e\beta^4}} \approx \omega\,. \tag{4.21}$$

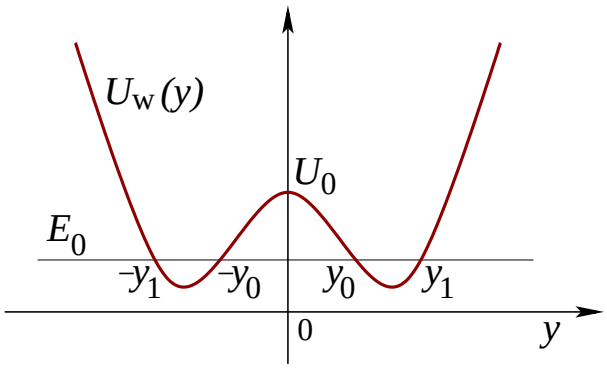

Figure 4.2: Sketch of the double-well potential $U_{\rm w}(y)$ in Eq. (4.16) with four turning points for the energy E_0.

So far, we derived the term $\Gamma\sigma_j^x$ in Eq. (4.15) via Eqs. (4.16), (4.17), (4.18), and (4.20). In order to simulate the remaining part, we propose to line up the pairs of quantum dots at equal distances λ (e.g., $\lambda = 600$ nm), where the parameters are supposed to obey the following hierarchy

$$\lambda \gg h > d \gg a\,. \tag{4.22}$$

In this limit, the interaction between the electrons will be dominated by the direct Coulomb repulsion between nearest neighbors $U_{\rm c}(x,y) = \sum_{j=1}^{n} U_{\rm c}^{j,j+1}$ with n denoting the number of electrons floating on the helium film. For $\lambda \gg d$, we may Taylor expand the Coulomb interaction into powers of y/λ due to $y \approx \pm d/2$. The zeroth-order term is constant and thus irrelevant while the first-order contributions vanish (up to boundary terms) after the sum over sites j. Thus, the leading term is bilinear in the electron positions

$$U_{\rm c}(x,y) \approx -\frac{e^2}{2\pi\varepsilon_0\,(\lambda+d+4a)^3}\sum_{j=1}^{n} y_j y_{j+1}\,, \tag{4.23}$$

and precisely corresponds to the $J\sigma_j^z\sigma_{j+1}^z$ term in Eq. (4.15) with the effective coupling

$$J = \frac{e^2(d+2a)^2}{8\pi\varepsilon_0(\lambda+d+4a)^3}\,. \tag{4.24}$$

As an alternative set-up, one may arrange the pairs of quantum dots in parallel (i.e., as a ladder), cf. Fig. (4.3). Adjusting the distance accordingly

$$\lambda' = (\lambda+d+4a)/\sqrt[3]{2}\,, \tag{4.25}$$

e.g., $\lambda' = 560$ nm instead of $\lambda = 600$ nm, we obtain the same coupling strength J at lowest order, provided that σ_j^z is identified with the electron position in alternating order. Combining the line and the ladder design then facilitates the realization of the two-dimensional Ising model, cf. Fig. (4.4).

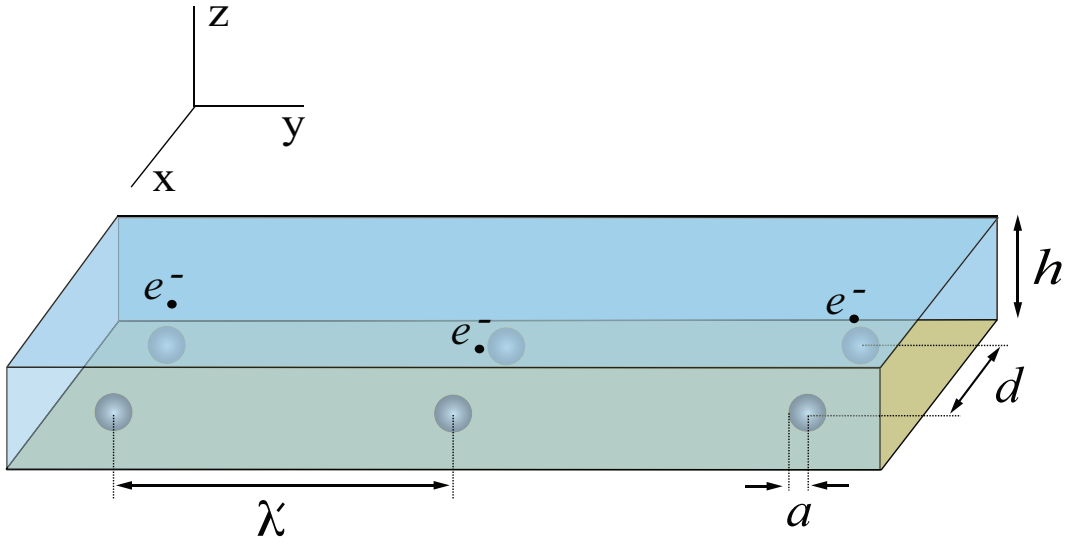

Figure 4.3: An alternative analogue quantum simulator. The pairs of quantum dots have been arranged in parallel.

4.1.4 Experimental parameters

For the example values given in the text, we obtain $\Gamma \approx 0.1$ K for the tunneling rate and the same value $J \approx 0.1$ K for the effective coupling, i.e., we are precisely in the quantum critical regime. However, deviations from this critical point should be easy to realize experimentally by varying the height h of the helium film, e.g., via changing the effective chemical potential difference between the thin helium film and the helium reservoir.[3] This deviation is possible because the tunneling rate depends strongly – in fact, exponentially – on h whereas the Coulomb force remains approximately constant, see also table (4.1). In order to see quantum critical behavior, i.e., to avoid thermal fluctuations, the temperature should ideally be well below this value 0.1 K (or at least not far above it).

Furthermore, the Coulomb repulsion energy between two electrons (zeroth-order term) of about 11 K would tend to destabilize the electron chain. Fortunately, this effect is compensated by the binding energy between the electron and its image on the sphere, which is around 13 K and thus stabilizes the electron chain. The probability for the electron to penetrate the helium film by tunneling to one of the golden spheres is extremely small (of order 10^{-16}) and can be neglected. Finally, the ground-state energy $E_0 \approx 1.4$ K (within the harmonic oscillator approximation) is reasonably well below the barrier height $U_0 \approx 3.1$ K such that the WKB approximation should provide a reasonable estimate.[4] On the other hand, $E_0 \approx 1.4$ K is a measure of the distance between the two lowest-lying states in Eq. (4.17) and the remaining excited states in

[3] This can be done, for example, by enclosing the reservoir in a capacitor with a variable voltage.

[4] The tunneling probability of 0.08 is also small enough.

h [nm]	100	105	110	115	120
Γ [K]	0.0471	0.0731	0.0918	0.1152	0.1387

Table 4.1: The tunneling rate Γ depends strongly on the height of the helium film h, e.g., varying h by 10%, Γ changes by 50%.

the double-well potential. As a result, these additional states do not play a role for temperatures well below one Kelvin and thus the Hamiltonian (4.15) provides the correct low-temperature description.

4.1.5 Read-out scheme

Having successfully simulated the Ising Hamiltonian (4.15), one is led to the question of how to actually measure its properties, e.g., how to detect signatures of quantum critical behavior. As one possibility, let us imagine having the golden spheres not grounded, but connecting them to small wires which allow us to address them individually or in suitable partitions. For example, applying a voltage of one μV between the spheres associated with spin up $|\uparrow\rangle$ and spin down $|\downarrow\rangle$, respectively, induces a perturbation Hamiltonian $\upsilon\,\sigma_j^z$ corresponding to a longitudinal field[5] of $\upsilon = \mathcal{O}(10^{-3}\mathrm{K})$, i.e., a weak perturbation $\upsilon \ll \Gamma$. Deep in the paramagnetic phase $\Gamma \gg J$, the response of the system to this weak perturbation $\upsilon \ll \Gamma$ is rather small

$$\langle \sigma_j^z \rangle \approx \frac{\upsilon}{\Gamma}\,. \tag{4.26}$$

Approaching the phase transition, however, the static susceptibility

$$\chi_\upsilon = \lim_{\upsilon \to 0} \langle \sigma_j^z \rangle / \upsilon\,, \tag{4.27}$$

grows and finally diverges at the critical point. In the broken symmetry phase, the perturbation $\upsilon\,\sigma_j^z$ lifts the degeneracy $\sigma_j^z \to -\sigma_j^z$ and hence the response is non-analytic, i.e., independent of the smallness of υ: e.g., for $J \gg \Gamma$, we have $\langle \sigma_j^z \rangle = \mathrm{sign}(\upsilon) = \pm 1$.
This signal $\langle \sigma_j^z \rangle$ indicating the phase transition can be picked up by measuring the voltage difference induced by the position of the electron. If the spheres are not grounded but isolated, the electron image charge induces a voltage difference of up to 13 mV between the two spheres. Clearly, this would constitute a large disturbance and thus one should put a resistor or capacitor between them in order to reduce the voltage difference to a few μV. However, since the associated charge transfer is small (a fraction of the elementary charge e), a site-by-site read-out is probably very hard to realize. Nevertheless, collecting signal from many electrons should lead to measurable currents. Preferably, this measurement should be done using other spheres than

[5] In addition to the transversal field $\Gamma\,\sigma_j^x$.

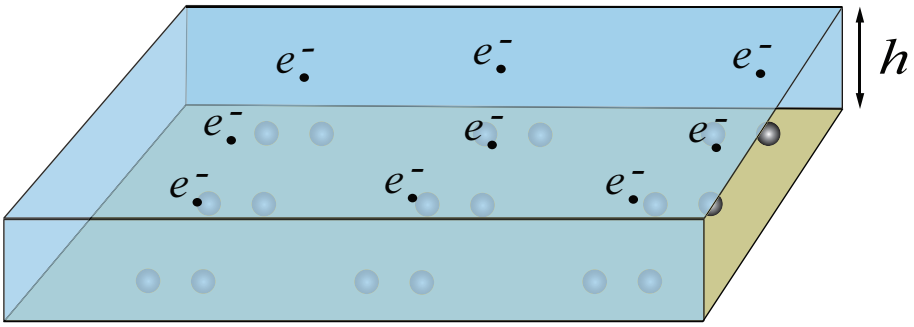

Figure 4.4: Sketch of the analogue quantum simulator for two-dimensional (spatial) Ising Model.

the one on which the external voltage has been applied. E.g., one could apply the external voltage of one μV on half of the electrons and measure (with suitably adapted internal resistances) the internal response $\langle\sigma_j^z\rangle$ on the other half – or in large enough sub-sets (partitions).
Comparing the signals from the different partitions then yields information about the correlator $\langle\sigma_i^z\sigma_j^z\rangle$. In addition to the static case, one could also study the time-resolved response $\langle\sigma_j^z(t)\rangle$ to a varying voltage $\upsilon(t')$, which is determined by the dynamical correlator $\langle\sigma_i^z(t')\sigma_j^z(t)\rangle$ in lowest-order response theory. Even in the absence of an externally imposed voltage, the chain induces spontaneous voltage fluctuations in the electrodes, which are strongest deep in the ferromagnetic phase. The variance of these fluctuations yields the correlator sum $\sum_{ij}\langle\sigma_i^z\sigma_j^z\rangle$ which is an order parameter for the phase transition and allows us to detect topological defects (i.e., kinks) which might have been produced during the sweep to the ferromagnetic phase.

4.1.6 Disorder and decoherence

In a real experimental set-up, the Hamiltonian will not be exactly equivalent to (4.15) due to imperfections such as electric stray fields, variations in the film thickness h and further geometric parameters a, d, and λ etc. Therefore, the original expression (4.15) will typically be altered to

$$H = -\sum_{j=1}^{n}\left\{\Gamma_j\,\sigma_j^x + J_j\,\sigma_j^z\sigma_{j+1}^z + \upsilon_j\sigma_j^z\right\}\,, \tag{4.28}$$

where $\Gamma_j = \bar{\Gamma} + \delta\Gamma_j$ and $J_j = \bar{J} + \delta J_j$. Assuming that the disorder parameters $\delta\Gamma_j$, δJ_j, and υ_j are much smaller than the excitation gap $\Delta = 2|J-\Gamma|$ of the undisturbed system[6] (in the

[6] According to the discussions in Sec. (3.5) of this Thesis, the diagonalized Hamiltonian of the quantum Ising model in a transverse field is given by Eq. (3.45), $H_{\rm sys}(t) = \sum_k \mathscr{E}_k(t)\left(\gamma_k^\dagger\gamma_k - 1/2\right)$ with the single particle energy $\mathscr{E}_k(t) = 2\sqrt{J^2+\Gamma^2-2J\Gamma\cos(ka)}$. In the continuum limit, the energy gap or the minimum excitation energy is always at $k=0$ and equals $\Delta = 2|J-\Gamma|$.

continuum limit), the impact of these imperfections will be suppressed. Near the critical point $J \approx \Gamma$, however, this argument fails. Still, for a finite number n of electrons, one retains a minimum gap[7] (within the symmetric or anti-symmetric subspace, respectively) of order J/n. Exploiting this gap might be suitable for a reasonably small systems, but for $n \geq 100$ electrons, the required accuracy on the sub-percent level is probably hard to achieve experimentally. For example, decreasing the diameter of the golden spheres by ten percent with the other values remaining the same as before, the tunneling rate increases by fifty percent.

For a sufficiently large number of electrons, the relevance of the disorder induced by imperfections near the critical point depends on the dimensionality of the system. In one spatial dimension, the critical exponent $\mathfrak{d} = 1$ of the Ising model indicates that the renormalization flow is directed away from the homogeneous situation, see, e.g., [37], which means that disorder becomes important at large scales $n \to \infty$. In this case, one would expect effects such as local paramagnetic regions inside the global ferromagnetic phase and percolation transitions etc. Therefore, turning this drawback into an advantage, one might generate these imperfections on purpose in order to study the impact of disorder onto the phase transition. In contrast to the original Hamiltonian (4.15), the above form (4.28) is no longer analytically solvable and hence much less is known about its properties.

Finally, in a real set-up, the system will also experience decoherence due to the inevitable coupling to the environment [44]. These effects could be incorporated by operator-valued variations $\delta\Gamma_j$, δJ_j, and υ_j associated to the degrees of freedom of the environment. According to [75], the main decoherence channels in the set-up under consideration are due to the coupling to ripplons, i.e., surface waves on the helium film. Their thermal fluctuations given in Eq. (4.14) have an amplitude of $\delta h = \sqrt{k_{\mathrm{B}}\mathcal{T}/\xi} \approx 0.06$ nm at $\mathcal{T} = 0.1$ K. Since δh is extremely small compared to $h = 110$ nm, the coupling terms and energy shifts induced by these height variations are negligible here. Furthermore, the energy ω of the ripplons itself depends on their wavenumber q via Eq.(4.13), $\omega^2 \approx q^3\xi/\varrho$. For typical wavelengths of the ripplons coupled to the electrons of order 100 nm, the ripplon energy is below 0.01 K and hence also negligible. Consequently, even though the ripplons might induce significant dephasing and decay of *excited* states, see [75], they basically do not affect the quantum *ground* state. However, near the quantum phase transition, where the energy levels become arbitrarily close, even these small ripplon couplings cause excitations – as we have studied extensively in the third chapter of this Thesis.

[7] At the critical point $J = \Gamma$, all the excitation energies $\mathscr{E}_k$ take their minimum values, $\mathscr{E}_k^{\min} = 2\,|J \sin(ka/2)|$. Since the pseudo-momenta k scale with the inverse n, see Eq. (3.44), the minimum gap near the critical point is of order J/n.

4.2 Quantum Simulator for the $O(3)$ Nonlinear σ Model

This section based on publication[8] [76] and we propose another design for the construction of a laboratory system based on present-day technology which simulates the quantum dynamics of the $O(3)$ nonlinear sigma model. Apart from its relevance in condensed-matter theory, this strongly interacting quantum field theory serves as an important toy model for quantum chromodynamics (QCD) since it reproduces many crucial properties of QCD.

4.2.1 The Nonlinear Sigma Model

Spontaneous symmetry breaking is one of the most typical phenomena in physics which acquires gapless particles in the spectrum of the system. These particles represent slowly varying fluctuations of the order parameter. The low energy interaction of these Goldstone particles are uniquely determined by the pattern of symmetry breaking and often described by the so called *nonlinear sigma model* (see, e.g., [77]-[96]). Nonlinear sigma models are field theories whose elementary fields or dynamical variables are maps from a space (the source space) to an auxiliary space (the target space). The Lagrangian governing the dynamics of the model measures the total energy of those maps. The classical solutions of the model, i.e., the solutions of the corresponding field equations, constitute the space of field configurations where the solitons of the model are localized. The dimension of the source space is called the dimension of the model so as the isometry group of the target space is the symmetry of the model.
Two dimensional nonlinear sigma models, in particular those with symmetry $O(3)$ are ubiquitous in physics (see, e.g., [97, 98]) with applications from condensed-matter physics (partly due to its relation to spin-systems such as anti-ferromagnets, see, e.g.,[99, 100, 101]) to high-energy physics [102, 103, 104] and, of course, quantum field theory [105]. For statistical mechanics the $O(N)$ nonlinear sigma model describe the infrared properties of the N-component classical Heisenberg ferromagnet as obtained from the low-temperature expansion [77]. This kind of universality is strongly related to the fact that those sigma models and equations governing their dynamics have a deep underlying geometric meaning which provides a powerful reason to explain the great interest of those models in physics and applied mathematics, see, e.g., [106].
The $O(N)$ sigma model in two-dimensional space-time is introduced as a field theory constrained to live on a sphere. It is described by the $O(N)$ and Poincaré invariant action

$$\mathfrak{L} = \frac{1}{2}\,\partial_\nu \boldsymbol{\sigma} \cdot \partial^\nu \boldsymbol{\sigma} = \frac{1}{2}\left[(\partial_t \boldsymbol{\sigma})^2 - c^2(\partial_x \boldsymbol{\sigma})^2\right] , \tag{4.29}$$

with the internal vector $\boldsymbol{\sigma} = (\sigma_1, \sigma_2, \ldots, \sigma_N) \in \mathbb{R}^N$ reflecting the $O(N)$-symmetry. So far, this

[8] R. Schützhold and S. Mostame, *Quantum simulator for the O(3) nonlinear sigma model*, JETP Lett. **82**, 248 (2005).

theory describes N independent free fields, but the constraint

$$\boldsymbol{\sigma}^2 = \sigma_1^2 + \sigma_2^2 + \cdots + \sigma_N^2 = \frac{N}{\mathfrak{g}^2}\,, \tag{4.30}$$

introduces an interaction corresponding to the coupling $\mathfrak{g} > 0$. For vanishing coupling $\mathfrak{g} \downarrow 0$, the curvature of the constraint sphere ($\boldsymbol{\sigma}^2 = N/\mathfrak{g}^2$) vanishes and we reproduce (locally) an effectively free theory. For finite coupling $\mathfrak{g} > 0$, we obtain a non-trivially interacting theory as long as $N \geq 3$, i.e., in the non-Abelian case. The classical ground state $\boldsymbol{\sigma} = \mathrm{const}$ is $O(N)$-degenerate, but quantum interaction lifts that degeneracy and gives the classical Goldstone modes a mass gap, see, e.g., [82]-[88].

4.2.2 Properties

The sigma model is *renormalizable* in 1+1 dimensions, cf. [93]-[96]. Furthermore, it is exactly *solvable* in the large-N limit, where it corresponds to massive free fields with sub-leading (in $1/N$) interaction terms, see, e.g., [82]. In order to give a brief review of the $O(N)$ sigma model in this limit, it is convenient to normalize $\boldsymbol{\sigma}$ fields to 1

$$\mathfrak{L} = \frac{N}{2\mathfrak{g}^2}\,\partial_\nu\boldsymbol{\sigma}\cdot\partial^\nu\boldsymbol{\sigma} \qquad , \qquad \boldsymbol{\sigma}^2 = 1\,. \tag{4.31}$$

The action $\mathcal{S}$ and the generating functional for the Green functions $\mathcal{Z}$ in Euclidean space-time can be written by virtue of a Lagrange multiplier β

$$\mathcal{S}[\boldsymbol{\sigma},\beta] = \frac{1}{2}\int d^2r\left\{\partial_\nu\boldsymbol{\sigma}\cdot\partial^\nu\boldsymbol{\sigma} - \frac{\beta}{\sqrt{N}}\left[\boldsymbol{\sigma}\cdot\boldsymbol{\sigma} - \frac{N}{\mathfrak{g}^2}\right]\right\}\,, \tag{4.32}$$

and

$$\mathcal{Z}[\boldsymbol{J}] = \int D\sigma\, D\beta\, \exp\left\{-\mathcal{S} + \int d^2r\; \boldsymbol{J}\cdot\boldsymbol{\sigma}\right\}\,. \tag{4.33}$$

The action (4.32) is bilinear in $\boldsymbol{\sigma}$ and therefore, the functional integral over σ in Eq. (4.33) is readily calculable

$$\mathcal{Z}[\boldsymbol{J}] = \int D\beta\, \exp\left\{-\mathcal{S}_{\text{eff}} + \frac{1}{2}\int d^2r\; \boldsymbol{J}\cdot\left[\frac{1}{-\partial^2 + \beta/\sqrt{N}}\,\boldsymbol{J}\right]\right\}\,, \tag{4.34}$$

with

$$\mathcal{S}_{\text{eff}} = \frac{N}{2}\,\mathrm{tr}\,\ln\left[-\partial^2 + \frac{\beta}{\sqrt{N}}\right] - \int d^2r\,\frac{\sqrt{N}}{2\mathfrak{g}^2}\,\beta\,. \tag{4.35}$$

where $1/\left(-\partial^2 + \beta/\sqrt{N}\right)$ is a symbolic notation for the Green function of the operator

$-\partial^2 + \beta/\sqrt{N}$. In Eq. (4.34), there exists a stationary point in β and the remaining functional integral can be solved via the saddle-point (or stationary phase) approximation. Lorentz invariance suggests that the stationary value of β is actually independent of r and we can denote this constant by $\sqrt{N}\Lambda^2$, where Λ is the scale parameter. Then $\beta = \sqrt{N}\Lambda^2 + \beta_{\rm qu}$, where deviations $\beta_{\rm qu}$ from the stationary point $\beta_{\rm c} = \sqrt{N}\Lambda^2$ describe quantum fluctuations of the β field. We might expand $\mathcal{S}_{\rm eff}$ in terms of $\beta_{\rm qu}$ assuming the fluctuations to be small

$$\begin{aligned}\mathcal{S}_{\rm eff} &= \frac{N}{2}\,{\rm tr}\ln\left(-\partial^2+\Lambda^2\right) - \frac{N}{2}\int d^2r\,\frac{\Lambda^2}{\mathfrak{g}^2} \\ &\quad + \frac{N}{2}\sum_{l=1}^{\infty}\frac{(-1)^{l+1}}{l}\,{\rm tr}\left[\frac{1}{-\partial^2+\Lambda^2}\,\frac{\beta_{\rm qu}}{\sqrt{N}}\right]^l \\ &\quad - \frac{\sqrt{N}}{2\mathfrak{g}^2}\int d^2r\,\beta_{\rm qu}\,. \end{aligned} \tag{4.36}$$

The first two terms in the expansion are inessential constants and the linear term in $\beta_{\rm qu}$ can be transformed in the following way

$${\rm tr}\left[\frac{1}{-\partial^2+\Lambda^2}\,\beta_{\rm qu}\right] = \int d^2r\;\langle r|\,\frac{1}{-\partial^2+\Lambda^2}\,|r\rangle\,\beta_{\rm qu} = \int\frac{d^2p'}{(2\pi)^2}\,\frac{1}{p'^2+\Lambda^2}\int d^2r\,\beta_{\rm qu}\,,$$

where p' denote momenta. The integral over momenta is ultraviolet divergent, so one must introduce a cut-off momentum p. The integral can be done explicitly and the answer turns out to be

$$\int\frac{d^2p'}{(2\pi)^2}\,\frac{1}{p'^2+\Lambda^2}\;\longrightarrow\;\frac{1}{4\pi}\ln\frac{p^2}{\Lambda^2}\,. \tag{4.37}$$

Moreover, for the procedure to be consistent with the saddle-point condition, the expansion of the effective action (4.36) should contain no term linear in $\beta_{\rm qu}$. This leads to

$$\frac{1}{\mathfrak{g}^2} = \frac{1}{4\pi}\,\ln\frac{p^2}{\Lambda^2} \tag{4.38}$$

The bilinear term in the expansion in $\beta_{\rm qu}$ of $\mathcal{S}_{\rm eff}$

$$\mathcal{S}^{(2)}_{\rm eff} = -\frac{1}{4}\,{\rm tr}\left[\frac{1}{-\partial^2+\Lambda^2}\,\beta_{\rm qu}\right]^2 = -\frac{1}{4}\int d^2r\,d^2r'\,\beta_{\rm qu}\,\mathfrak{F}(r-r')\,\beta_{\rm qu}(r')\,, \tag{4.39}$$

describes the propagation of β particles. Their propagator evidently reduces to $D^{\beta}(p') = -2/\mathfrak{F}(p')$, where $\mathfrak{F}(p')$ is the Fourier transform of $\mathfrak{F}(r-r')$

$$\begin{aligned}\mathfrak{F}(p') &= \int\frac{d^2\mathfrak{r}}{(2\pi)^2}\frac{1}{(\mathfrak{r}^2+\Lambda^2)\,[(p'+\mathfrak{r})^2+\Lambda^2]} \\ &= \frac{1}{2\pi}\,\frac{1}{\sqrt{p'^2(p'^2+4\Lambda^2)}}\,\ln\frac{\sqrt{p'^2+4\Lambda^2}+\sqrt{p'^2}}{\sqrt{p'^2+4\Lambda^2}-\sqrt{p'^2}}\,. \end{aligned} \tag{4.40}$$

However, the function $D^{\beta}(p')$ has no poles in p'^2 and only a cut starting at $p'^2 = -4\Lambda^2$. Therefore, strictly speaking, the β field does not corresponds to any real particles. Knowing the propagator $D^{\beta}(p')$ one can easily calculate $\mathcal{Z}[\boldsymbol{J}]$ by perturbation theory.
The running coupling of the sigma model $\mathfrak{g}(p^2)$ in Eq. (4.38) generates *asymptotic freedom*

$$\mathfrak{g}^2(p^2 \gg \Lambda^2) \propto \frac{1}{\ln(p^2/\Lambda^2)}\,. \tag{4.41}$$

Indeed, at small distances $p \to \infty$ and for fixed Λ the running coupling $\mathfrak{g}(p^2)$ vanishes ($\mathfrak{g} \to 0$) and the constariant (4.30) which creates strong interactions at small momenta, leaves the theory asymptotically free. Eq. (4.41) also implies the so-called *dimensional transmutation*. In analogy to QCD, the classical scale invariance $x^{\nu} \to \Omega\, x^{\nu}$ is broken dynamically corresponding to the dimensional transmutation $\mathfrak{g} \to \Lambda$. Furthermore, the sigma model generates *non-vanishing vacuum condensates* in the operator product expansion. The β field develops a non-vanishing vacuum expectation value $\langle 0|\,\beta\,|0\rangle = \sqrt{N}\Lambda^2$, which automatically leads to the non-vanishing vacuum condensates $\langle 0|\,\mathfrak{L}\,|0\rangle \neq 0$ and also reproduces the trace anomaly $\langle 0|\,T^{\nu}_{\nu}\,|0\rangle \neq 0$ (see, e.g., [82]).
For $N = 3$, the sigma model exhibits *instantons*.[9] The configurational space in which the $\boldsymbol{\sigma}$ fields are defined is topologically equivalent to a two-dimensional sphere. On the other hand, in the $O(3)$ model the $\boldsymbol{\sigma}$ fields live on the same two-dimensional sphere,

$$\sigma_1^2 + \sigma_2^2 + \sigma_3^2 = \frac{3}{\mathfrak{g}^2}\,. \tag{4.42}$$

Thus, there should exist topologically non-equivalent classes of field configurations corresponding to topologically distinct mappings of the two spheres on each other $\left(\mathbb{S}_2 \to \mathbb{R}^2\right)$[10] cf. [79]-[82].

4.2.3 The Analogue

In order to reproduce the quantum dynamics of the the 1+1 dimensional $O(N)$ σ-model according to Eqs. (4.29) and (4.30), let us consider a large number of perfectly insulating thin hollow spheres with the radius R lined up at equal distances Δx with single electrons being captured

[9] An instanton is a classical solution to equations of motion with a finite, non-zero action, either in quantum mechanics or in quantum field theory. More precisely, it is a solution to the equations of motion of the classical field theory on a Euclidean spacetime. In such a theory, solutions to the equations of motion may be thought of as critical points of the action that might be local maxima of the action, local minima, or saddle points. In quantum field theory, they appear in the path integral as the leading quantum corrections to the classical behavior of a system, and also they can be used to study the tunneling behavior in various systems such as a Yang-Mills theory [107].

[10] It is also clear that for an $O(N)$ group with $N > 3$ all mappings $\left(\mathbb{S}_2 \to \mathbb{R}^{N-1}\right)$ are topologically equivalent to the trivial one and, hence, instantones are absent.

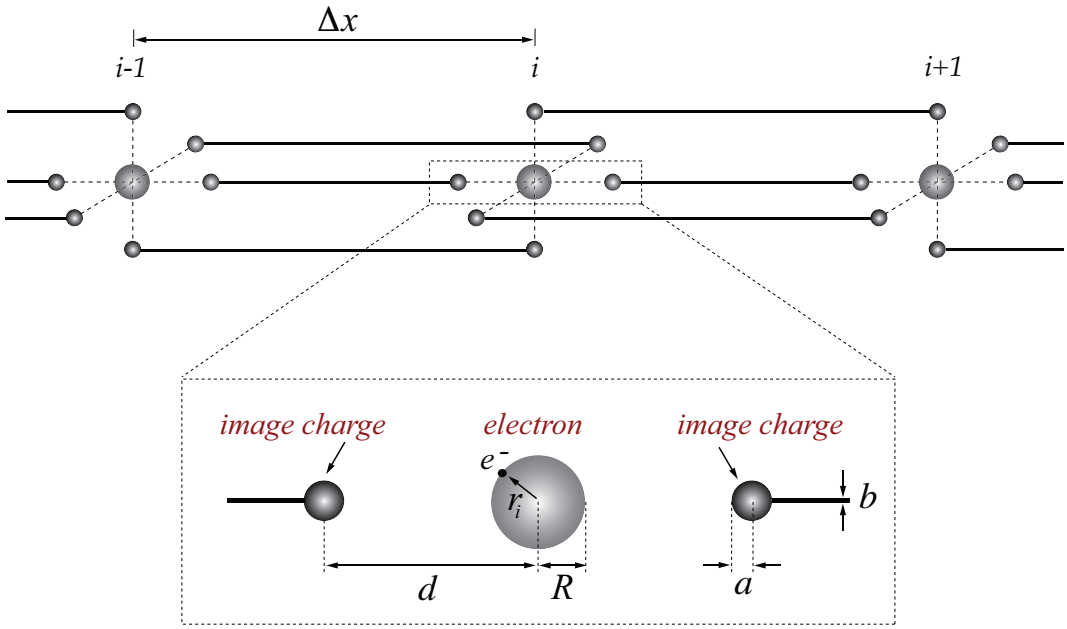

Figure 4.5: Sketch of the proposed analogue quantum simulator. The solid lines and spheres denote (super) conductors and the hollow spheres are insulators containing single electrons. Shown are just three elements of a long chain (top) and a close-up view (bottom) with the involved length scales.

by the polarizability (inducing a finite extraction energy) on each of the hollow spheres. These insulating spheres are surrounded by an arrangement of superconducting spheres (radius a) and wires (radius b) as depicted in Fig. (4.5), which generate controlled interactions of the confined electrons via their image charges. The involved length scales including the typical wavelength of the excitations λ, the distance of elements (lattice spacing) Δx, the distance between the insulating and the conducting spheres d, the radii of the insulating and conducting spheres R and a and wires b, cf. Fig. (4.5), are supposed to obey the following hierarchy

$$\lambda \gg \Delta x \gg d \gg R, a \gg b\,. \tag{4.43}$$

The total Lagrangian for the system of electrons reads

$$\mathfrak{L} = \sum_i \left[\frac{m_e}{2}\, \dot{\boldsymbol{r}}_i^{\,2} - U(\boldsymbol{r}_{i+1}, \boldsymbol{r}_i) \right] , \tag{4.44}$$

with m_e being the mass of the electrons and $U(\boldsymbol{r}_{i+1}, \boldsymbol{r}_i)$ their interaction potential, where only nearest neighbors are taken into account in view of the assumptions (4.43). The images of the electron charges e on the superconducting spheres

$$\mathfrak{q}_{(i,\pm)} = -\frac{a}{|\boldsymbol{r}_i \pm d\,\boldsymbol{e}_x|}\, e\,, \tag{4.45}$$

with $\boldsymbol{e}_x = \boldsymbol{\Delta x}/\Delta x$, induce the interaction potential $U(\boldsymbol{r}_{i+1}, \boldsymbol{r}_i)$ which can be simplified in the limit of the assumptions (4.43)

$$\begin{aligned} U(\boldsymbol{r}_{i+1}, \boldsymbol{r}_i) &= \frac{1}{2}\left\{ -\frac{ae^2}{4\pi\varepsilon_0 \left(\boldsymbol{r}_i - d\,\boldsymbol{e}_x\right)^2} + \frac{2a^2e^2}{4\pi\varepsilon_0 d^2 \left|\boldsymbol{r}_i - d\,\boldsymbol{e}_x\right|} \frac{2d - \left|\boldsymbol{r}_{i+1} - \boldsymbol{r}_i\right|}{4a + \Delta x/\ln(\Delta x/b)} \right. \\ &\qquad \left. -\frac{ae^2}{4\pi\varepsilon_0 \left(\boldsymbol{r}_i + d\,\boldsymbol{e}_x\right)^2} + \frac{2a^2e^2}{4\pi\varepsilon_0 d^2 \left|\boldsymbol{r}_i + d\,\boldsymbol{e}_x\right|} \frac{2d - \left|\boldsymbol{r}_{i+1} - \boldsymbol{r}_i\right|}{4a + \Delta x/\ln(\Delta x/b)} \right\} \\ &\approx \frac{a^2e^2}{4\pi\varepsilon_0 d^4} \frac{(\boldsymbol{r}_{i+1} - \boldsymbol{r}_i)^2}{4a + \Delta x/\ln(\Delta x/b)}\,, \end{aligned} \tag{4.46}$$

where the first addend in the denominator on the right-hand side is due to the capacitance of the conducting spheres $4\pi\varepsilon_0 a$ and the second one due to the capacitance of the long wires $2\pi\varepsilon_0 \Delta x/\ln(\Delta x/b)$. Comparing the resulting Lagrangian in Eqs. (4.44) and (4.46) with the one in Eq. (4.29), we can read off the effective propagation speed

$$c_{\text{eff}} = \sqrt{\frac{e^2}{4\pi\varepsilon_0 m_e} \frac{2a^2\Delta x^2/d^4}{4a + \Delta x/\ln(\Delta x/b)}}\,. \tag{4.47}$$

Since the first term under the root represents the classical electron radius (of order 10^{-15} m), the effective propagation speed c_{eff} is much smaller than the speed of light in vacuum $c_0 \gg c_{\text{eff}}$ for realistic parameters (see below), i.e., we obtain a large slow-down. Furthermore, we may identify the effective coupling for $N = 3$

$$\mathfrak{g}_{\text{eff}} = \sqrt{3}\,\frac{d}{R} \sqrt[4]{\frac{4\pi\varepsilon_0}{m_e e^2} \frac{4a + \Delta x/\ln(\Delta x/b)}{2a^2}}\,, \tag{4.48}$$

where the first term under the root is the classical electron radius over the square of the fine structure constant. The value of the effective coupling can be tuned by varying the ratio $d/R \gg 1$ and may well be of order one (see parameters below). Strictly speaking, the above equation determines the value of the running coupling $\mathfrak{g}_{\text{eff}}(p^2)$ at a length scale corresponding to the lattice spacing Δx (lattice renormalization scheme). In complete analogy to Λ_{QCD}, the coupling

$$\mathfrak{g}^2_{\text{eff}}(p^2 \gg \Lambda_\sigma^2) \propto \frac{1}{\ln(p^2/\Lambda_\sigma^2)} \tag{4.49}$$

determines the induced scale of dynamical symmetry breakdown Λ_σ of the σ-model (dimensional transmutation). This important quantity sets all other length scales such as the mass gap (see, e.g., [83]-[88]) and must satisfy the condition (4.43) for consistency, i.e., $\Lambda_\sigma \Delta x \ll 1$. Finally, identifying (again for $N = 3$)

$$\boldsymbol{\sigma}(x = i\Delta x) = \frac{\sqrt{3}}{\mathfrak{g}_{\text{eff}}} \frac{\boldsymbol{r}_i}{R}\,, \tag{4.50}$$

the continuum limit $\sum_i \Delta x \to \int dx$ for $\lambda \gg \Delta x$ of Eq. (4.44) generates the Lagrangian (4.29) of the $O(3)$ nonlinear sigma model with the constraint (4.30) being implemented by $\boldsymbol{r}_i^2 = R^2$.

4.2.4 Disturbances

Of course, for a realistic proposal, it is essential to estimate the impact of the contributions which have been omitted so far. The additional kinetic terms due to inductances L of the wires are negligible $LI^2 \ll m_e \dot{\boldsymbol{r}}^2$ provided that

$$\frac{4a\, c_{\text{eff}}^2}{\Delta x}\, \ln\left(\frac{\Delta x}{b}\right) \ll 1 \tag{4.51}$$

holds, i.e., for a sufficiently large slow-down (as one would expect). For the same reason, the influence of the zero-point fluctuations of the electromagnetic field (inductance of free space) is negligible.

In contrast to sequential quantum algorithms, where errors may accumulate over many operations, the quantum simulation under consideration is basically a ground state problem and hence more similar to adiabatic quantum computing which we have discussed earlier in the second chapter of this Thesis. In this case, decoherence can be neglected as long as the interaction energies of the disturbances are much smaller than the energy gap between the ground state and the first excited state [13, 26]. For the nonlinear σ-model, this gap is determined by the induced scale Λ_σ (in analogy to QCD). Therefore, the energies of all perturbations (e.g., impurities in the material) must be much smaller than the gap of order $c_{\text{eff}}\Lambda_\sigma$. In particular, in order to see quantum behavior (where the Heisenberg uncertainty relation becomes important), the temperature must be small enough

$$k_{\text{B}}\mathcal{T} \ll c_{\text{eff}}\Lambda_\sigma\,. \tag{4.52}$$

Another issue concerns the spins of the electrons, which have been omitted so far. Fortunately, we may fix the electron spins by a small external magnetic field (see the next paragraph) and the various spin-spin and especially spin-orbit coupling terms are negligible (in comparison to $c_{\text{eff}}\Lambda_\sigma$) for the parameters provided below.

4.2.5 Phase Diagram

Before investigating the impact of an external magnetic field, let us turn to the phase diagram of the nonlinear σ-model in terms of the temperature $\mathcal{T}$ and the chemical potential μ. For low temperatures $k_{\text{B}}\mathcal{T} \ll c_{\text{eff}}\Lambda_\sigma$ and small chemical potentials $\mu \ll c_{\text{eff}}\Lambda_\sigma$, we basically get the usual vacuum state. Note that the introduction of a chemical potential necessitates the definition of a particle number (which is a nontrivial issue in interacting theories). In the σ-model, this can be achieved by means of the Noether current corresponding to the global $O(3)$ invariance $\boldsymbol{j}_\nu = \boldsymbol{\sigma} \times \partial_\nu \boldsymbol{\sigma}$ and the associated global charge along some internal axis $\boldsymbol{n}$ with $\boldsymbol{n}^2 = 1$

$$Q = \frac{1}{c_{\text{eff}}}\, \boldsymbol{n} \cdot \int dx\; \boldsymbol{\sigma} \times \dot{\boldsymbol{\sigma}}\,. \tag{4.53}$$

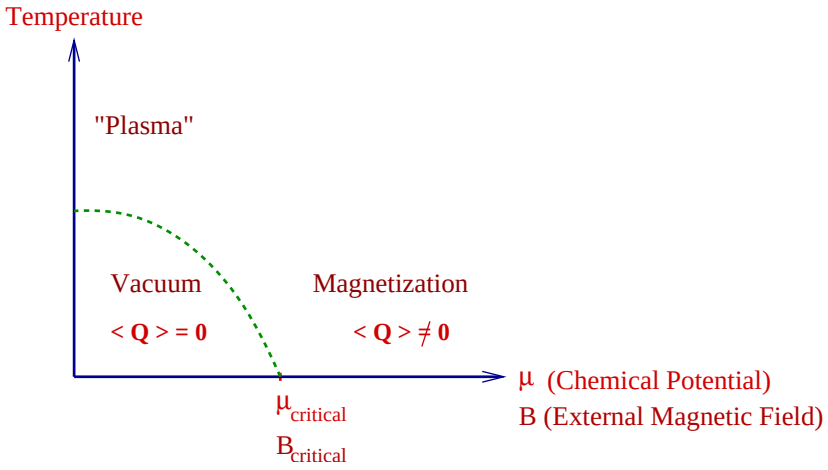

Figure 4.6: Phase diagram of the nonlinear sigma model in terms of the temperature $\mathcal{T}$ and the chemical potential μ. The structure of the ground state changes when the effective chemical potential exceeds the energy gap of order $c_{\text{eff}}\Lambda_\sigma$ and the above Noether current acquires a non-vanishing expectation value. In our laboratory system, the chemical potential corresponds to an external magnetic field $\boldsymbol{B}$ and at the critical field B_{crit} where the quantum phase transition occurs, the energy of the electron spins is of the same order as the gap.

For the laboratory system, the Noether charge Q is just the total (orbital) angular momentum in units of $\hbar$. Note that still many charges $Q \gg 1$ are required to generate one magnetic flux quantum (due to $c_0 \gg c_{\text{eff}}$).
In terms of the chemical potential defined with respect to this (dimensionless) Noether charge, the grand-canonical Hamiltonian H_{gc} reads

$$H_{\text{gc}} = H_0 + \mu_{\mathcal{N}}\mathcal{N} = H_0 + \mu_Q Q\,. \tag{4.54}$$

Translating this expression back to our laboratory system in Eq. (4.44), we observe that the chemical potential exactly corresponds to an external magnetic field $\boldsymbol{B}$ inducing the additional term $\dot{\boldsymbol{r}}\cdot\boldsymbol{A} = \dot{\boldsymbol{r}}\cdot(\boldsymbol{r}\times\boldsymbol{B})/3 = \boldsymbol{B}\cdot(\dot{\boldsymbol{r}}\times\boldsymbol{r})/3$

$$\mu_{\text{eff}} = \frac{e}{3m_e}\,B\,. \tag{4.55}$$

The second-order term $e^2\boldsymbol{A}^2/m_e$ is three orders of magnitude smaller for the parameters given below and can be neglected. When the effective chemical potential μ_{eff} exceeds the energy gap of order $c_{\text{eff}}\Lambda_\sigma$, the structure of the ground state changes and the above Noether current $\boldsymbol{j}_\nu$ acquires a non-vanishing expectation value – quantum phase transition, see, e.g., [83]-[88] and also cf. Fig. (4.6).
At the critical field $B_{\text{crit}} = \mathcal{O}(m_e c_{\text{eff}}\Lambda_\sigma/e)$ where this quantum phase transition occurs, the energy of the electron spins is of the same order as the gap $\boldsymbol{\mu}_s\cdot\boldsymbol{B} = \mathcal{O}(c_{\text{eff}}\Lambda_\sigma)$ and thus much

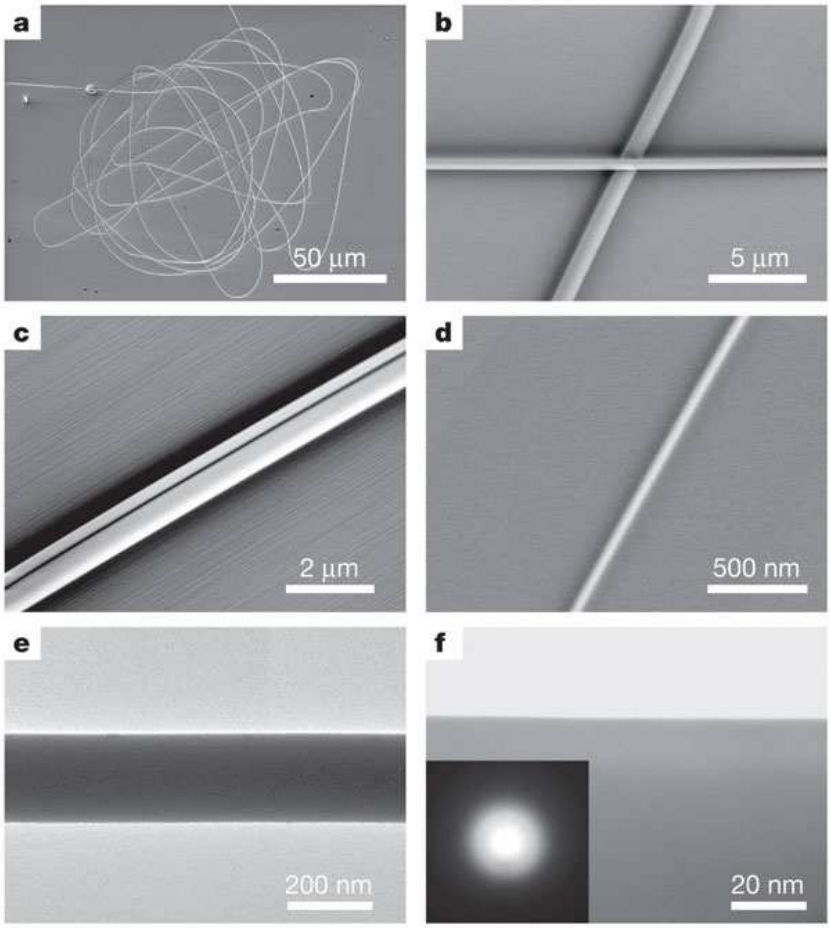

Figure 4.7: (**a**) A coiled 260-nm-diameter silica wire with a total length of about 4 mm. (**b**) Two crossed 570-nm and 1,100-nm diameter wires. (**c**) Two parallel 170-nm and 400-nm diameter wires. (**d**) A silica nanowire with a diameter of about 50 nm. (**e**) A 240-nm-diameter silica wire. (**f**) The surface of a 330-nm-diameter silica wire; the electron diffraction pattern (inset) demonstrates that the wire is amorphous [108].

bigger than the temperature. Hence one can fix the electron spins with much smaller external magnetic fields $B \ll B_{\rm crit}$ without disturbing the vacuum state too much. On the other hand, it is also possible to explore the full phase diagram (e.g., cross the quantum phase transition, monitored by a SQUID) by increasing the external magnetic field – which is completely equivalent to changing the chemical potential (and hence the number of particles). For the set of parameters discussed below, the critical field $B_{\rm crit}$ is of order milli-Tesla.

4.2.6 Experimental Parameters

The aforementioned constraints, in particular Eqs. (4.43) and (4.52), provide the frame of a window of opportunity for the experimental realization of the proposed quantum simulator –

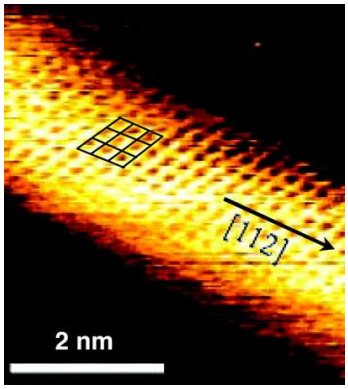

Figure 4.8: A silica nanowire with a diameter of about 3 nm [109].

which is (fortunately) open to present-day technology, see Figs. (4.7) and (4.8). Let us first explore the limit set by the ultra-low temperatures. For solid bodies of reasonable size, one can reach temperatures of order 10 μK by electron gas cooling via spin relaxation.
If we choose our parameters according to $b = 100$ nm, $R = 400$ nm, $a = 500$ nm, $d = 2.5$ μm, and $\Delta x = 12.5$ μm, we obtain $\mathfrak{g}_{\text{eff}} = \mathcal{O}(1)$, $c_{\text{eff}} \approx 10^4\,\text{m/s}$, $\Lambda_\sigma^{-1} \approx 125$ μm, and $c_{\text{eff}}\Lambda_\sigma$ corresponds to 600 μK, which satisfies all of the above assumptions reasonably well. Alternatively, we may start from the present state of nanotechnology which facilitates the production of nanowires with a radius of order nanometer[11] . If we explore this limit and choose $b = 1$ nm, $R = 12$ nm, $a = 5$ nm, $d = 25$ nm, and $\Delta x = 125$ nm, we obtain a similar value for $\mathfrak{g}_{\text{eff}}$ and $c_{\text{eff}} \approx 10^5\,\text{m/s}$, but now $c_{\text{eff}}\Lambda_\sigma$ corresponds to a temperature of order Kelvin. The range between μK and fractions of a Kelvin as well as between nanometers and micrometers provides a two or three orders of magnitude wide window of opportunity and the optimum experimental parameters are probably somewhere in the middle.
The thin superconducting wires can be switched on and off by local variations of the temperature (below and above the critical value). If the interaction $U(\boldsymbol{r}_{i+1}, \boldsymbol{r}_i)$ is switched off, the energy spectrum of the electrons is determined by the usual spherical harmonics

$$E_\ell = \frac{1}{2m_e}\frac{\ell(\ell+1)}{R^2}\,. \tag{4.56}$$

The energy gap between the s-state ($\ell = 0$) and the p-state ($\ell = 1$), i.e., without interaction $U(\boldsymbol{r}_{i+1}, \boldsymbol{r}_i)$, is one order of magnitude larger than with interaction $c_{\text{eff}}\Lambda_\sigma$. Consistently, the interaction potential $U(\boldsymbol{r}_{i+1}, \boldsymbol{r}_i)$ between the electrons on different spheres is of the same order of magnitude as the gap between the s-state ($\ell = 0$) and the p-state ($\ell = 1$) on a single sphere leading to strong entanglement of the ground state. If we want to switch on the interaction $U(\boldsymbol{r}_{i+1}, \boldsymbol{r}_i)$ adiabatically (e.g., via changing the temperature of the wires) satisfying the

[11] S. T. Lee and his research group, at the city university of Hong Kong, have produced silicon nanowires with diameters approaching 1 nm (2003), see also Fig. (4.8).

condition for the adiabatic theorem

$$\frac{\langle\psi_0|\,\dot{H}\,|\psi_1\rangle}{\Delta E_{01}^2} = \varepsilon \ll 1\,, \tag{4.57}$$

in order to stay in the ground state $|\psi_0\rangle$, the typical adiabatic switching time should be longer than a few picoseconds. Finally, it might be interesting to look at the energies of spin-spin coupling, $\mu_0 e^2/4\pi m_e^2(\Delta x)^3$ and also spin-orbit coupling, $ae^2/4\pi\varepsilon_0 R m_e^2 d^3$. For the parameters discussed above, the various spin-spin and spin-orbit coupling energies are at least two orders of magnitude smaller than $c_{\text{eff}}\Lambda_\sigma$ and thus negligible.

4.2.7 Summary and Outlook

The proposed set-up allows a direct access to the quantum state and hence an investigation of the strong entanglement (e.g., in the ground state or near the quantum phase transition). This could be done via state-selective radio/micro-wave spectroscopy of transitions from the levels in Eq. (4.56) to some higher-lying empty and isolated internal level (of the semi-conductor) with a sharp energy, for example (fluorescence measurement). Generating the radio/micro-waves via a circuit (wave-guide) facilitates the position control of the measurement (vicinity of the inductance loop). Furthermore, one may also switch off the wires (e.g., by locally increasing the temperature) before the measurement. It is also possible to create particles (and their anti-particles), which can be used to study the S-matrix, for example, via the illumination with (left and right) circular polarized radio/micro-wave radiation, cf. Eq. (4.53) and the subsequent remarks. Another interesting point is the robustness or fragility of non-perturbative properties (such as the instanton density) with respect to a small coupling to external degrees of freedom. After having handled and understood the 1+1 dimensional situation, the extension to 2+1 dimensions should not be very problematic. The 2+1 dimensional $O(3)$ nonlinear σ-model loses some of the properties discussed above, but also acquires novel features, such as skyrmions which are described by the topological current $j^\rho = \epsilon^{\mu\nu\rho}\,\boldsymbol{\sigma}\cdot(\partial_\mu\boldsymbol{\sigma}\times\partial_\nu\boldsymbol{\sigma})$. The inclusion of an explicit $O(3)$-symmetry breaking term $\boldsymbol{n}\cdot\boldsymbol{\sigma}$ should be easy in 1+1 and 2+1 dimensions. Note that we did not incorporate a topological (Chern-Simons type) θ-term $\mathcal{L}_\theta = \theta\,\epsilon^{\mu\nu}\,\boldsymbol{\sigma}\cdot(\partial_\mu\boldsymbol{\sigma}\times\partial_\nu\boldsymbol{\sigma})$ in our 1+1 dimensional scenario (in analogy to the θ-term $G^*_{\mu\nu}G^{\mu\nu}$ in QCD), whose implementation is less straight-forward. Further interesting topics are the behavior of strongly interacting quantum field theories (such as QCD and the σ-model) during the cosmic expansion and the (long-range) entanglement of QCD vacuum state (which might be used as a tool for diagnosis and a resource).

5 Conclusion

In the second chapter, we focused on the adiabatic approach to quantum computation. Although adiabatic quantum computation seems to differ from the sequential quantum computing, it has been proved that these two models are polynomially equivalent [29]. The adiabatic quantum computer operates near the instantaneous ground state of a time-dependent Hamiltonian and can therefore be expected to be insensitive to relaxation and open system effects among the excited states. This expected resilience to various kinds of open system effects makes it a promising candidate for robust quantum computation. As a main result of the second chapter, we stated that the first-order correction given in Eqs. (2.41) and (2.42) which has frequently been used as a condition for adiabatic quantum computation, does not yield a good estimate for the computational error [32]. Instead , the remaining real excitations after the dynamics present a better estimate. In contrast to the previous studies based on the Landau-Zener formula which the optimal run-time scales with the inverse of the square of the minimum gap, our general arguments implies that the optimal run-time scales with the inverse of the minimum gap. Although this achievement is merely polynomial and not as impressive as an exponential speedup, in practice it may be useful. As we discussed in Sec. (2.4.4), when the minimum gap of a time-dependent Hamiltonian scales exponentially with the inverse of the size of the problem, we would expect an exponential scaling of the run-time required to reach a fixed fidelity.
Quantum phase transitions are investigated in the third chapter of this Thesis. In the continuum limit (large number of qubits), adiabatic quantum algorithms display a remarkable similarity to sweep through quantum phase transitions [21]. Based on this similarity, it seems [22] that adiabatic quantum algorithms corresponding to second-order quantum phase transitions should be advantageous compared to isolated avoided level crossings (which are analogous to first-order transitions). For an adiabatic quantum algorithm (Grover's search routine [25]) based on a single isolated avoided level crossing [55], the impact of decoherence induced by a low-temperature bath with a well-behaved spectral distribution does not destroy the scalability of the system. However, as a main result of the third chapter we demonstrated that the situation is very different for second-order transitions. We focused our attention on the impact of decoherence caused by a small coupling to a rather general reservoir for the quantum Ising chain in a transverse field, which is considered a prototypical example [37] for a second-order quan-

tum phase transition. It turned out that for the decoherence channel which is always present, the impact of decoherence increases with system size, i.e., number of spins/qubits. According to the analogy between adiabatic quantum algorithms and quantum phase transitions, this result suggests scalability problems of the corresponding adiabatic quantum algorithm which is mainly different from the first-order quantum phase transitions. Therefore, in order to construct a scalable adiabatic quantum algorithm in analogy to the Ising model, suitable error-correction methods will be required.

Quantum simulators are the focus of the forth chapter. In the first section of this chapter Sec. (4.1), we have proposed a design for the simulation of the quantum Ising model with a system of electrons floating on a liquid helium film adsorbed on a silicon substrate [61]. Since the energy level splitting (tunneling rate) depends exponentially on the thickness of the helium film, we may tune the system through the quantum phase transition by changing the thickness of the helium film – which might even be feasible in a time-dependent manner, cf. [45]. The quantum critical behaviour and the created topological defects (kinks) could be detected via measuring the voltages induced on the spheres, see Fig. (4.1). Furthermore, a suitable generalization to two spatial dimensions, see Fig. (4.4), might be relevant for adiabatic quantum algorithms, see, e.g., [43]. Note that the realization of a sequential quantum computer based on a set of electrons floating on a helium film has been proposed in [75]. In contrast, our proposal is not suited for universal computations, but (as one would expect) should be easier to realize experimentally. Exploring a different limit, where many eigenstates of the double-well potential contribute, the proposed set-up could simulate the lattice version of interacting field theories such as the $\lambda\phi^4$-model in 1+1 dimensions. Finally, moving the pairs of spheres closer together ($\lambda = d$), one could simulate the Fermi-Hubbard model, even though only in specific corner of the phase diagram corresponding to small filling and large interactions.

In the second section of the forth chapter, Sec. (4.2), we have demonstrated that it is possible to construct a quantum simulator for the $O(3)$ nonlinear σ-model with present-day technology. Such a restricted quantum computer would allow the comparison, for a controllable scenario, between perturbative and non-perturbative analytical methods (renormalization flow [78], [93]-[101], instantons [79, 80, 81], operator product expansion and vacuum condensates, low-energy theorems and sum rules [82], the S-matrix [83]-[88] etc.) as well as numerical results [89]-[92] on the one hand with real quantum simulations on the other hand. In contrast to most of the numerical simulations, for example, the proposed quantum simulator works in real (laboratory) time, i.e., it is not necessary to perform a Wick rotation to Euclidean time. This advantage facilitates the study of the evolution of excitations, for example collisions (S-matrix etc.).

Apart from above points of interest, the construction of such restricted quantum computers, which are especially dedicated to the simulation of the Ising model and the $O(3)$ nonlinear σ-model, would be interesting feasibility studies for more general quantum simulators for a

comparably well understood (yet nontrivial) system. Finally, experience shows that the availability of new tools (such as the proposed quantum simulators) yielding new tests/results usually lead us to a new level of understanding in physics with possibly unexpected outcomes.

6 Appendix A

6.1 The Landau-Zener Formula

In 1932, Zener [35] published the exact solution to a one-dimensional semi-classical model for nonadiabatic transitions. As Landau [34] had formulated and solved the same model independently, it came to be known as the Landau-Zener model. Despite its limitations, it remains an important example of a nonadiabatic transition. Even in systems for which accurate calculations are possible, application of the Landau-Zener model can provide useful *first estimates* of nonadiabatic transition probabilities. Alternatively, for complex systems, it may offer the only feasible way to obtain transition probabilities.

The Landau-Zener formula provides an analytic solution to the equations of motion governing the transition dynamics of a 2-level quantum mechanical system, with a time-dependent Hamiltonian varying such that the energy separation of the two states is a linear function of time. The formula gives the probability of a nonadiabatic transition between the two energy states. The system starts, in the infinite past, in the lower energy eigenstate and we wish to calculate the probability of finding the system in the upper energy eigenstate in the infinite future, a so-called Landau-Zener transition. For infinitely slow variation of the energy difference (i.e., a Landau-Zener velocity of zero), the adiabatic theorem tells us that no such transition will take place, as the system will always be in an instantaneous eigenstate of the Hamiltonian at that moment in time. At non-zero velocities, transitions occur with probability as described by the *Landau-Zener formula*.

Let us consider a two-level system Hamiltonian $H(t)$. Denoting the eigenvalues of $H(t)$ by $E_0(t)$, $E_1(t)$ and corresponding normalized eigenvectors by $|n_0(t)\rangle$, $|n_1(t)\rangle$, respectively, the formula reads

$$P \approx \exp\left\{-2\,\tau\left|\Im\left(\int_0^{z_0} dz\ [E_1(z) - E_0(z)]\right)\right|\right\}\ , \tag{6.1}$$

where P is the probability of the transition from initial eigenstate $|n_0(-\infty)\rangle$ at time $-\infty$ to the eigenstate $|n_1(+\infty)\rangle$ at time $+\infty$, z_0 is a point in the complex-time plane where $E_1(z_0) = E_0(z_0)$

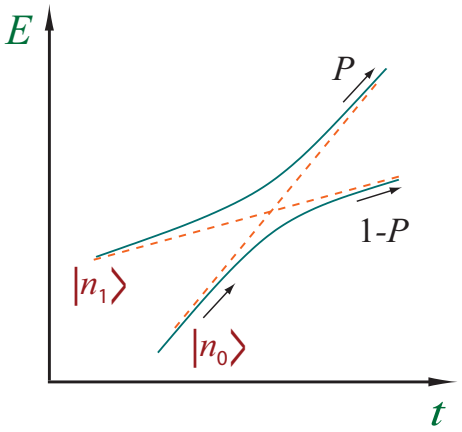

Figure 6.1: Schematic of a Landau-Zener crossing. Assuming a system prepared in the eigenstate $|n_0\rangle$ in the infinite past, the Landau-Zener formula provides the transition probability from this initial state to the eigenstate $|n_1\rangle$, which the system will be in the infinite future.

and τ is a multiplicative factor.[1] This formula assumes that the eigenvalues have an analytic extension property to the complex-time plane. The infinite times should be understood in a limiting sense and the eigenvalues $E_0(t)$ and $E_1(t)$ are assumed to have no crossing on the real axis. When the eigenvalues depend on time analytically, the Landau-Zener formula not only predicts exponentially fast approach to adiabatic limit, but also predicts the precise rate of the approach.[2]

In adiabatic quantum computation, somewhere during the computation the energy gap is smallest. This minimum gap sets the run-time for solving the problem and is therefore the dangerous point for the system leaving the ground state. For a large class of problems, the evolution through this minimum gap point is equivalent to a *Landau-Zener crossing*, where the two lowest eigenstates are the levels in an effective two-level system. The Landau-Zener problem has a long history and analytical results for the probability of leaving the ground state even in the presence of strongly coupled environments are available [113]. Therefore the probability of leaving the ground state for adiabatic quantum computation can be analyzed by treating the physics of the anticrossing in the Landau-Zener framework, even in the presence of noise.

[1] The adiabatic limit of a slowly changing Hamiltonian is formally related to the large τ limit [111].

[2] For more details see. e.g., [111, 112].

7 Appendix B

7.1 Further Generalizations of the Error Estimate

In this appendix, we present further generalizations of the error estimate discussed in Sec. (2.4). From an experimental point of view, the time-dependence of the Hamiltonian

$$H(t) = [1 - s(t)]H_0 + s(t)H_{\mathrm{f}}\,, \tag{7.1}$$

will most certainly vanish asymptotically $\dot{H}(t < 0) = \dot{H}(t > T) = 0$ or at least be negligible – which automatically implies $h(0) = h(1) = 0$, where $h(s)$ is the same as defined in Eq. (2.45)

$$\frac{ds}{dt} = \Delta E(s)h(s)\,, \tag{7.2}$$

Furthermore, realistic Hamiltonians should be described by C^∞-interpolations[1] (*Natura non facit saltus*). By using a C^∞-test function which was matched at $t_1 = 0.1T$ and $t_2 = 0.9T$ to the usual dynamics $s(t)$, compare dotted lines in Fig. (7.1) bottom panel, we have implemented an interpolation scheme with such an adiabatic switching on and off $\dot{s}(0) = \dot{s}(T) = 0$. For the investigated adiabatic implementation of the Grover search routine, see Sec. (2.4.4), this scheme does not affect the final result considerably. The reason for this robustness lies in the fact that the matrix element $F_{nm} = \langle m(s)|\, H'(s)\, |n(s)\rangle$ is peaked around $s = 1/2$ and $h(0)$ as well as $h(1)$ are small enough already without the adiabatic switching on and off. Therefore, one can expect the dominant non-adiabatic corrections to arise from the behavior around the minimum gap, which was unaffected by the test function.
However, the situation is completely different for the example considered in Sec. (7.1.2) below. In that case the exponential suppression of the final error as a function of the run-time requires a smooth C^∞-interpolation – with other dynamics such as C^0 (just continuous) or C^1 (differentiable once), the final error is merely polynomially small, cf. Fig. (7.2).

[1] C^∞-interpolations are interpolations with a test function which is infinitely smooth, i.e., an infinite number of times continuously differentiable.

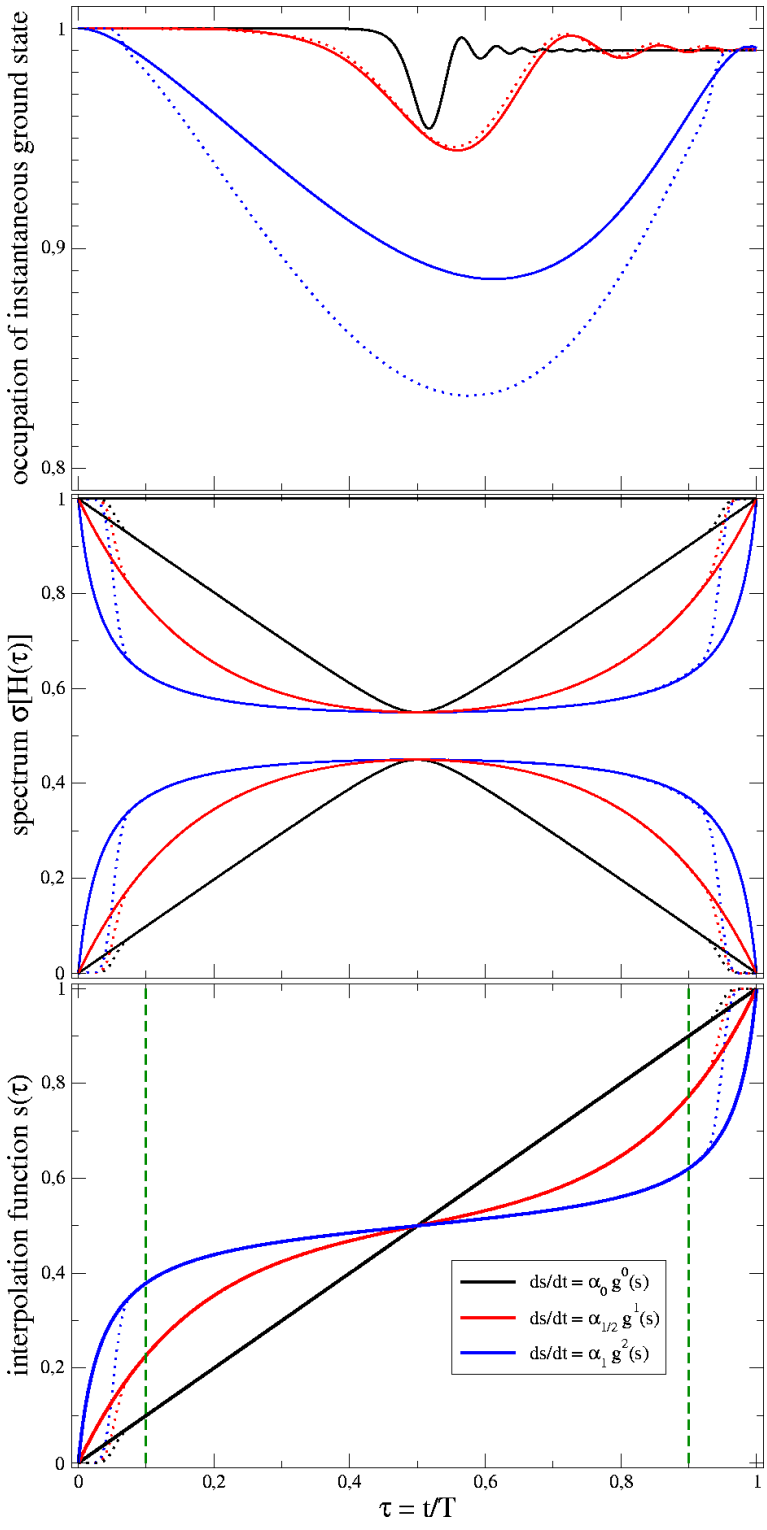

Figure 7.1: Evolution of the interpolation function $s(t)$ (**bottom panel**), the spectrum $\sigma[s(t)]$ (**middle panel**), and the occupation of the instantaneous ground state (**top panel**) versus the rescaled time $\tau = t/T$ for an adiabatic Grover search problem with $N = 100$ states. For each interpolation (different line styles), T was adapted to reach 99% of final fidelity. Thin dotted lines represent C^∞-interpolations smoothed with a test function.

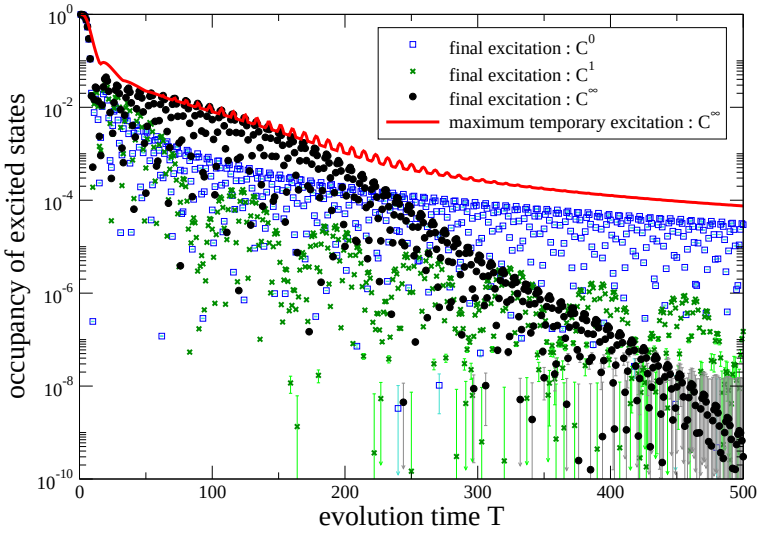

Figure 7.2: Evolution of the final and the maximum intermediate (red line) excitations with the runtime T for the example (7.5). The exponential falloff in the final excitations is only visible, if a smooth C^∞-interpolation (black circles) is used, whereas the scaling of the intermediary excitations (red line) is always polynomial. The suppression of the final error for C^0 or C^1-interpolations (blue squares and green crosses) is also merely polynomial.

7.1.1 Nonlinear Interpolation

Although we have chosen a linear interpolation scheme (7.1) in order to satisfy the trace constraint (2.43),

$$\mathrm{tr}\{H[s(t)]\} = \mathrm{const.} \qquad \forall\, s \in [0,1]\,, \tag{7.3}$$

the presented analysis can be generalized easily to more general non-linear interpolations.[2] The argumentation based on the analytic continuation works in the same way provided that the functional dependence $H_{\mathrm{nl}}(s) = f(H_{\mathrm{i}}, H_{\mathrm{f}}, s)$ does not involve extremely large or small numbers.

As an illustrative example, we consider the Grover's search problem with the same initial and final Hamiltonians but a quadratic interpolation scheme

$$\begin{aligned} H_{\mathrm{nl}}(s) &= [(1-s)H_{\mathrm{i}} + sH_{\mathrm{f}}]^2 + s(1-s)\,\frac{2N-2}{N^2}\,\mathcal{I} \\ &= (1-s)^2 H_{\mathrm{i}} + s^2 H_{\mathrm{f}} + s(1-s)\left[\{H_{\mathrm{i}}, H_{\mathrm{f}}\} + \frac{2N-2}{N^2}\,\mathcal{I}\right], \end{aligned} \tag{7.4}$$

[2] Note that, *linear* refers to the straight connection line between initial and final Hamiltonian in equation (7.1) and should not be confused with the different velocities $s(t)$ at which this line is traversed.

where $\{\cdot,\cdot\}$ denotes the anti-commutator. The identity operator $\mathcal{I}$ has been added in order to ensure $\mathrm{tr}\{H_{\mathrm{nl}}\} = N-1$, cf. Eq. (7.3). Although the spectrum of this non-linear interpolation is slightly distorted compared to the linear one, the fundamental gap is the same as in equation (2.60),

$$\Delta E(s) = \sqrt{1 - 4\left(1 - \frac{1}{N}\right) s(1-s)} \approx \sqrt{4\left(s - \frac{1}{2}\right)^2 + \frac{1}{N}}\,,$$

and hence same interpolation functions $s(t)$, applied to the above Hamiltonian, should reproduce the scaling predictions mentioned in Sec. (2.4).

7.1.2 Degeneracy

So far, we have restricted our considerations to the instantaneous ground state and a single first excited state. Let us now consider a very simple example (see also [28]) in which there is still a unique ground state, but many degenerate first excited states: In terms of single-qubit Pauli matrices σ_x and σ_z, the M-qubit Hamiltonian reads

$$H(s) = \frac{1}{2}\sum_{j=1}^{M}\left[\mathbf{1} - s\sigma_z^{(j)} - (1-s)\sigma_x^{(j)}\right]\,, \tag{7.5}$$

where we have used a linear interpolation (7.1) for simplicity. In this example, the Hamiltonian can be decomposed completely into independent and equal single-qubit contributions and hence the time-evolution operator factorizes, i.e., it is sufficient to solve the dynamics of a single qubit. Furthermore, the Hamiltonian is invariant under any permutation of the qubits. The instantaneous ground states for all values of s are symmetric under this permutation group and hence unique, but the first excited states are not – leading to a M-fold degeneracy (i.e., there are M equivalent first excited states). Hence, the fundamental gap between the ground state and each one of these first excited states is the same as for one qubit and thus independent of the number of qubits

$$\Delta E(s) = \sqrt{1 - 2s(1-s)}\,. \tag{7.6}$$

In some sense, this simple example represents a limiting case opposite to Grover's algorithm: The energy gap $\Delta E(s)$ and the matrix elements $F_{nm} = \langle m(s)|\, H'(s)\, |n(s)\rangle$ do not scale with the number M of qubits and the F_{nm} are neither small initially nor finally. Instead, the scaling with system size manifests itself in the M-fold degeneracy of the first excited states. As a result of the M-independent gap structure, the adiabatic switching is crucial for achieving the exponential suppression of the final error. Fig (7.2) displays the final error probabilities for a smooth C^∞-interpolation and for C^0 and C^1-interpolations for comparison. These numerical

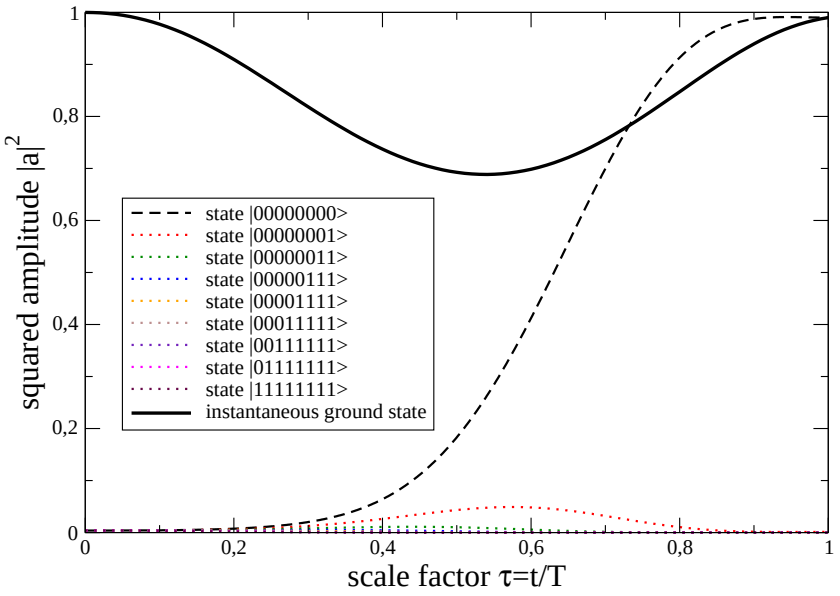

Figure 7.3: Occupation of the instantaneous ground state and some selected computational basis states for the Hamiltonian in (7.5) for an $M = 8$ qubit system. Temporarily, the system leaves the instantaneous ground state, but the runtime T has been adjusted such that the final fidelity is 99%.

simulations confirm that the falloff is exponential in the C^∞-case but merely polynomial for C^0 and C^1.

Another interesting point of this simple example is the difference between the intermediate and the final occupation of the ground state, see Figs. (7.2) and (7.3). According to the first-order result in Eq. (2.41)

$$a_m(t) \;\approx\; a_m^0 e^{i\vartheta_m(t)} - i\left[\sum_{n\neq m} a_n^0 \frac{\langle m|\,\dot{H}\,|n\rangle}{\Delta E_{nm}^2}\, e^{i\varphi_{nm}}\right]_0^t , \tag{7.7}$$

and the aforementioned factorization of the time-evolution operator, the intermediate excitation probability scales as

$$p_{\text{int}} = \sum_{m>0} |a_m|^2 = \mathcal{O}\left(\frac{M}{T^2\Delta E^4}\right) = \mathcal{O}\left(\frac{M}{T^2}\right) , \tag{7.8}$$

since the gap ΔE is independent of M. On the other hand, the final error probability (assuming a C^∞-interpolation) is exponentially suppressed

$$p_{\text{fin}} = \mathcal{O}\left(M \exp\{-T\Delta E\}\right) = \mathcal{O}\left(M \exp\{-T\}\right) , \tag{7.9}$$

and hence the two error probabilities can be vastly different $p_{\text{int}} \gg p_{\text{fin}}$, cf. Fig. (7.3). In fact, by increasing the number of qubits, the occupancy of the instantaneous ground state can be

made arbitrarily small. Moreover, the run-time condition derived from the first-order result in Eqs. (7.7) and (7.8)

$$T_0 = \mathcal{O}(\sqrt{M})\,, \tag{7.10}$$

yields a scaling which is far too pessimistic compared with the correct final error probability assuming a C^∞-interpolation

$$T_\infty = \mathcal{O}(\ln M)\,. \tag{7.11}$$

Note that non-smooth interpolations (e.g., C^0 or C^1) would also yield a polynomial scaling $T = \mathcal{O}(M^x)$ similar to Eq. (7.10). On the other hand, the scaling behavior in Eqs. (7.9) and (7.11) is just what one would obtain by immersing the system in Eq. (7.5) into a zero-temperature environment and letting it decay towards its ground state. Therefore, using non-smooth interpolations (e.g., C^0 or C^1) or naively demanding the first-order estimate in Eq. (2.41), the adiabatic algorithm would be even slower than this simple decay mechanism.

8 Notation

Throughout this thesis natural units with $\hbar, c_0 = 1$ are used. Lowercase Greek indices such as μ, ν vary from 0 (time) to 3 (space) and describe space-time components. Furthermore, the following symbols are employed:

$\mathfrak{A}$	excitation amplitude
$\boldsymbol{B}$	external magnetic field
$\mathbb{C}$	set of all complex numbers
C_{12}	controlled not gate
$\mathfrak{d}$	critical exponent
e	elementary charge
g	interpolation function
g_e	acceleration due to gravity
$\mathfrak{g}$	running coupling
E_n	eigenenergy
$\mathscr{E}$	single particle energy
$H^{(2)}$	Hadamard gate
H	Hamiltonian
H_0	initial Hamiltonian
H_f	final Hamiltonian
$\mathcal{H}$	Hilbert space
i	imaginary unit
$\Im$	imaginary part
$\mathcal{I}$	identity operator
I_a	controlled phase inversion
J	exchange energy

k	pseudo-momentum
k_e	wavevector of an electron
k_B	Boltzmann constant
K_n	modified Bessel function
K	kelvin
$\mathfrak{L}$	Lagrangian
m	meter
m_e	electron mass
nm	nanometer
$\mathbb{N}$	set of all natural numbers
$\mathcal{O}(N)$	order of N
p	momentum
$\mathfrak{q}$	charge
$\boldsymbol{q}$	ripplon momentum vector
Q	Noether charge
$\mathcal{Q}$	gate sequence
$\mathfrak{Q}$	ripplon normal coordinate
$\boldsymbol{r}$	spatial coordinate
$\mathbb{R}$	set of all real numbers
$\Re$	real part
$\mathcal{S}$	Euclidean action
$\mathbb{S}_2$	two-sphere
t	time coordinate
T	total evolution time
$\mathcal{T}$	temperature
tr	trace
$\mathcal{U}$	unitary transformation
U	potential energy
χ	static susceptibility
δ_{ij}	Kronecker delta
δ	deviation
Δ	difference
ϵ	small parameter
ε	relative static permittivity
γ	Bogoliubov operators
Γ	transverse field
Λ	length scale
ω	frequency

$\boldsymbol{\mu}_s$	electron magnetic moment
$\mu_{\mathcal{N}}, \mu_Q$	chemical potential
μ_{eff}	effective chemical potential
μm	micrometer
μK	microkelvin
ρ	density
ϱ	density operator
$\sigma^x, \sigma^y, \sigma^z$	Pauli operators
$\boldsymbol{\sigma}$	fields in sigma model $(\sigma_1, \sigma_2, \ldots, \sigma_N)$
ϑ	Berry phase
υ	weak perturbation
Υ	correlation length
ξ	surface tension
$\wedge$	logic conjunction
$\forall$	for all
$\in$	member of
$\oplus$	addition modulo 2
$\otimes$	tensor product
$\perp$	orthogonal
$\dagger$	adjoint
$\sum$	sum
$\prod$	product
$\|0\rangle, \|1\rangle$	basis vectors of a single-qubit space
$\|\uparrow\rangle$	spin up along the z axis
$\|\downarrow\rangle$	spin down along the z axis
$\|\rightarrow\rangle$	spin polarized along the x axis
$\|n\rangle, \|\psi\rangle$	eigenvector
$\|\Psi\rangle$	state vector
$\|X\rangle$	basis vector in a Hilbert space
$\langle\cdot\|\cdot\rangle$	scalar Fock space product
$\|\cdot\|$	absolute value
$[\cdot, \cdot]$	commutator $[A, B] = AB - BA$
$\{\cdot, \cdot\}$	anti-commutator $\{A, B\} = AB + BA$

List of Figures

Bibliography

[1] R. P. Feynman, *Simulating physics with computers*, Int. J. Theor. Phys. **21**, 467 (1982).

[2] R. P. Feynman, *Quantum mechanical computers*, Found. Phys. **16**, 507 (1986).

[3] D. Deutsch, *Quantum theory, the Church-Turing principle and the universal quantum computer*, Proc. R. Soc. Lond. A **400**, 97 (1985).

[4] P. Shor, *Algorithms for quantum computation: Discrete logarithms and factoring*, In Proc. 35th Annual Symposium on Foundations of Computer Science, page 124, Los Alamitos, CA: IEEE Computer Society Press (1994).

[5] L. Grover, *A fast quantum mechanical algorithm for database search*, In Proc. 28th Annual ACM Symposium on the Theory of Computation, page 212, New York: ACM Press (1996).

[6] S. Hallgren, *Polynomial-time quantum algorithms for Pell's equation and the principal ideal problem*, In Proc. of the 34th Annual ACM Symposium on the Theory of Computation, page 653, New York: ACM Press (2002).

[7] E. Farhi, J. Goldstone, S. Gutmann and M. Sipser, *Quantum computation by adiabatic evolution*, pre-print: `quant-ph/0001106` (2000).

[8] A. M. Childs, E. Farhi, and J. Preskill, *Robustness of adiabatic quantum computation*, Phys. Rev. A **65**, 012322 (2001).

[9] M. S. Sarandy, and D. A. Lidar, *Adiabatic quantum computation in open systems*, Phys. Rev. Lett. **95**, 250503 (2005).

[10] W. M. Kaminsky and S. Lloyd, *Scalable architecture for adiabatic quantum computing of NP-hard problems*, in *Quantum computing and quantum bits in mesoscopic systems* by A. Leggett and P. Silvestrini, Eds. (Kluwer Academic, 2003); pre-print: `quant-ph/0211152`.

[11] G. Alber, M. Mussinger, and A. Delgado, *Dynamical stabilization of Grover's algorithm with embedded quantum codes*, Proc. SPIE **4429**, 37 (2001).

[12] D. S. Johnson, C. H. Papadimitriou, *The traveling salesman problem*, E. L. Lawler, J. K. Lenstra, A. H. G. Rinnooykan, D. B. Shmays, Eds. (Wiley, New York, 1985), p. 37.

[13] E. Farhi, J. Goldstone, S. Gutmann, J. Lapan, A. Lundgren, and D. Preda, *A Quantum adiabatic evolution algorithm applied to random instances of an NP-Complete problem*, Science **292**, 472 (2001).

[14] S. Kirkpatrick and B. Selman, *Critical behavior in the satisfiability of random Boolean expressions* Science **264**, 1297 (1994).

[15] S. L. Braunstein, H. Lo, P. Kok, Ed. , *Scalable quantum computers: Paving the way to realization*, (Wiley-VCH, 2001).

[16] J. I. Cirac and P. Zoller, *Quantum computation with cold trapped ions*, Phys. Rev. Lett. **74**, 4091 (1995).

[17] C. H. Bennett, G. Brassard, C. CrÃ©peau, R. Jozsa, A. Peres, and W. K. Wootters, *Teleporting an unknown quantum state via dual classical and Einstein-Podolsky-Rosen channels*, Phys. Rev. Lett. **70**, 1895 (1993).

[18] S. Lloyd, *Universal quantum simulators*, Science **273**, 1073 (1996).

[19] M. A. Nielsen and I. L. Chuang, *Quantum computation and quantum information*, (Cambridge University Press, Cambridge, England, 2000).

[20] A. Messiah, *Quantum mechanics*, (John wiley and Sons, 1958).

[21] J. I. Latorre and R. Orús, *Adiabatic quantum computation and quantum phase transitions*, Phys. Rev. A **69**, 062302 (2004).

[22] R. Schützhold and G. Schaller, *Adiabatic quantum algorithms as quantum phase transitions: First versus second order*, Phys. Rev. A **74**, 060304(R) (2006).

[23] C.-P. Sun, *High-order quantum adiabatic approximation and Berry's phase factor*, J. Phys. A **21**, 1595 (1988).

[24] J. W. Brown and R. V. Churchill, *Fourier series and boundary value problems*, (McGraw-Hill, New York, 1993).

[25] J. Roland and N. J. Cerf, *Quantum search by local adiabatic evolution*, Phys. Rev. A **65**, 042308 (2002).

[26] A. M. Childs, E. Farhi, J. Goldstone, and S. Gutmann, *Finding cliques by quantum adiabatic evolution*, Quant. Inf. Comp. **2**, 181 (2002).

[27] M. Žnidarič, *Scaling of the running time of the quantum adiabatic algorithm for propositional satisfiability*, Phys. Rev. A **71**, 062305 (2005).

[28] E. Farhi, J. Goldstone, Sam Gutmann and Daniel Nagaj, *How to make the quantum adiabatic algorithm fail*, International Journal of Quantum Information **6**, 503 (2008).

[29] D. Aharonov, W. van Dam, J. Kempe, Z. Landau, S. Lloyd, and O. Regev, *Adiabatic quantum computation is equivalent to standard quantum computation*, 45th Annual IEEE Symposium on Foundations of Computer Science, 42-51, (2004); SIAM Journal of Computing **37**, 166 (2007).

[30] M. S. Sarandy, L. A. Wu, and D. A. Lidar, *Consistency of the adiabatic theorem*, Quant. Inf. Proc. **3**, 331 (2004).

[31] S. Das, R. Kobes, and G. Kunstatter, *Energy and efficiency of adiabatic quantum search algorithms*, J. Phys. A **36**, 2839 (2003).

[32] G. Schaller, S. Mostame, and R. Schützhold, *General error estimate for adiabatic quantum computing*, Phys. Rev. A **73**, 062307 (2006).

[33] N. D. Birrell and P. C. W. Davies, *Quantum fields in curved space*, (Cambridge University Press, Cambridge, England 1982).

[34] L. Landau, *Zur Theorie der Energieübertragung.*, Physics of the Soviet Union **2**, 46 (1932).

[35] C. Zener, *Non-adiabatic crossing of energy levels*, Proceedings of the Royal Society of London, Series A **137** 692 (1932).

[36] W. H. Press, B. P. Flannery, S. A. Teukolsky, W. T. Vetterling, *Numerical recipes in C*, (Cambridge University Press, Cambridge, England 1994).

[37] S. Sachdev, *Quantum phase transitions*, (Cambridge University Press, Cambridge, UK, 1999).

[38] J. E. Bunder and R. H. McKenzie, *Effect of disorder on quantum phase transitions in anisotropic XY spin chains in a transverse field*, Phys. Rev. B **60**, 344 (1999).

[39] K. H. Fischer, and J. A. Hertz, *Spin glasses*, (Cambridge University Press, Cambridge, UK, 1993).

[40] A. Das, and B. K. Chakrabarti, *Quantum annealing and related optimisation methods*, (LNP **679**, Springer-Verlag, Heidelberg, 2005).

[41] G. E. Santoro, R. Martoňák, E. Tosatti, and R, Car, *Theory of quantum annealing of an Ising spin glass*, Science **295**, 2427 (2002).

[42] T. Kadowaki, and H. Nishimori, *Quantum annealing in the transverse Ising model*, Phys. Rev. E **58**, 5355 (1998).

[43] IEEE Spectrum online, Tech Talk, February 13th (2007).

[44] S. Mostame, G. Schaller, and R. Schützhold, *Decoherence in a dynamical quantum phase transition of the Ising chain*, Phys. Rev. A **76**, R030304 (2007).

[45] J. Dziarmaga, *Dynamics of a quantum phase transition: Exact solution of the quantum Ising model*, Phys. Rev. Lett. **95**, 245701 (2005).

[46] G. Schaller, and R. Schützhold, *The role of symmetries in adiabatic quantum algorithms*, pre-print: `arXiv:0708.1882` (2007).

[47] M. Žnidarič, and M. Horvat, *Exponential complexity of an adiabatic algorithm for an NP-complete problem*, Phys. Rev. A **73**, 022329 (2006).

[48] R. Schützhold, M. Uhlmann, Y. Xu and Uwe R. Fischer, *Sweeping from the superfluid to Mott phase in the Bose-Hubbard model*, Phys. Rev. Lett. **97**, 200601 (2006).

[49] R. Schützhold, *Dynamical zero-temperature phase transitions and cosmic inflation/deflation*, Phys. Rev. Lett. **95**, 135703 (2005).

[50] G. Vidal, J. I. Latorre, E. Rico, and A. Kitaev, *Entanglement in quantum critical phenomena*, Phys. Rev. Lett. **90**, 227902 (2003).

[51] W. H. Zurek, U. Dorner, and P. Zoller, *Dynamics of a quantum phase transition*, Phys. Rev. Lett. **95**, 105701 (2005).

[52] B. Damski, *The simplest quantum model supporting the Kibble-Zurek mechanism of topological defect Production: Landau-Zener transitions from a new perspective*, Phys. Rev. Lett. **95**, 035701 (2005).

[53] K. Sengupta, S. Powell, and S. Sachdev, *Quench dynamics across quantum critical points*, Phys. Rev. A **69**, 053616 (2004).

[54] A. Fubini, G. Falci and A. Osterloh, *Robustness of adiabatic passage through a quantum phase transition*, New J. Phys. **9**, 134 (2007).

[55] M. Tiersch and R. Schützhold, *Non-Markovian decoherence in the adiabatic quantum search algorithm*, Phys. Rev. A **76**, 030304 (2007).

[56] P. Jordan and E. Wigner, *Über das Paulische Äquivalenzverbot (Over the Pauli equivalence prohibition),* Z. Phys. 47, 631 (1928).

[57] S. Katsura, *Statistical mechanics of the anisotropic linear Heisenberg model*, Phys. Rev. **127**, 1508 (1962).

[58] M. H. S. Amin, Peter J. Love, and C. J. S. Truncik, *Thermally assisted adiabatic quantum computation*, Phys. Rev. Lett. **100**, 060503 (2008).

[59] A. M. Childs, E. Deotto, E. Farhi, J. Goldstone, S. Gutmann and A. J. Landahl, *Quantum search by measurement*, Phys. Rev. A **66**, 032314 (2002).

[60] G. Schaller, *Adiabatic preparation without quantum phase transitions,* pre-print: `arXiv:0807.2516` (2008).

[61] S. Mostame and R. Schützhold, *Quantum simulator for the Ising model with electrons floating on a helium film*, pre-print: `arXiv:0803.1093` (2008).

[62] D. Porras and J. I. Cirac, *Effective quantum spin system with trapped ions,* Phys. Rev. Lett. **92**, 207901 (2004).

[63] E. Y. Andrei, Ed., *Two-dimensional electron systems on Helium and other cryogenic substrates*, (Academic Press, New York, 1991).

[64] C. C. Grimes and T. R. Brown, *Direct spectroscopic observation of electrons in image-potential states outside liquid Helium*, Phys. Rev. Lett. **32**, 280 (1974).

[65] G. D. Gaspari and F. Bridges, *Electron-ripplon scattering on the surface of liquid Helium*, Journal of Low Temperature Physics **21**, 535 (1975).

[66] W. T. Sommer, *Liquid Helium as a barrier to electrons*, Phys. Rev. Lett. **12**, 271 (1964).

[67] P. M. Platzman and G. Beni, *Comment on plasmon linewidth experiments for electrons on a Helium surface*, Phys. Rev. Lett. **36**, 626 (1976).

[68] M. W. Cole, *Properties of image-potential-induced surface states of insulators*, Phys. Rev. B. **2**, 4239 (1970).

[69] Samuel Safran, *Statistical thermodynamics of surfaces, interfaces, and membranes*, (Academic Press, New York, 1994).

[70] E. Wigner, *On the interaction of electrons in metals*, Phys. Rev. **46**, 1002 (1934).

[71] H. Ikezi and P. M. Platzman, *Stability of helium films charged with electrons*, Phys. Rev. B. **23**, 1145 (1981).

[72] X. L. Hu and A. J. Dahm, *Stability of charged thin helium films*, Phys. Rev. B. **42**, 2010 (1990).

[73] J. Angrik, A. Faustein, J. Klier and P. Leiderer, *Electrons above Helium films on metal substrates*, Journal of Low Temperature Physics, **137**, 335 (2004).

[74] M. Razavy, *Quantum theory of tunneling*, (World Scientific, 2003).

[75] P. M. Platzman and M. I. Dykman, *Quantum computing with electrons floating on liquid helium*, Science **284**, 1967 (1999).

[76] R. Schützhold and S. Mostame, *Quantum simulator for the O(3) nonlinear sigma model*, JETP Lett. **82**, 248 (2005).

[77] M. Gell-Mann and M. Levy, *The axial vector current in beta decay*, Nuovo Cim. **16**, 705 (1960).

[78] A. M. Polyakov, *Interaction of Goldstone particles in two-dimensions; Applications to ferromagnets and massive Yang-Mills fields*, Phys. Lett. B **59**, 79 (1975).

[79] A. M. Polyakov and A. A. Belavin, *Metastable states of two-dimensional isotropic ferromagnets*, JETP Lett. **22**, 245 (1975) [Pisma Zh. Eksp. Teor. Fiz. **22**, 503 (1975)].

[80] A. A. Belavin, A. M. Polyakov, A. S. Shvarts and Y. S. Tyupkin, *Pseudoparticle solutions of the Yang-Mills equations*, Phys. Lett. B **59**, 85 (1975).

[81] V. A. Fateev, I. V. Frolov and A. S. Shvarts, *Quantum fluctuations of instantons in the nonlinear σ model*, Nucl. Phys. B **154**, 1 (1979).

[82] V. A. Novikov, M. A. Shifman, A. I. Vainshtein and V. I. Zakharov, *Two-dimensional σ models: Modeling nonperturbative effects of quantum chromodynamics*, Phys. Rept. **116**, 103 (1984) [Sov. J. Part. Nucl. **17**, 204 (1986); FECAA **17**, 472-545 (1986)].

[83] M. Luscher, *Quantum nonlocal charges and absence of particle production in the two-dimensional nonlinear σ model*, Nucl. Phys. B **135**, 1 (1978).

[84] M. Luscher and K. Pohlmeyer, *Scattering of massless lumps and nonlocal charges in the two-dimensional classical nonlinear σ model*, Nucl. Phys. B **137**, 46 (1978).

[85] A. B. Zamolodchikov and A. B. Zamolodchikov, *Factorized S-matrices in two dimensions as the exact solutions of certain relativistic quantum field models*, Annals Phys. **120**, 253 (1979).

[86] A. M. Polyakov and P. B. Wiegmann, *Theory of nonabelian Goldstone bosons in two dimensions*, Phys. Lett. B **131**, 121 (1983).

[87] P. B. Wiegmann, *Exact solution of the $O(3)$ nonlinear σ model*, Phys. Lett. B **152**, 209 (1985).

[88] P. Hasenfratz, M. Maggiore and F. Niedermayer, *The exact mass gap of the $O(3)$ and $O(4)$ nonlinear σ models in $D = 2$*, Phys. Lett. B **245**, 522 (1990).

[89] G. Martinelli, G. Parisi and R. Petronzio, *Monte Carlo simulations for the two-dimensional $O(3)$ nonlinear σ model*, Phys. Lett. B **100**, 485 (1981).

[90] K. Symanzik, *Continuum limit and improved action in lattice theories: II. $O(N)$ nonlinear sigma model in perturbation theory*, Nucl. Phys. B **226**, 205 (1983).

[91] Y. Iwasaki, *Renormalization group analysis of lattice theories and improved lattice action: Two-dimensional nonlinear $O(N)$ σ model*, Nucl. Phys. B **258**, 141 (1985).

[92] U. Wolff, *Asymptotic freedom and mass generation in the $O(3)$ nonlinear σ model*, Nucl. Phys. B **334**, 581 (1990).

[93] E. Brezin, J. Zinn-Justin and J. C. Le Guillou, *Renormalization of the nonlinear σ model in $2 + \epsilon$ dimension*, Phys. Rev. D **14**, 2615 (1976).

[94] E. Brezin and J. Zinn-Justin, *Renormalization of the nonlinear σ model in $2 + \epsilon$ dimensions – Application to the Heisenberg ferromagnets*, Phys. Rev. Lett. **36**, 691 (1976).

[95] W. A. Bardeen, B. W. Lee and R. E. Shrock, *Phase transition in the nonlinear σ model in $2 + \epsilon$ dimensional continuum*, Phys. Rev. D **14**, 985 (1976).

[96] S. Hikami and E. Brezin, *Loop calculations in the two-dimensional nonlinear σ model*, J. Phys. A **11**, 1141 (1978).

[97] F. S. A. Cavalcante, M. S. Cunha and C. A. S. Almeida, *Vortices in a nonminimal Maxwell-Chern-Simons $O(3)$ sigma model*, Phys. Lett. B **475**, 315 (2000).

[98] T. Tsurumaru, I. Tsutsui, *On topological terms in the $O(3)$ nonlinear sigma model*, Phys. Lett. B **460**, 94 (1999).

[99] A. M. Tsvelik, *Quantum field theory in condensed matter physics*, (Cambridge University Press, Cambridge, 1995).

[100] P. M. Chaikin and T. C. Lubensky, *Principles of condensed matter physics*, (Cambridge University Press, Cambridge, 1995).

[101] J. Zinn-Justin, *Quantum field theory and critical phenomena*, Int. Ser. Monogr. Phys. **113**, 1 (2002).

[102] C. Albertsson, U. Lindstrom and M. Zabzine, $N = 1$ *supersymmetric sigma model with boundaries – I*, Comm. Math. Phys. **233**, 403 (2003).

[103] C. Albertsson, U. Lindstrom and M. Zabzine, $N = 1$ *supersymmetric sigma model with boundaries – II*, Nuclear Physics B **678**, 295 (2004).

[104] H. Otsu, T. Sato, H. Ikemori and S. Kitakado, *Solitons of sigma model on noncommutative space as solitons of electron system*, JHEP **07**, 52 (2004).

[105] Y. Mishchenko and Chueng-Ryong Ji, *A novel variational approach for quantum field theory: Example of study of the ground state and phase transition in nonlinear sigma model*, Int. J. Mod. Phys. A **20**, 3488 (2005).

[106] R. Capovilla and J. Guven, *Helfrich-Canham bending energy as a constrained nonlinear sigma model*, J. Phys. A **38**, 2593 (2005).

[107] R. Rajaraman, *Solitons and Instantons*, (Amsterdam, North Holland, 1987).

[108] L. Tong, R. R. Gattass, J. B. Ashcom, S. He, J. Lou, M. Shen, I. Maxwell, and E. Mazur, *Subwavelength-diameter silica wires for low-loss optical wave guiding*, Nature **426**, 816 (2003).

[109] D. D. D. Ma, C. S. Lee, F. C. K. Au, S. Y. Tong and S. T. Lee *Small-Diameter Silicon Nanowire Surfaces*, Science **299**, 1874 (2003).

[110] A. M. Dykhne, *Adiabatic perturbation of discrete spectrum states*, Sov. Phys. JETP **14**, 941 (1962).

[111] V. Jakšić and J. Segert, *On the Landau-Zener formula for two-level systems*, J. Math. Phys. **34**, 2807 (1993).

[112] C. Wittig, *The Landau-Zener Formula*, Journal of Physical Chemistry B **109**, 8428 (2005).

[113] Ping Ao and J. Rammer, *Quantum dynamics of a two-state system in a dissipative environment*, Phys. Rev. B **43**, 5397 (1991).

List of Publications

- Sarah Mostame and Ralf Schützhold,
  Quantum simulator for the Ising model with electrons floating on a helium film,
  Phys. Rev. Lett. **101**, 220501 (2008)
  Virtual Journal of Quantum Information, Vol. **8**, Iss. 12
- Sarah Mostame, Gernot Schaller, and Ralf Schützhold,
  Decoherence in a dynamical quantum phase transition of the transverse Ising chain,
  Phys. Rev. A **76**, 030304 (*Rapid Communication*) (2007);
  Virtual Journal of Quantum Information, Vol. **7**, Iss. 9;
  Virtual Journal of Nanoscale Science and Thechnology, Vol. **16**, Iss. 14
- Gernot Schaller, Sarah Mostame, and Ralf Schützhold,
  General error estimate for adiabatic quantum computing
  Phys. Rev. A **73**, 062307 (2006);
  Virtual Journal of Quantum Information, Vol. **6**, Iss. 6 (2006)
- Ralf Schützhold and Sarah Mostame,
  Quantum simulator for the O(3) nonlinear sigma model,
  JETP Lett. **82**, 248 (2005);
  Pisma Zh. Eksp. Teor. Fiz. **82**, 279

Acknowledgement

I am most grateful to Prof. Dr. Ralf Schützhold for giving me the opportunity in his research group and helping me all along to do the Thesis. His sharp insights and enthusiasm for quantum theory were a constant source of inspiration for my work. It is also a special pleasure to thank Dr. Gernot Schaller for his valuable guidance and discussions. Particularly, I thank Prof. Dr. Rüdiger Schmidt who took the role of the supervisor.

I wish to thank all of my friends, colleaguse and officemates. Among all those people who made my last years a wonderful time, I am especially grateful to Azar Moghtased-Azar, Caroline Semmling, Sara Jabbari Farouji, Fatemeh Ghasemi and last but not least, Farideh Saeed-Mehr, Michael Uhlmann and Markus Tiersch.

I am particularly thankful to my family: my uncle Ali-Akbar Jahani-Saber, my sister Raana Mostame, my brother Sassan Mostame and specially my parents Sakineh-Soltan Jahani-Saber and Fazlollah Mostame for their great love and support during all my studies. I appreciate the freedom my parents have given me to choose my way in life and carry out my wishes.

Above all, my warmest thanks go to Reza Farhadifar whose endless love, great support and encouragements made it possible for me to follow my dreams.

Erklärung

Hiermit versichere ich, daß ich die vorliegende Arbeit ohne unzulässige Hilfe Dritter und ohne Benutzung anderer als der angegebenen Hilfsmittel angefertigt habe; die aus fremden Quellen direkt oder indirekt übernommenen Gedanken sind als solche kenntlich gemacht. Diese Arbeit wurde bisher weder in Inland noch im Ausland in gleicher oder ähnlicher Form einer anderen Prüfungsbehörde vorgelegt.

Dresden, den 02. Oktober 2008

Sarah Mostame